Variability Analysis of a Sample of Potential Southern Calibration Sources

A thesis submitted in partial fulfilment of the
requirements for the degree of

MASTER OF SCIENCE

of

RHODES UNIVERSITY

by

FAITH HUNGWE

June 2009

Abstract

A considerable number of Very Long Baseline Interferometry (VLBI) surveys have been conducted in the northern hemisphere and very few in the southern hemisphere mostly because of a lack of telescopes and therefore adequate baseline coverage. Thus there is a deficit of calibrator sources in the southern hemisphere. Further, some of the most interesting astronomical objects eg. the galactic centre and the nearest galaxies (the small and large Magellanic Clouds) lie in the southern hemisphere and these require high resolution studies. With a major expansion of radio astronomy observing capability on its way in the southern hemisphere (with the two SKA (Square Kilometre Array) precursors, meerKAT (Karoo Array Telescope) and ASKAP (Australian SKA Pathfinder), leading to the SKA itself) it is clear that interferometry and VLBI in the southern hemisphere need a dense network of calibration sources at different resolutions and a range of frequencies. This work seeks to help redress this problem by presenting an analysis of 31 southern sources to help fill the gaps in the southern hemisphere calibrator distribution. We have developed a multi-parameter method of classifying these sources as calibrators. From our sample of 31 sources, we have 2 class A sources (Excellent calibrators), 16 class B sources (Good calibrators), 9 class C sources (Poor calibrators) and 4 class D sources (Unsuitable calibrators).

Acknowledgements

I would like to acknowledge and extend my heartfelt gratitude to the following people who have made the completion of this thesis possible:

- My advisor, Dr Roopesh Ojha for his inspiring guidance and unconditional availability during the whole period of my study.
- My advisors, Dr Michael Bietenholz and Prof Roy Booth for their help and motivation.
- The United States Naval Observatory for providing the data.
- The South African SKA project for their financial support.
- My friends and workmates for their vital encouragement and support.

I owe a profound debt of gratitude to my parents for unconditionally supporting and sacrificing for me. I will forever be grateful for their confidence in me. Thank you for believing in me.

List of Figures

Contents

Chapter 1

Introduction

1.1 Background

High angular resolution radio astronomy is done using interferometers. These require calibrators, for correction of systematic effects and effects of the atmosphere on the measured visibilities. Atmospheric fluctuations cause perturbations in visibility phase which, if not corrected, seriously limit both the sensitivity and image quality of an interferometric array. Due to the limited number of telescopes, and therefore baseline coverage, few surveys for calibrators have been carried out in the southern hemisphere and hence, there are fewer calibrators in the south.

There is an expansion of radio astronomy observing capability on the way in the southern hemisphere with the two SKA (Square Kilometer Array) precursors, meerKAT (Karoo Array Telescope) and ASKAP (Australian Square Kilomter Array Pathfinder), leading to the SKA itself. This will make the need for calibrators in the south more acute. Currently, the method of correcting perturbations in the visibilities involves periodic observations of a nearby calibrator. Self-calibration can also be used but is limited to very bright sources and it only removes antennas-based errors. Also, for small arrays, a significant fraction of the phase and amplitude information cannot be recovered and information about absolute position is lost.

This project was begun with the aim of looking for calibrators in the south, with the SKA and the South African meerKAT as drivers. These new instruments will greatly expand the VLBI capabilities in the south and most of this expansion will be at lower frequencies, hence this study at 2.3 GHz. A significant amount of time was spent doing background work on surveys done in the southern hemisphere. Some of the surveys looked at include the VLA sky survey at 1.4 GHz, the Parkes Survey and the Molonglo Survey but none of these are VLBI surveys. While several surveys have been carried out in the northern hemisphere, including but not limited to, the VLBA calibrator Survey 1- 6 (Beasley et al., 2002; Fomalont et al., 2003; Petrov et al., 2005, 2006; Kovalev et al., 2007; Petrov et al., 2008) and several surveys to densify the International Celestial Reference Frame (Fey & Charlot, 1996, 1997, 2000), very few VLBI surveys have been carried out in the southern hemisphere. Some of the VLBI surveys that have been carried out in the southern hemisphere include the C-Band Southern Hemisphere VLBI Survey of Compact Radio Sources (Shen et al., 1997, 1998a) and

Observations of Southern ICRF sources at 8.4 GHz (Ojha et al., 2004, 2005). The figure 1.1 gives a good illustration of the lack of calibrators in the southern hemisphere.

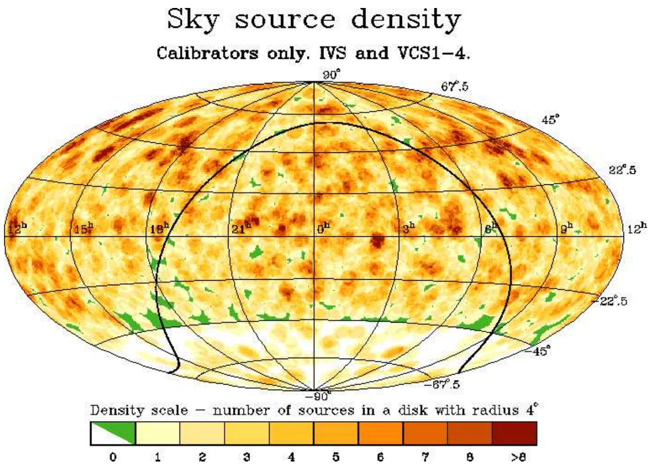

Figure 1.1: Sky distribution of calibrators from the VLBA Calibrator Survey. Note the lack of a dense network of calibrators in the south (Petrov et al., 2006).

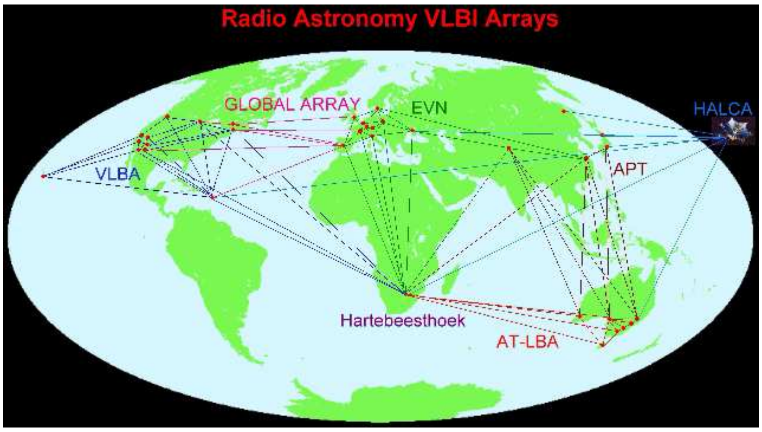

Figure 1.2: Global distribution of VLBI stations, note the lack of telescopes in the southern hemisphere. Taken from http://www.hartrao.ac.za

An ideal calibrator would look the same to all observing antennas on all baselines. It should be bright, compact, unresolved and should not vary. A calibrator source should also be separated from the target sources by as small an angle as possible. Therefore, it is desirable to have calibrator sources evenly distributed across the whole sky.

In practice, at radio wavelengths, the primary flux calibrators are mostly powerful radio galaxies, Active Galactic Nuclei (AGN), which exist at the centre of about 10% of all galaxies. There are several types of AGN but they can be grouped into radio-loud and radio quiet AGN. Radio quiet AGN include LINERs, Seyfert Galaxies and Radio Quiet quasars. The radio loud AGN include Blazars, Radio Loud Galaxies and Radio Loud Quasars and their fundamental source of power is believed to be accretion of matter onto a super-massive black hole.

Radio loud AGN, in particular quasars, are known to vary at all wavelengths at which they have been studied. Early in the study of AGN physics, it was discovered that quasars vary significantly on timescales as short as a few days leading to the interpretation that the radiation must come from a region of size the order of light days. This means that you have a body the size of the solar system radiating hundreds of times as much energy as an entire galaxy, making quasars some of the brightest radio objects in the sky. So, despite the fact that they vary, quasars are some of the most compact of AGN. They are also well distributed around the sky and because they are very distant objects, they have stable positions in the sky. All these qualities make quasars the AGN of choice when looking for calibrators.

As mentioned before, this work seeks to characterize a selection of southern radio sources, and determine their suitability as calibrators for southern VLBI experiments, especially ones using MeerKAT and the SKA. In particular, I will determine the amount of source structure and its variation, as well as the amount of flux density variation in order to determine suitability of each as a calibrator.

1.2 The Square Kilometre Array

1.2.1 The SKA

The SKA project was born as an international project and countries were invited to put in bids to host the telescope. In 2006, South Africa and Australia were short listed as hosts and both countries began to work on demonstrator telescopes for SKA. Australia is working on ASKAP and South Africa is developing meerKAT. These two telescopes will have much shorted baselines and therefore less resolution than the SKA but the plan is that they will contribute towards the development of the SKA and the proposed sites.

With a receiving area of one million square metres, the SKA will be the largest telescope ever (Carilli & Rawlings, 2004). It will be an interferometric instrument with many small antennas. Some antennas will form a dense inner core and the other antennas will be further apart as you move away from the centre. About 20% of the collecting area will be within a 1 km diameter and 50% within a 5 km diameter. 75% of the total collecting area will be within 150 km and maximum baselines will be at least 3000 km from the array centre giving an angular resolution of $< 0.02/f$ GHz arcsecond. It is expected to operate in the frequency range 70 MHz to 25 GHz. It will have simultaneous independent observing bands, with 2 polarizations at each of the two independent frequencies. A dynamic range of $> 10^6$ and image fidelity of $> 10^4$ between 0.5 and 25 GHz, over a declination range of 90°is planned.

Key Science Projects

Originally, the SKA was to detect HI in normal galaxies at high redshifts but due to developments in other branches of astronomy, the SKA is now expected to answer questions ranging from the the origin and evolution of cosmic magnetism, galaxy evolution and cosmology to the existence of other life-forms. Below, are some of the SKA key science areas.

i) **Epoch of Reionisation:** The low-frequency SKA is expected to probe the Dark Ages and the epoch of reionisation. Imaging neutral hydrogen is expected to give the most direct probe of the transition of the inter-galactic medium from a neutral to an ionised state.

ii) **Cosmic Magnetism:** The SKA will track the origin and evolution of magnetic fields in galaxies by measuring Faraday rotation towards large numbers of background sources.

iii) **Cradle of Life:** The SKA will provide sufficient sensitivity to search for pre-biotic molecules and maybe 'leakage' of radio emissions from nearby extraterrestrial civilizations.

iv) **Strong field tests of Gravity:** Many of the current tests and attempts at detecting gravitational wave emission rely on just a few known pulsars. The SKA will conduct a two-pronged program that will first discover new pulsars and then do high-precision timing to probe fundamental physics (Cordes, 2009). The SKA will, among other things, survey the Galaxy with the aim of increasing by an order of magnitude, the number of millisecond pulsars and neutron star binary systems suitable for further timing.

v) **Cosmology and Galaxy Evolution:** The original driver for a collecting area of 1 km^2 were studies of the 21-cm hyperfine transition of HI over cosmological distances. The ultimate goal is to have surveys analogous to optical surveys like the Sloan Digital Sky Survey (SDSS) but unaffected by dust obscuration (Myers, 2009).

   The relationship between AGN and Star Formation is not clear but both are known to evolve, reaching a peak at $z \approx 2$. The SKA is expected to answer questions about when the first massive black holes formed, whether it was before or after the first galactic scale assemblies of stars (Putman, 2009). It is also expected to show the role of jet feedback by observations of radio synchrotron emission from both supernovae and massive blackhole accretion. The SKA with its unique combination of sensitivity and resolution will also allow, for the first time, the study of "normal" galaxies and radio-quiet AGN at cosmological redshifts.

vi) **The Dynamic Radio Sky:** Most instruments in astronomy become famous for findings other than what they were designed for and the SKA is not expected to be an exception. The promise of the SKA for exploring the dynamic radio sky is threefold: (1) Its high sensitivity and large area of view will enable complete surveys over large portions of the sky. (2) Both line and continuum surveys offer a natural platform for synoptic operation to cover the sky repeatedly; and (3) computational and algorithmic advances will enable observations to achieve multiple science goals (Lazio, 2009; Kellermann, 2009).

1.2.2 meerKAT

The new South African radio telescope meerKAT will be the largest radio telescope in the Southern hemisphere when completed. meerKAT is scheduled for completion by the end of 2012, the first phase of construction has already begun. meerKAT is planned to have 80 dishes, each of diameter 12 m, and it will be located in the Karoo radio protected, radio-quiet zone in the Northern Cape province of South Africa. The working specifications are listed in Table 1.1. As well as being a significant radio telescope in its own right, meerKAT will serve as a pathfinder for the SKA, and will also serve as a sensitive element in global and southern hemisphere VLBI arrays.

Specifications	Reference Design
Feed	Single-pixel wide-band
Lower Freq	500 MHz
Upper Freq	10 GHz
Dish Diameter	12 m
Number of Dishes	80
T_{sys}	30K
Min Baselines	20 m
Aperture Efficiency	0.7
Correlator architecture	FX

Table 1.1: meerKAT specification. Table adapted from Jonas (2007).

In particular, meerKAT will have baselines up to 80 km (Booth, private communication) and will operate at frequencies up to 10 GHz. The maximum resolution of meerKAT on its own will therefore be on the order of 100 milliarcseconds, giving a maximum resolution of ground-based VLBI arrays including meerKAT at, for example, 2.3 GHz, will be a few milliarcseconds. The sources in existing calibrator lists, such as the ATCA calibrator list, might all be heavily resolved at these resolutions, and therefore no longer suitable to use as calibrators. It is important therefore, to examine potential calibrator sources at higher resolution, which is the aim of this thesis.

1.2.3 ASKAP

The Australian SKA Pathfinder (ASKAP) will comprise 36 12m antennas. It is designed to be high speed survey instrument with a high dynamic range. It will have maximum baselines of about 6 km. ASKAP will be located in western Australia with construction due to start in late 2009. The full ASKAP is planned to be fully operational by 2013.

1.3 Interferometry and Very Long Baseline Interferometry

1.3.1 VLBI

The 31 selected sources were observed using the technique of Very Long Baseline Interferometry (VLBI). This technique uses a number of antennas that are not physically connected to look at astronomical objects. It has the advantage of much higher angular resolution relative to single dish telescopes and connected interferometers.

When using VLBI, data is recorded on tape recorders or disk packs and then correlated before it is available to the astronomer. Because there is no direct link between the antennas, they can be placed just about anywhere on earth or in space, allowing baselines of up to and greater than (using an antenna space eg. VLBI Space Observatory Programme 2 (VSOP2) the diameter of the earth. At centimetre wavelengths, this yields milliarcsecond resolution, giving VLBI instruments the highest resolution for any telescope in astronomy. The

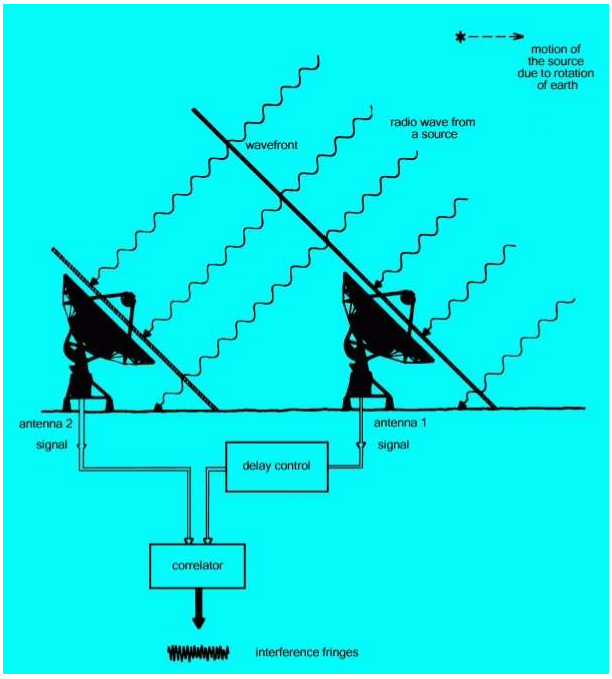

Figure 1.3: Schematic diagram showing a two-element interferometer.

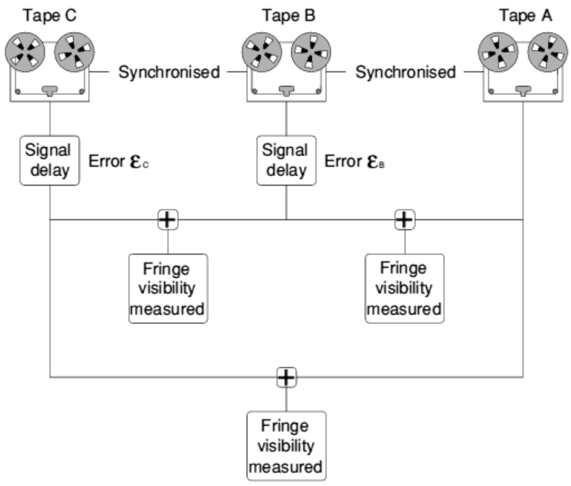

Figure 1.4: Schematic diagram showing playback of data from each telescope in a VLBI array. Atomic signals recorded with the data help to synchronise the playback of data from the different telescopes.

technique of VLBI was primarily developed for studies of quasars and radio-bright galaxies. By the mid-60s, it was obvious some radio sources had features of small angular size that could not be resolved by conventional connected element interferometers. The variation timescales of some of the radio sources provided an indication of the angular size of the objects in question. A group at the University of Manchester developed the technique of radio linked interferometers. This technique had a natural limit of about 100 km. After increasing the baseline of the interferometer to this distance, they then raised the operating frequency from 158 MHz to 408 MHz. It became obvious that in order to observe and characterise the structure in radio sources in much greater detail, even longer baselines were necessary, which required a move from the radio link to tape recorders and much later to disk packs. Recording data at each station prior to correlation required local oscillators with sufficient time stability to maintain the phase relationship between the elements of the VLBI instrument. Technical developments in the mid-60s made this possible with new frequency standards. Most stations now use hydrogen masers which have a time stability of about 1 part in 10^{14}.

VLBI uses non-connected antennas to look at radio-objects in the sky. Because there is no link between the antennas, the data is recorded on either tape recorder or disk packs and processed at a later stage. Along with the data, time stamps are also written and are used later to synchronise the data streams and allow them to be correlated with the proper time alignment. Most stations use a hydrogen maser as a clock for short term stability and synchronisation via the GPS satellite system for long term stability.

A correlator predicts delay for a given baseline and synchronises the recorded data during playback. In order to detect "fringes", signals from the same wavefront have to be correlated to each other. The correlator generates a correlation function for each pair of antennas which is directly comparable to the complex visibilities of a 'normal' connected element interferometer.

Because the data come from different telescopes, there is need to calibrate the data to correct for telescope sensitivity, system temperature, gain, correlator effects, instrumental phase, ionospheric and tropospheric effects. This is described in chapter 3.

1.3.2 The Very Long Baseline Array (VLBA)

Observations of the sources studied in this thesis were made using the Very Long Baseline Array (VLBA) as the core for all observations together with a global array of antennas. The VLBA is a VLBI array, primarily designed as an imaging instrument.

With 10 identical 25-m antennas situated in different locations in the United States of America, the telescope has a resolution of about 1 milliarcseconds (mas) allowing detailed analysis of parsec scale extra-galactic objects like AGN. It is the only interferometric instrument in the world that was built solely for the purpose of VLBI. On the longest baselines (Mauna Kea in Hawaii to St. Croix in the US Virgin Islands), the VLBA spans more than 9000 km. The location of the antennas were chosen for optimum u-v coverage.

A wide range of receivers covering frequencies from 300 MHz to 43 GHz are installed on the antennas to make it possible to do different kinds of science. The VLBA has smaller antennas compared to those traditionally used for VLBI e.g., Greenbank (100 m), Medicina (32 m), Tsukuba (34 m) and so care was taken to compensate for sensitivity limitations. The antennas have a high-gain shaped design with an efficiency of about 70% compared to about 50% common to most large VLBI antennas. This makes it possible to do short

Figure 1.5: The 10 antennas of the VLBA. *c*ourtesy:http://www.vlba.nrao.edu

scans and to observe weak sources (Napier, 1995).

All the antennas have an alt-az mounting. The antennas slew fairly rapidly 90° per min in azimuth and 30° per min in elevation , making it ideal for geodetic and astrometric observations used by the RRFID. The VLBA can observe up to 8 different frequencies in a quasi-simultaneous manner. 2 frequencies (S and X-band) were observed simultaneously for the data used in this thesis.

Chapter 2

Active Galactic Nuclei (AGN)

AGN make good calibrators and they have been instrumental in driving the development of VLBI. This chapter looks at AGN in detail, their properties, classification and emission mechanisms.

The optical identification in 1963 of radio sources 3C273 (Schmidt, 1963) and 3C48 (Greenstein, 1963) ushered in a new era in extra-galactic astronomy. It proved the existence of an energy source that produced more energy than an entire galaxy yet had a star-like appearance. Later discoveries showed that these radio sources were in fact radio galaxies and the star-like appearance was due to the existence of energetic phenomena at the central region or nuclei of these galaxies. Radio galaxies are some of the most energetic and largest galaxies in the universe. They form a sub-class of active galactic nuclei (AGN) which are powerful sources of radiation and which exist in the centre of about 10% of all galaxies. Their luminosities range from 10^{40} ergs^{-1} to 10^{47} ergs^{-1}. The term AGN is generally used to describe both the central region and the galaxy hosting the AGN.

2.1 Properties of AGN

AGN are known to exhibit the following properties:

i) They are very small in angular size.

ii) AGN have high luminosities, comparable to or greater than that of an entire galaxy (ranging from 1% to 10^4 times the luminosity of a normal galaxy).

iii) AGN are known to be bright at almost all wavelengths they have been observed.

iv) AGN are known to have very prominent emission lines which are very different to those of most stars and galaxies whose lines are very weak and mostly in absorption.

v) Most AGN are weakly polarised but about 10% of them are strongly polarised. The polarisation is mostly linear with typical fractional polarisation of a few percent. Circular polarisation has been detected in AGN at levels typically less than a percent (Wardle et al., 1998).

vi) Variability, AGN are known to vary at almost all wavelengths at which they have been observed.

2.2 Classification of AGN

AGN can be classified into radio-loud and radio-quiet AGN. About 10% of AGN are radio-loud with the rest being radio-quiet. Radio-quiet AGN include LINERs, Seyfert galaxies and radio quiet quasars. Radio-loud AGN are made up of radio loud quasars, blazars and radio galaxies. All AGN are characterised by very high luminosities which cannot be attributed to stars (Curran et al., 2000). Seyfert galaxies and quasars form the two largest subclasses of AGN, the fundamental difference between them being the amount of radiation emitted by the most central region. Seyfert galaxies have a quasar like nucleus but the host galaxy is clearly detectable whilst quasars have a star-like appearance.

2.2.1 Radio-quiet AGN

Seyfert Galaxies

Seyfert galaxies, are named after Carl Seyfert who discovered them in 1943. He was the first to see that these galaxies were similar and formed a distinct class. Almost all Seyferts are spiral galaxies. They are low luminosity galaxies ($M_B \geq -21.5 + logH_o$) and are found in the local universe. The original definition was primarily morphological (Seyfert, 1943) but now Seyfert galaxies can be classified into two groups, based on the absence or presence of broad bases on the permitted line in their spectra, (Khachikian & Weedman, 1974).

- Seyfert 1 galaxies have two sets of emission lines (broad lines and narrow lines) superposed on one another. The broad lines come from high electron density regions which are relatively close to the core and are seen in permitted lines only. They have widths of up to 8500 kms^{-1}.

- Seyfert 2 galaxies have only one set of emission lines (narrow lines) present. They display both permitted and forbidden emission lines. The have widths between $100-1000$km s^{-1} and arise from the low density ionised gas relatively far from the core. Weak broad lines have been detected in some Seyferts that were originally thought to be Seyfert 2s, making the distinction between Seyfert 1 and 2s blurred. In order to account for this, scientists believe the different pictures presented by Seyferts depends on whether the galaxies are seen axis-on or not and that there is just one type of Seyfert galaxy (see section on the Unified Scheme).

LINERs

LINERs are the most common type of AGN. They are low-ionisation nuclear emission line region galaxies. They are spectroscopically similar to Seyfert 2 galaxies but have stronger low-ionisation lines. They usually contain a compact core similar to that seen in radio galaxies and quasars but it is much weaker.

2.2.2 Radio-loud AGN

Quasars

Quasars are defined as objects with broad emission lines and an absolute magnitude $M_B \leq -23$. At radio wavelengths, they can can have both a compact and extended components. The position of the compact component is often coincident with that of an optically identified quasar. The extended component is made up of twin lobes on either side of the nucleus and is linked to the compact component by tightly collimated emission jets. The extent of these lobes can range from a few parsecs to several megaparsecs in giant radio galaxies. The lobes can be classified into two classes, FR I and FR II, depending on luminosity and morphology (Fanaroff & Riley, 1974). Although the initial classification was based on the ratio of the distance between the brightest components on either side of the nuclei (galaxies with a ratio of ≤ 0.5 were put into class 1 and those with a ratio greater than 0.5 were put in class 2), it turned out the low luminosity galaxies were found in class 1 whilst the high luminosity galaxies generally fell into class 2.

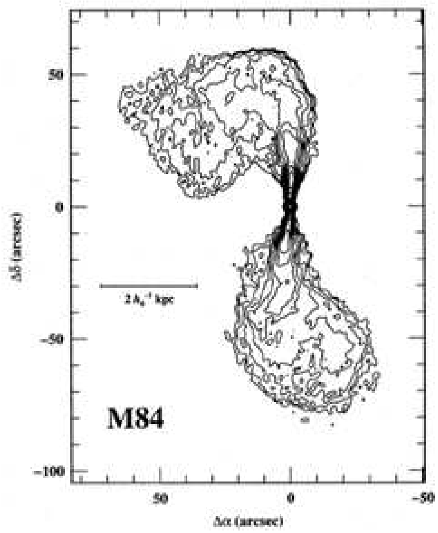

Figure 2.1: VLA map of FR-I galaxy M84 at 4.9 GHz. (Laing & Bridle, 1987)

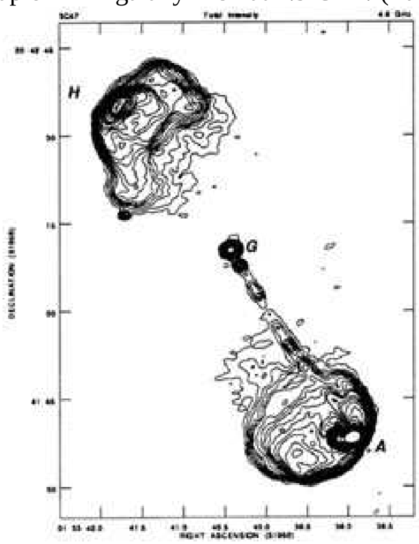

Figure 2.2: A VLA map of FR-II galaxy 3C 47 (Bridle et al., 1994).

FR-I sources are generally weaker radio sources with a very bright core component and they show an edge-darkened morphorlogy. Jets are detected in a large fraction of FR-I sources. These can begin as single lobes close to the centre of the galaxy but they become double sided and continuous, a few parsecs from the core.

FR-II sources have edge-brightened lobes and very faint cores with one or more hot spots at the outermost edge of the lobes. The jets have small opening angles and are generally one-sided. This one-sidedness occurs from milliarcsecond scales to up to kiloparsec scales.

Quasars are distinguished from Seyferts by the fact they are generally unresolved in Palomar Sky Survey Photographs ie they are very compact, making them ideal for use as calibrators.

Radio Galaxies

Like Seyferts, radio galaxies are classified based on their emission lines. There are two types of radio galaxies; broad-line radio galaxies (BLRGs) and narrow-line radio galaxies (NLRGs). Unlike Seyferts that are generally hosted by spiral galaxies, radio galaxies are generally hosted by giant elliptical galaxies.

Blazars

Blazars are radio-loud AGN that display very strong and variable continuum emission at all wavelengths. They comprise BL Lac Objects (named after the prototype, BL Lacertae) and Optically Violent Variables (OVVs). Their variation is very rapid and large compared to 'normal' AGN eg $\Delta m \geq 0.1$ mag in the visible spectrum.

2.3 Emission Mechanisms

AGN have been detected in all wavebands, from x-rays, through the optical and into the radio. Radio emission is thought to come from both thermal and non-thermal processes, bremsstrahlung and synchrotron radiation respectively. The total emission from the galaxy comes from all emission processes but synchrotron emission makes up by far the largest fraction of the total radio emission. No other emission mechanism can compete with synchrotron emission in producing polarised emission in the radio regime.

2.3.1 Synchrotron Emission

Synchrotron radiation was first suggested by Alfvén & Herlofson (1950) as the emission mechanism responsible for the very bright radio emission. Alfvén & Herlofson (1950) proposed that "the nonthermal radiation is emitted by relativistic electrons moving in intricately tangled magnetic fields of extended coronas believed to surround certain kind of stars". In 1963, Oke (1963) noted that the energy distribution from spectrophotometry results did not resemble a black body and inferred a contribution from synchrotron radiation. The justification for the identification of synchrotron emission as the mechanism responsible for radio emission is that it naturally produces polarised emission and this has been observed for almost all AGN. Synchrotron emission is produced as a result of helical motion of a relativistic electron, of charge e and mass m, moving at a velocity v in a magnetic field of strength B. The acceleration of the charge is always perpendicular to the field. The frequency, ν, of the projected orbit on a plane normal to B, is

$$\nu_g = \frac{eB}{2\pi\gamma mc} \tag{2.1}$$

where $\gamma = (1 - v^2/c^2)^{-1/2}$ and c is the speed of light. The emitted power P is given as:

$$P = \frac{2}{3} r_o^2 c \beta^2 \gamma^2 B^2 sin^2\theta, \quad r_o = \frac{e^2}{mc^2} \tag{2.2}$$

where $\beta = v/c$. In radio astronomy, we observe radiation from an ensemble of electrons. For a homogeneous and isotropic ensemble of electrons with energy density distribution N(E)dE, the total power emitted by the electrons as a function of frequency of the emitted radiation is given by

$$P(\nu) = \int_{E_1}^{E_2} P(E,\nu) N(E) dE \tag{2.3}$$

where $P(\nu)$ is the energy emitted per unit time per unit frequency interval from electrons with energies in the range E and $E + dE$. For a power law energy spectrum given by $N(E)dE = N_\circ E^{-p} dE$, where $N_\circ$ and p are constants, in a limited range $E_1 < E < E_2$,

the emitted spectrum has the very simple power law form

$$P(\nu) \propto \nu^{-\alpha}, \quad \alpha = \frac{p-1}{2} \tag{2.4}$$

where α, the spectral index, is usually positive.

The steep spectrum ($\alpha > 0.5$) emitted by the lobes of radio galaxies is a consequence of the relative lifetimes of electrons with different energies: high-energy electrons lose energy more quickly than those at lower energies, leading to an overall curvature of the spectrum. The flat radio spectrum typical of compact cores may be due to opacity effects, equivalent to superposing the emission from many discrete, self-absorbed synchrotron sources (Phinney, 1985). Synchrotron self-absorption occurs usually at very low frequencies when the compact radio source becomes opaque to its own radiation. This results in a steep ($\alpha = -\frac{5}{2}$) turn down in the radio spectrum at low frequency which depends on magnetic field and angular size of the source and produces a low frequency cut off of the spectrum.

2.4 Superluminal Motion

The development of VLBI provided very high angular resolution for AGN studies. Scientists had always suspected that AGN would have structure at very small scale because of the very rapid flux variability. Observations (including this thesis) have shown the presence of multiple components. Whitney et al. (1971), after observing quasars that had been observed earlier by Knight et al. (1971), discovered that the angular separation of the components translated to a linear separation rate of about 10 times the speed of light.

Cohen et al. (1971) also observed the same kind of phenomenon in 3C 273 and 3C 279. These components were seen to have proper motion, moving further and further apart. The observed proper motions imply transverse speeds of close to and greater than the speed of light. Apparent superluminal motion has now been

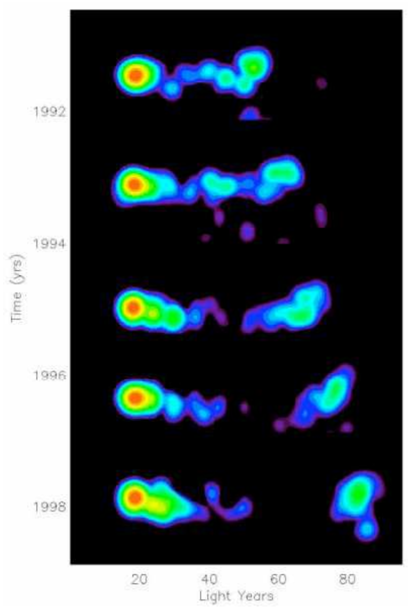

Figure 2.3: K-band image showing movement of a jet component of the source 3C 279 through 5 epochs from 1994 to 1998. The separation is given in light years and shows speeds greater than the speed of light. This image is part of a larger set of 28 images made by Wehrle et al. (2001) using the VLBA.

observed in a number of quasars and radio galaxies.

The generally accepted explanation for apparent speeds greater than the speed of light is that the superluminal speeds are due to a geometric effect where a jet pointing nearly towards the observer with a small angle θ, will almost overtake its own radiation creating the illusion of transverse speeds greater than the speed of light. This apparent speed is referred to as superluminal motion and can be expressed as:

$$\beta_{app} = \frac{\beta \sin\theta}{1 - \beta \cos\theta} \tag{2.5}$$

β_{app} can greatly exceed unity.

2.5 Unification Models

The unification model is currently the most accepted model to explain the different types of AGN. AGN are generally thought to be powered by gravitational accretion onto a supermassive black hole (SMB) at the centre of the galaxy (Begelman et al., 1984; Blandford, 1990). The different types of AGN that are observed are thought to depend on observer orientation.

2.5.1 Unified Model

The unified model tries to unify Seyfert 1 and Seyfert 2 galaxies as being one type. Using the technique of spectro-polarimetry, considerable progress to find and understand interrelation between the two types of Seyfert galaxies was made. The technique revealed several cases of type 2 Seyfert galaxies with obscured type 1 regions.

2.5.2 Grand Unified Model

The figure below shows a schematic diagram of AGN according to the Grand Unified Model. The AGN consists, as mentioned, of a SMB in the centre, surrounded by an accretion disk which widens at the edges, forming a torus that envelopes the whole AGN.

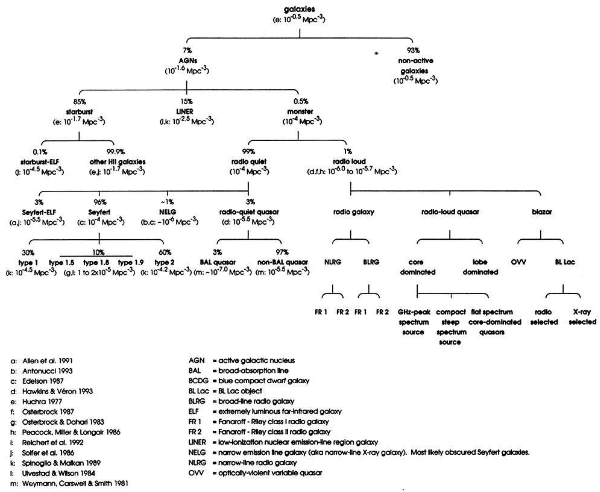

Figure 2.4: Figure below shows a schematic diagram of AGN according to the Grand Unified Model. *courtesy: http://www.auger.org/news/PRagn/. Image credit:NASA.*

As matter falls into the SMB, some of the gravitational potential energy is converted into observable radiation and kinetic energy of the jets. The BLR are located in the inner regions of the AGN, ie the central 1 parsec. The outer clouds form the NLR which can extend to a few parsecs. Now, depending on the orientation, it is possible one can see only the narrow line regions and not see the broad line region directly. The Grand Unification Model is not perfect as it does not explain a number of phenomenon. In particular, it does not explain the presence of both radio-loud AGN and radio quiet ones, but it provides a good framework on which further investigations of AGN can be made.

Chapter 3

Observation and Data Analysis

The observations used in this thesis were carried out in the course of geodesy experiments. Hartebeesthoek Radio Astronomy Observatory has for many years been involved in geodesy experiments in the global VLBI network (see Fig 1.1). Through this involvement, we were able to begin a collaboration with the United States Naval Observatory (USNO) and this thesis uses data from the USNO's Radio Reference Frame Image Database (RRFID).

3.1 Source Selection

3.1.1 The RRFID

The selected sources are a subset of sources from the Relativistic Jets In RRFID Kinematic Survey (Piner et al., 2007). The RRFID is the result of the USNO's ongoing program to image the radio reference frame sources on a regular basis, to monitor them for variability and structural change. It observes simultaneously at 2.3 GHz and 8.4 GHz.[1]

The Radio Reference Frame Image Database is a database of about 6700 images of over 700 sources compiled from geodetic and astrometric VLBI experiments. These observations began in 1994 and are ongoing, with the latest one at the time of writing being the January 2009 epoch. Sources in the RRFID were chosen solely for their suitability for astrometry and geodesy. The observation epochs are not equally spaced between 1994 and 1998. After 1998, the Research and Development VLBI (RDV) series of experiments (see Table 3.1) use a spacing of 2 months but they do not observe all the RRFID sources in all epochs. More recently, the RRFID has begun to include observations at 23 and 43 GHz.

3.1.2 The RRFID Kinematic Survey

Piner et al. (2007) discuss jet kinematics in a subset of the RRFID sources, concentrating on the 8.4 GHz observations. This thesis looks at the 2.3 GHz observations of the southern sources in Piner's kinematic survey,

[1] The web site for the RRFID is located at http://rorf.usno.navy.mil/RRFID.

hereafter known as the Southern Sample.

The Piner et al. survey is made up of the RRFID sources that have been observed at three or more epochs from July 1994 to December 1998. This yielded a sample of 87 sources with a total of 966 8-GHz images and an average of 11 epochs for each source. The best observed source had a total of 19 epochs. The RRFID Kinematic survey is one of the first large sample Kinematics survey to study jet kinematics with a smaller average epoch spacing than previous VLBI surveys and so is potentially very important (Piner et al., 2007).

3.1.3 The Southern Sample

This sample of 31 sources was chosen from the RRFID Kinematic Survey done at 8.4 GHz, the only qualification being that the sources were southern sources. They cover a declination range of 0° to about -50°. For meerKAT, and for the purposes of this thesis, 2.3 GHz observations of southern hemisphere sources were selected giving 31 southern sources with an average of about 20 epochs between July 1994 and January 2008, with the best observed source having been observed at 32 epochs. In total, about 620 epochs of data were worked on. Epochs later than 1998 are not used in the original work by Piner et al. (2007). These were included to see the long term variation of the sources and also to get the latest behaviour of these sources. As in the RRFID Kinematic Survey, the epoch spacing is not regular except after 1998 where the RDV series of experiments were done every 2 months. This sample shall be known as the Southern Sample and the sources are listed in table 3.1.

3.2 Observations

Observations were made using the ten telescopes of the VLBA, Hartebeesthoek (South Africa) when it was available and up to 10 other antennas across the globe. Inclusion of the global array greatly improves the u-v coverage on long baselines and higher declinations. At lower declinations, the beam becomes greatly elongated in the north-south direction due to poor u-v coverage. Hartebeesthoek greatly improves u-v coverage for sources far south which make up the sample for this thesis. Unfortunately, Hartebeesthoek was not available for all epochs and not all VLBA antennas can see far south, leaving huge gaps in the u-v coverage of most southern sources. A perfect image can only be made if all points in the u-v plane are measured. This is never the case and large holes in the u-v coverage make it more difficult to make correct and unique images.

About 100 sources were observed in each observing run, each running for 24 hours with an average on-source time of 15 minutes. The on-source time is not continuous, but divided into scans of between 1 and several minutes spaced in time to give optimal u-v coverage.

Eight IF's were recorded simultaneously, each 8 MHz wide, with 4 at 2.3 GHz and 4 at 8.4 GHz for a total of 32 MHz in each frequency band. Observations were made in a dualfrequency bandwidth synthesis mode to facilitate delay measurements for astrometry. Observations of this mode also allow imaging at both frequency bands.

Table 3.2 shows the 32 experiments included in this thesis. The earlier experiments (1994-1996) used only the 10 antennas of the VLBA and are more randomly spaced in time. The later experiments correspond with the beginning of the RDV experiments, starting on January 30 1997 and have been continued to date, with

Table 3.1: The Southern 2.3 GHz Sample.

B1950 Source Name	Other Name	Epochs	Optical Identification	z
0003-006		24	BL Lac	0.35
0104-048		28	BL Lac	0.58
0238-084	NGC1052	16	Galaxy	0.005
0336-019	CTA26	25	Quasar	0.85
0402-362		17	Quasar	1.42
0454-234		27	Quasar	1.00
0458-020		26	Quasar	2.29
0727-115		32	Quasar	1.59
0919-260		17	Quasar	2.30
0920-397		16	Quasar	0.59
1034-293		27	Quasar	0.31
1124-186		26	Quasar	1.05
1144-379		23	Quasar	1.05
1145-071		16	Quasar	1.34
1253-055	3C279	3	Quasar	0.54
1255-316		14	Quasar	1.92
1313-333		17	Quasar	1.21
1334-127		25	Quasar	0.54
1351-018		13	Quasar	3.71
1424-418		18	Quasar	1.52
1451-375		14	Quasar	0.31
1514-241		16	BL Lac	0.05
1622-253		24	Quasar	0.79
1741-038		28	Quasar	1.05
1908-201		23	Quasar	1.12
1921-293		23	Quasar	0.35
1954-388		21	Quasar	0.63
1958-179		9	Quasar	0.65
2052-474		10	Quasar	1.49
2243-123		22	Quasar	0.63
2255-282		20	Quasar	0.93

Optical identifications from the catalogue of Véron-Cetty & Véron (2003)

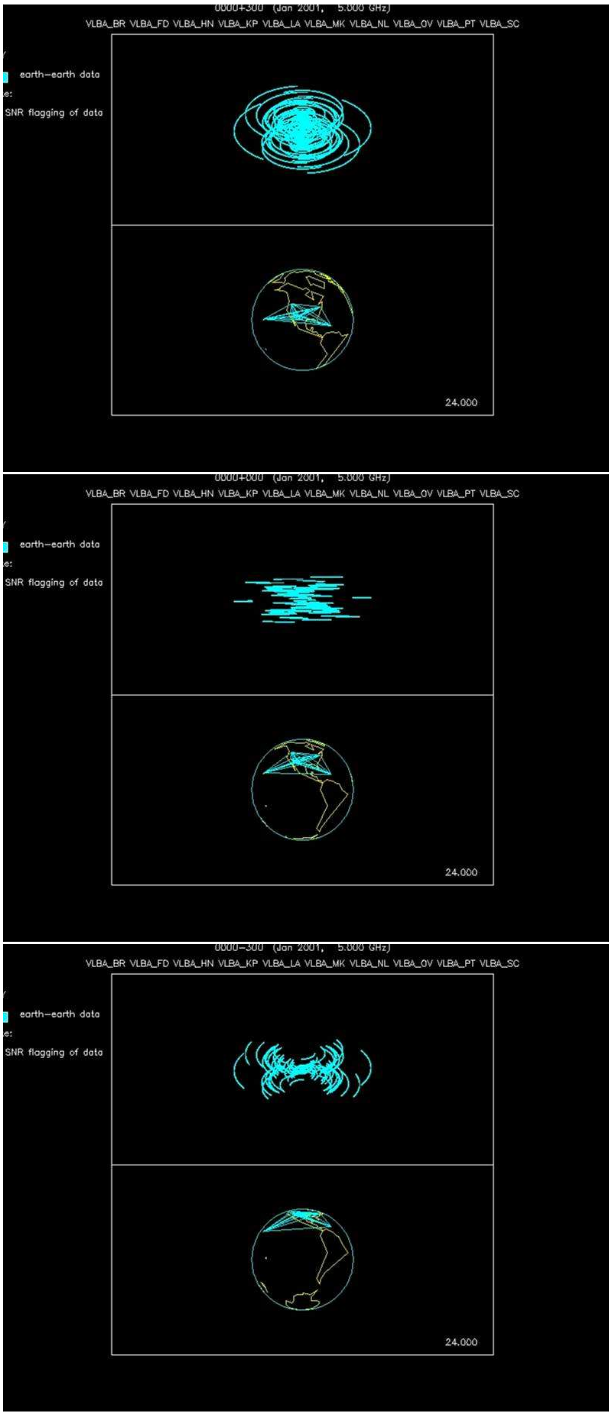

Figure 3.1: Example u-v coverages obtained using the VLBA only at three different source declinations: from the top, 30°, 0° and $-30°$. This represents the minimal u-v coverage for our observations since all of our observing runs used the VLBA, but many also used additional antennas, resulting in better u-v coverage than illustrated.

Table 3.2: Details of each observing epoch.

Epoch	Code	Antennas
1994JUL08	BR005	VLBA
1995APR12	BR025	VLBA
1995JUL24	RDGE02	VLBA
1995OCT02	RDGE03	VLBA
1995OCT12	BF012	VLBA
1996APR23	BE010a	VLBA
1997JAN10	BF025a	VLBA
1997JAN11	BF025B	VLBA
1997JAN30	RDV01	VLBA+GcGnKkMcOnWf
1997MAR31	RDV02	VLBA+GcGnKkMcOnWf
1997MAY19	RDV03	VLBA+GcGnKkMcOnWf
1997JUL24	RDV04	VLBA+GcGnKkMcOnWf
1997SEP08	RDV05	VLBA+GcGnKkOnWf
1997DEC17	RDV06	VLBA+GcGnKkMcOnWf
1998FEB09	RDV07	VLBA+GcGnKkMcNyOnWf
1998APR15	RDV08	VLBA+GcGnKkMcNyOnWf
1998JUN24	RDV09	VLBA+GcGnKkMcNyOnWf
1998AUG10	RDV10	VLBA+GcGnKkMcNyOn
1998DEC21	RDV12	VLBA+GcGnKkMcNyWf
1999JUN21	RDV16	VLBA+GcHhKkMcNyOnTsWfWz
2000OCT23	RDV23	VLBA+GcGgHhKkMaMcNyTsWfWz
2001MAY09	RDV28	VLBA+GcHhKkMcNyOnTsWfWz
2002JAN16	RDV31	VLBA+GcGgKkMcNyOnTsWfWz
2004JUL14	RDV45	VLBA+GcGgKkMcOnTsWfWz
2006JUL11	RDV57	VLBA+ApHoMcNyWfWz
2006SEP13	RDV59	VLBA+HoMcNySvTcWfWz
2007JAN24	RDV61	VLBA+KbNySvTcWfWz
2007JUN26	RDV63	VLBA+HhKbKkNyWz
2007JUL10	RDV64	VLBA+HhKbOnWz
2007AUG01	RDV65	VLBA+HhKbNyTcWfWz
2007DEC05	RDV66	VLBA+HhKbNyOnSvTsWzZc
2008JAN23	RDV67	VLBA+KbKkNyTsWfWzZc

Table 3.3: Details of the antennas used at each observing epoch.

CODE	NAME	LOCATION	DIAMETER (m)
Ap	ALGONQUIN	Algonquin Park, Canada	46
Gc	GILCREEK	Fairbanks,AK USA	29.5
Gg	GGAO MV3	Greenbelt, MD USA	5
Gn	NRAO20	Greenbank, WV USA	20
Hh	HARTEBEESTHOEK	Johannesburg, South Africa	26
Ho	HOBART	Tasmania, Australia	26
Kk	KOKEE	Kokee Park, HI USA	20
Ma	MATERA	Matera, Italy	20
Mc	MEDICINA	Medicina, Italy	32
Ny	NYALES20	Ny Alesund, Norway	20
On	ONSALA60	Onsala, Sweden	20
Sv	SVETLOE	Lenigrad, Russia	32
Tc	TIGO	Concepcion, Chile	6
Wf	WESTFORD	Westford, MA USA	18
Ts	TSUKUB32	Tsukuba, Japan	34
Wz	WETTZELL	Wettzell, Germany	20
Zc	ZELENCHUKSKAYA	Karachaevo-Cherkessia, Russia	32

observations roughly every 2 months. The best observed source was observed at all 32 epochs with an average of 20 epochs per source.

3.3 Data Reduction

3.3.1 Calibrating with AIPS

The data only becomes available to the astronomer after it has been correlated. The data from all the antennas were correlated with the VLBA correlator at the Array Operations Center in Socorro, New Mexico. The correlator outputs AIPS readable UVFITS files. Before the data can be used, it must be calibrated and processed.

We calibrated the observed data using NRAO's Astronomical Imaging Processing System (AIPS). With Roopesh Ojha of the USNO, I calibrated the January 2008 with 100 sources at both frequencies, 2.3 and 8.4 GHz. The rest of the data was calibrated by the USNO which maintains the RRFID.

Several AIPS 'tasks' and 'verbs' are used to manipulate the data. When data is first read into AIPS, several tables are created and filled with information describing the data. These tables contain information such as antenna names, geometric data, system temperature and other useful details of the observations.

Calibration and editing tasks in AIPS create more tables which include tables with bandpass information, flagging information, baseline or correlator information and gain solution from the calibration routines. These tables can later be applied to the data as the AIPS tasks do not alter the data directly. When one is satisfied with the calibration and editing, the AIPS task SPLIT is then used to apply the different tables to the data. The task also writes u-v data for individual sources which can then be used for imaging and modelfitting.

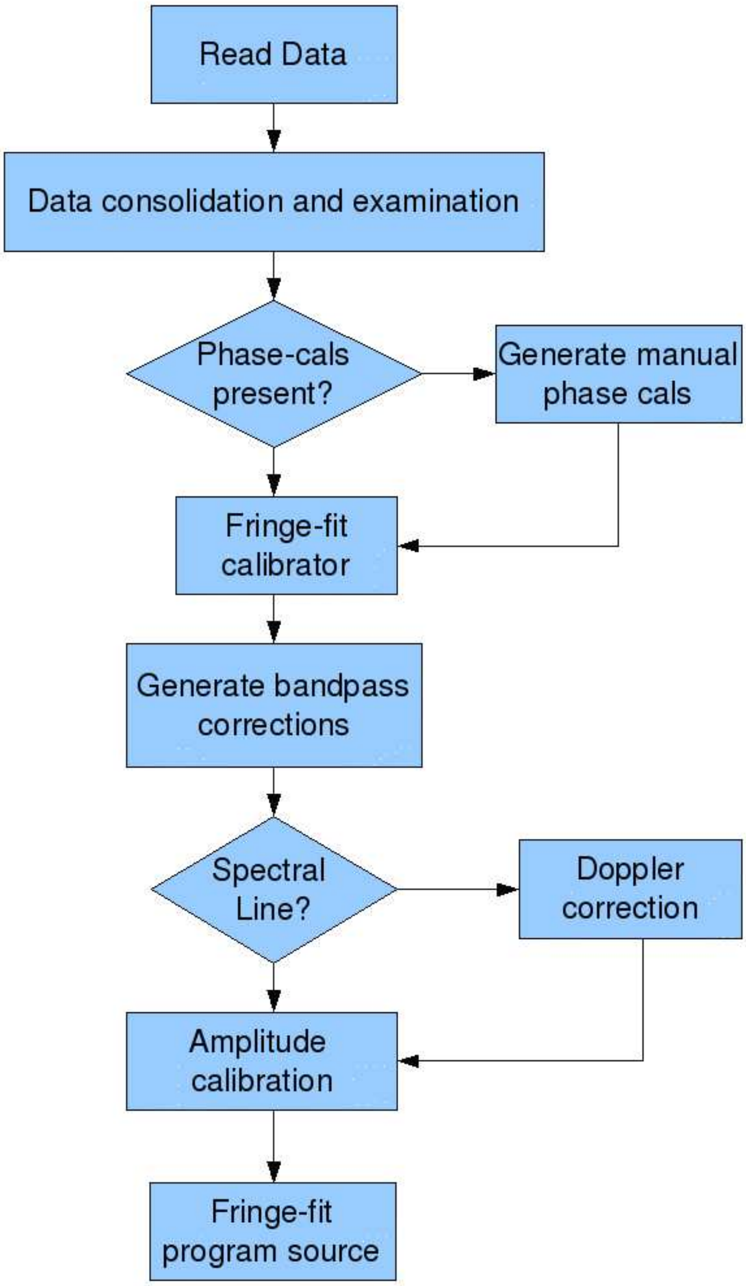

Figure 3.2: Block diagram showing data calibration in AIPS. Not all of these steps were necessary for our data. Figure adapted from Very Long Baseline Interferometry and the VLBA. (Diamond, 1995).

Data Examination and Consolidation

The multi-source data in FITS format, is loaded into AIPS. After reading the data into AIPS, the data quality was checked, particularly for corrupted data in the first record of the scans and for dead antennas. We also checked for RF interference, erratic amplitudes and missing antennas. AIPS provides several ways to examine and display data. LISTR, PRTAN, PRTUV were used to view the observation time per source, the list of antennas and the raw visibilities. After examining the data and making necessary changes (mostly removing obviously corrupt data), one can start the calibration process. Figure 3.2 shows the general steps carried out when calibrating VLBI data. Not all of these steps were necessary for our data and the procedures used are explained below.

Amplitude Calibration

The system temperature (T_{sys}) tables and gain curves that are generated during observations are used to correct the amplitudes. Because we had non-VLBA antennas, calibration files for these antennas had to be manually edited and formatted to add the information supplied by the different antennas and to bring them to AIPS format. This information is then read into the system temperature and gain curves tables in AIPS using ANTAB.

To do the actual amplitude calibration, the AIPS task APCAL is used. This reads data and generates the amplitude gain curves. These curves are applied to the data and produces the visibility data in units of Jansky.

Fringe-fitting the Program Sources

Fringe fitting is the process of calculating the residual delay as well as their time derivates (delay rates). It takes out the time variation in the data. The task FRING calculates the rates and these are then applied to the data. After fringe fitting, all phase differences and slopes are removed and the phases line-up between the IFs.

Additonal Amplitude Calibration

Amplitude calibration was improved by using observations of sources whose core flux density is known to be $\geq 90\%$ of the total flux density. A single amplitude gain correction factor is derived for each antenna based on fitting a Gaussian model to the core component. This is after applying initial amplitude calibration based on the system temperature tables and gain curves mentioned above. Gain correction factors are then calculated based on the difference between the observed and the model visibilities. The amplitude gain correction factors are then applied to the target sources. This is a non-standard procedure and it results in improvement of about 20% in the amplitude calibration.

3.3.2 Imaging

Data imaging and modelfitting were done using the Caltech Difference Mapping program, Difmap[2]. Difmap is an interactive program which directly reads the standard UV FITS files.

[2]Difmap was written by Martin Sherpherd and is part of the Caltech VLBI Software Package

Difmap can be used for calibrating, editing, imaging and modelfitting but for this thesis, Difmap was used for imaging and modelfitting. Whereas large packages like AIPS split tasks into separate programs, in Difmap these tasks are functions within one single program. This simplifies the user interface. Difmap also has a scripting facility which is different from most packages. It maintains a log file which records command lines verbatim and messages as comments and so the log file can be used as a script. Difmap is easy to install and manage and is highly interactive, making it ideal when it comes to data editing, imaging and modelfitting.

Interferometric arrays do not form images of the radio sky directly. An image is formed by:

- Fourier Inversion - Formation of an initial dirty image from the visibility samples collected by an interferometric array.
- Deconvolution - Correction of the effect of the Fourier plane sampling deficiencies on the dirty image.
- Self-calibration - Correction of the effects of calibration errors on the deconvolved image.

RADPLT produces a plot of amplitude against u-v radius. Editing data in this mode is not ideal as it is baseline based whereas systematic errors are mostly antenna-based. UVPLOT produces a plot of u-v coverage and TPLOT displays every time interval for which there exists data for each telescope. The display which is produced can be manipulated in a number of ways.

The imaging begins after the data has been inspected and bad points edited out. First, the image size and cell size should be set. The image size is at least twice the maximum source size since Difmap can only deconvolve the inner quarter of the image. An image size of 1024 pixels was used for most of this data.

The cell size used for all the images in the 2.3 GHz data used for this thesis was 0.3 milliarcseconds, less than a fifth of the beam size. The sources were first imaged in Difmap automatic mode. Generally, this mode fails for about one third of the sources which had structure that is complex or too extended for the automatic script to handle. These have to be redone by hand in interactive mode. For the southern sources in this sample, almost all had to be imaged by hand due to the poor u-v coverage.

Both natural and uniform weighting were used. Uniform weighting gives more weight to the longer baselines and less weight to the short baselines, this provides a higher resolution but degrades the point source sensitivity. After imaging, the map can be viewed using the command MAPPLOT. This command generates a dirty map of the source which is the image of the source convolved with the beam of the interferometer. To begin with, I used a small CLEAN window of 0.7 times the beam width around the brightness peak in the dirty image for most sources.

To start the deconvolution process, one must choose the number of iterations and also define the loop gain. Once entered, these values become the default values. The CLEAN algorithm does the actual deconvolution of the dirty map. A loop gain of 5% was used.

When a model of the source is subtracted from a dirty map, what remains is the residual map and the point in Difmap is to progressively build a model of the source by cleaning from the residual map. MAPPLOT is used to view the residual map. After CLEANing, the phases are self calibrated using SELFCAL. Phase selfcal calculates the non-closure phases of the source for a minimum of 3 telescopes.

Again, one picks the brightest component with PEAKWIN and runs CLEAN and SELFCAL. Difmap uses a chi-squared fit for the model and so one must keep track of the sigma level. MAPPLOT, PEAKWIN, CLEAN and SELFCAL are iterated until sigma is no longer decreasing and the CLEANed flux is no longer increasing. To view the CLEAN map, one types MAPPLOT CLN. One can check whether the model fits the data by typing RADPLOT, which shows a plot of visibility amplitude against u-v radius. The model will be superimposed in red on the data. If the model does not fit well with the data at short baselines, one should switch to natural weighting which gives more weight to the shorter baselines and therefore more sensitivity but degrades the resolution. CLEAN and self calibration must be performed again until sigma is no longer decreasing and the flux in the clean model is no longer increasing. When this is done, one can start the amplitude self calibration.

Amplitude calibration was done using GSCALE which computes a single amplitude correction factor for each antenna for each IF and GSCALE TRUE lets the telescope parameters float freely and this was used for the data. MAPPLOT and RADPLOT were used to see the effect of the different commands on the model. On average, GSCALE improved the model on the short baselines. SELFCAL TRUE, TRUE, 120 perform amplitude and phase self calibration with a solution interval of 2hours. It is best to start with long solution interval and then shorten the solution interval as the model improves. Again CLEAN and SELFCAL are looped until sigma is constant. After this, the solution interval can be changed. All the while, MAPPLOT and RADPLOT are being used to check how closely the model resembles the data. When one has done enough iterations of SELFCAL and CLEAN and is satisfied with the model of the data and the image produced, the image can be saved by typing SAVE FILENAME. Difmap will then produce 5 files, one of which is the parameter file which is a Difmap environment file and contains details of the image. It is this file that is loaded into Difmap when one wants to do modelfitting.

3.3.3 Modelfitting

Modelfitting is used to parameterize characteristics of the source, in particular, to determine component locations and brightnesses. These include the flux density of individual components and their distance from the core. Like imaging, it is an iterative procedure but in modelfitting one has to give the initial guess for the parameter vector. I did the modelfitting image plane by fitting elliptical Gaussians to the image. The model is fit by least-squares, that is by minimizing the χ^2 residual between the image and the sum of the model components at each pixel location.

When modelfitting in Difmap, one loads the parameter file that is produced after imaging. It contains the image information when the image was saved. After loading the edited data into Difmap the model is deleted using the command CLRMOD.

- The established model is subtracted from the visibility data and is incrementally built up from the source model.
- The tentative model represents an attempt to model the difference between the data and the established model.

Elliptical Gaussian components were used only to represent the core component or a very bright jet component if the residuals remaining from a circular Gaussian model were too large and made it difficult to continue modelfitting using the residual map. Otherwise, circular Gaussian models were mostly used.

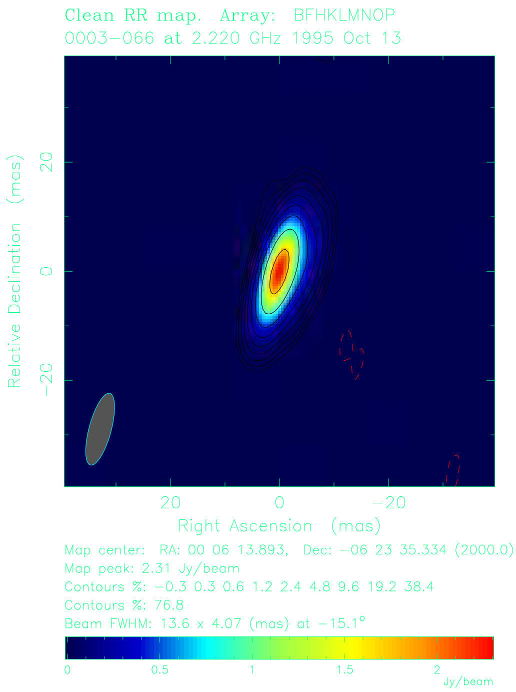

Figure 3.3: Image of 0003-066. The image was made from data at the frequency and date indicated at the top, in right circular polarization (IEEE convention). The peak brightness and contour levels, given in % of the peak are indicated below. The FWHM beamsize is also given below and indicated graphically in the lower left of the image.

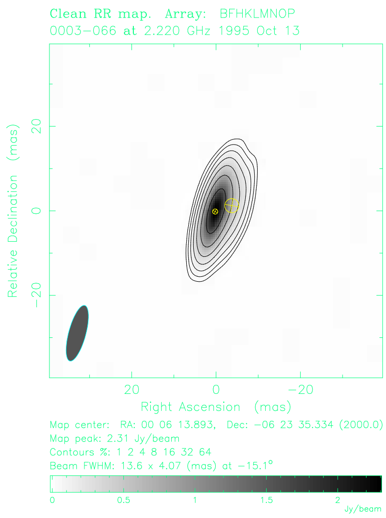

Figure 3.4: Image of 0003-066, at frequency and observing date indicated. The peak brightness, contour levels, and FWHM size of the restoring beam are given below. The yellow circles show the two model components fitted by Difmap, with the size of the circle showing the FWHM size of an elliptical Gaussian fitted to the image plane data.

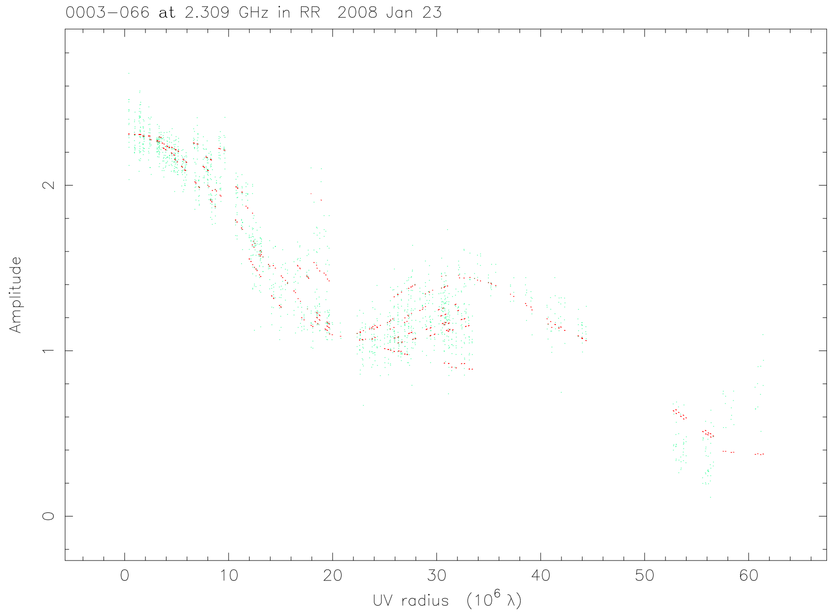

Figure 3.5: A plot of visibility amplitude against u-v radius for 0003-066 showing the modelfit to the data. The modelfit is in red and although it is satisfactory, it is not as good as the fit produced by the hybrid images shown below.

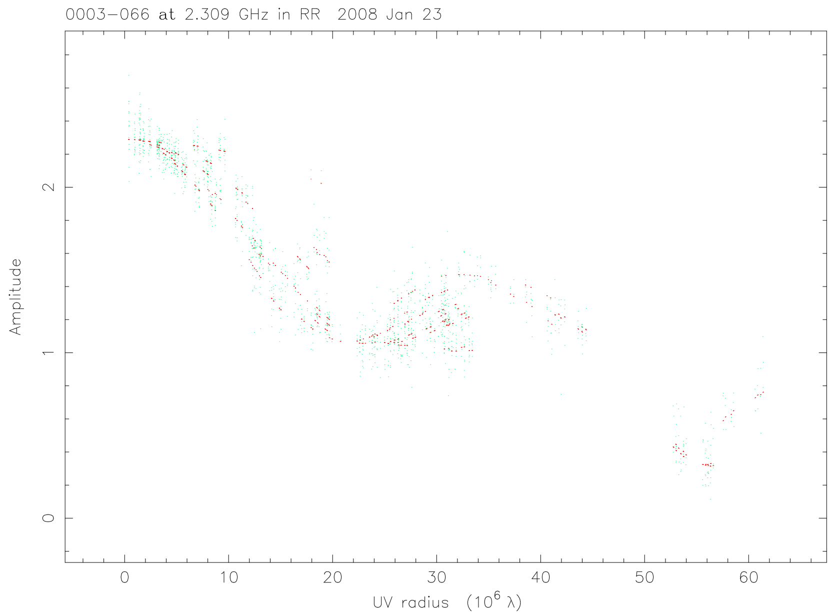

Figure 3.6: A plot of visibility amplitude against u-v radius for 0003-066. The model is superimposed in red on the data and shows a much better fit to the image data which have many CLEAN components compared to the modelfits.

The modelfits generally describe the visibility data well but these models may not be unique because of incomplete sampling in the u-v plane.

Chapter 4

Results

4.1 Calibrator Classification

4.1.1 Classification Scheme

The results are presented in this chapter. We use a combination of the variation of core flux density with time, the ratio of model core flux density to total flux density (core compactness) and the radial extent within which 95% of the flux density is contained (weighted and unweighted), to evaluate the usefulness of these sources at 2.3 GHz. These measures were each given a weight and the total of these gives a figure which determines which class a source falls into.

The image was given a maximum weight of 10% and this was based on a subjective evaluation of the image at one epoch. The core flux variation has a weight of 10% since most of the sources will be unresolved by meerKAT, the compactness 40%, the weighted and unweighted radial extent 20% each.

The compactness weight was determined using values of the actual compactness by factors shown in Table 4.1.

Table 4.1: Source Compactness weighting distribution.

Compactness(%)	Weight(%)
0-60	0
60-70	10
70-80	20
80-90	30
90-100	40

The weighted and unweighted radial extent were weighted using the variability index by factors shown in Table 4.2.

Table 4.2: Distribution of weights for the weighted and unweighted radial extent.

Index	Weighting(%)
0-0.2	20
0.20-0.40	16
0.40-0.60	8
0.60-0.80	4
0.80 and above	2

The core flux density was weighted using the variability index by the factors shown in Table 4.3.

Table 4.3: Distribution of weights for the Core Flux Density.

Core Flux Density Variability Index	Weighting (%)
0-0.20	10
0.20-0.40	8
0.40-0.60	6
0.60-0.80	4
0.80 and above	2

The class A to D the source falls into depends on its overall score summed up from the weighting schemes discussed above. No single measure is adequate to pass judgement on the sources but we are developing a way to assign sources into four calibrator categories, A through D based on their overall properties (see below).

A - Source should score a total of 80% to 100%. (Excellent calibrator).

B - A total of 60% to 80% (Very good calibrator).

C - Source should score a total of between 40% to 60% (Good calibrator)

D - Any source below 40%.(Unsuitable as calibrator, use with caution).

One image is shown for each source to give an idea of the source structure. I have reproduced these images from the USNO RRFID data. The peak brightness, contour levels, and FWHM size of the restoring beam are given in the image. I made the core flux density plots from the modelfits I performed on the data. All optical identifications are from the Véron-Cetty & Véron (2003) Catalogue unless otherwise stated and all modelfits are shown in Appendix A.

4.1.2 Core Flux Density

A good calibrator should be relatively bright at the frequency of observation to be easily detectable. It also has to be stable with minimal flux density variation over time. I determined the core flux density, S_{core} for each source over all epochs using the Gaussian component I fit to the core of each source. This is represented as a graph of flux density vs time for each source for all epochs. From the core flux density, I computed the mean core flux density ($\bar{S}$) averaged over all epochs in which the source was observed. The extent to which the core flux density varies over time can be characterised by the core flux density variability index ($\sigma_{core}/\bar{S}$) where σ_{core} is the core flux density standard deviation. A value of 0.0 indicates no variation over time.

4.1.3 Source Compactness

The compactness (C), is defined as the ratio of the Model Core Flux Density to the Source Flux Density, (S_{core}/S_{total}), as determined by the Gaussian model fits to the visibility data. It provides an indication of how point-like a source is and also provides a way to track source structure changes from epoch to epoch. The compactness is shown, over time for each source in form of a graph of compactness vs time. The compactness was determined by running a program which calculates core flux density over the total flux density by taking the sum of CLEAN components within one synthesised beam and dividing by the sum of all components. The average compactness, $\bar{C}$, was computed for each source over all epochs. As with the core flux density index, I also computed the source compactness variability index ($\sigma_C/\bar{C}$) where σ_C is the compactness standard deviation. A value of 0.0 for the source compactness index indicates no variation over time.

4.1.4 Unweighted Radial Extent

This is the radial extent within which 95% of the source flux density is contained. This provides a measure of how extended a source is. Plots of radial extent vs time were made for both the weighted (see below) and unweighted radial extent. The mean ($\bar{R}_{UW}$) and standard deviation were also calculated as was the variability index ($\sigma_{R_{UW}}/\bar{R}_{UW}$) where $\sigma_{R_{UW}}$ is the unweighted radial extent standard deviation.

4.1.5 Weighted Radial Extent

This is the flux density-weighted radial extent and gives another measure of core- dominance (Ojha et al., 2004). It can be defined as:

$$R_W = \frac{\sum_i S_i r_i}{\sum_i S_i} \tag{4.1}$$

where r_i is the radius at which the ith CLEAN component has flux density S_i.

The mean ($\bar{R}_W$) and standard deviation were also calculated as was the variability index ($\sigma_{R_W}/\bar{R}_W$) where σ_{R_W} is the weighted radial extent standard deviation.

4.2 Results

4.2.1 0003-066

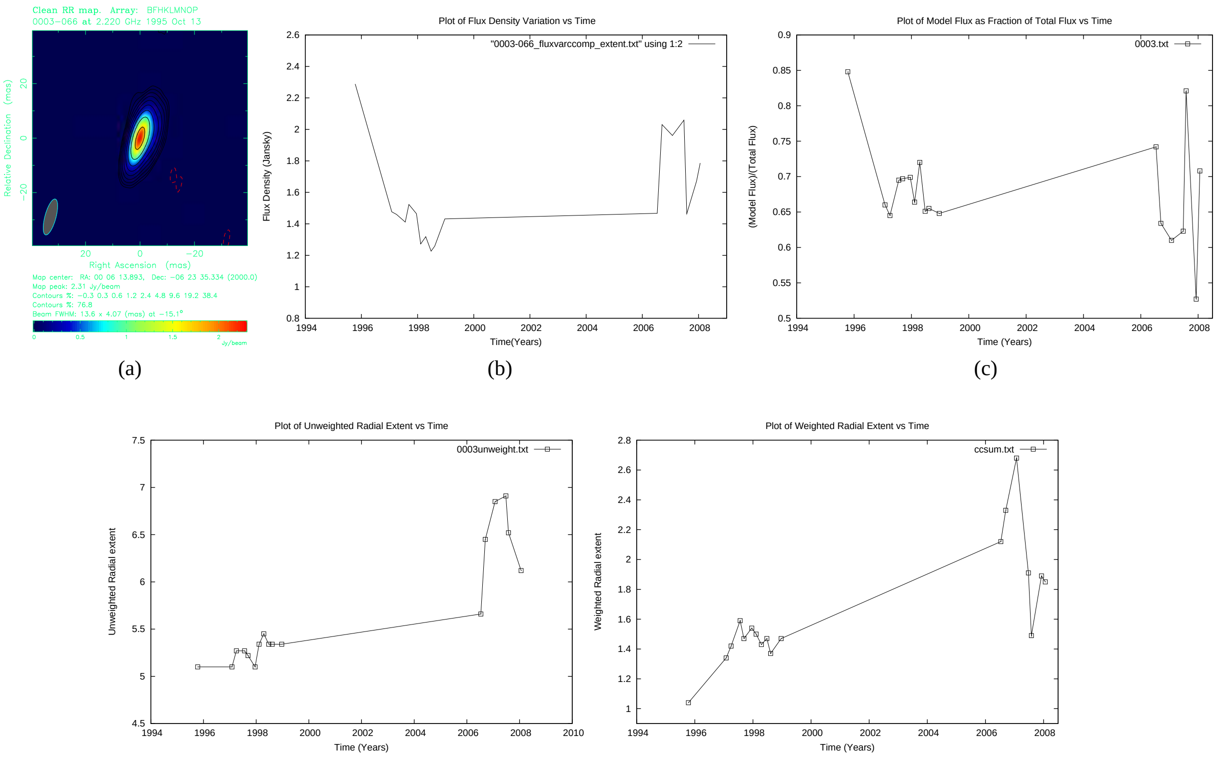

(a) (b) (c)

(d) (e)

Figure 4.1: (a):Source image:0003-066. (b):Plot of Flux Density Variation. (c):Source Compactness. (d): Unweighted radial extent. (e): Weighted radial extent

This source has been optically identified as a BL Lac object at a redshift of 0.35.

The source is well fitted, for all epochs, by two Gaussian components, the core and a single component. At its brightest (fig (b)), around 1995, the source is very compact and has about 85% of the total flux density contained in the core. The source flux density falls between 1995 and June 1998, the compactness also falls from 85% to 65%. This could be due to ejection of a component. On average, the source is not very compact with a mean compactness of 68%. The radial extent within which 95% of the flux density is contained also increases fig(d) as does the weighted radial extent fig(e).

The flux density standard deviation is 0.31 Jy from a mean of 1.59 Jy, giving a flux density index of 0.20. The mean of the compactness is 68% while standard deviation is 7% and the index of 0.11. The unweighted radial extent standard deviation is 2.22 mas from a mean of 6.17 mas giving an index of 0.36. The weighted radial extent standard deviation is 0.40 mas giving an index of 0.24. The mean radial extent is 1.66 mas.

This has been classified a **class C source**.

4.2.2 0104-408

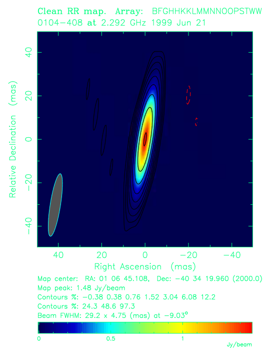

(a)

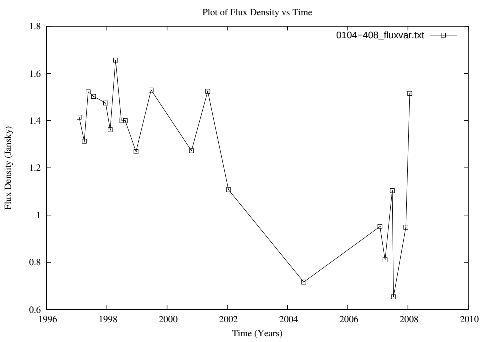

(b)

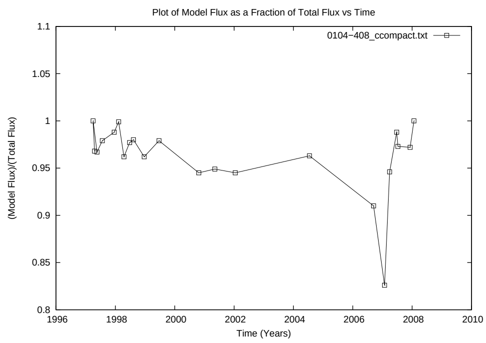

(c)

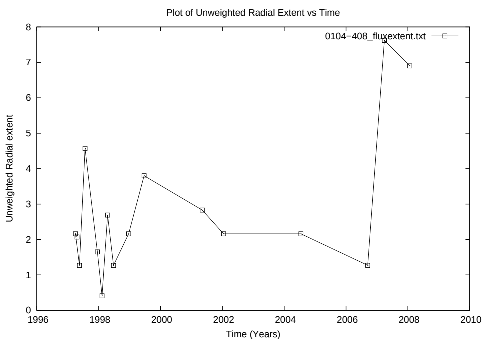

(d)

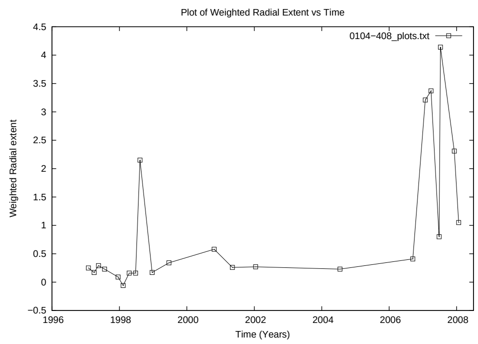

(e)

Figure 4.2: (a):Source image:0104-408. (b):Plot of Flux Density Variation. (c):Source Compactness. (d): Unweighted radial extent. (e): Weighted radial extent

This is a 19th magnitude BL Lac object at a redshift of 0.58. The core flux density varies between about 1.3 Jy and 1.7 Jy between 1995 and 2001 but falls to 1.1 Jy in 2002. Modelfits show the presence of a single additional component in 2002. Modelfits for later epochs show a single but much weaker component, falling to as low as 0.7 Jy in 2004. The flux density in the core goes up for later epochs, reaching 1.5 Jy in early 2008, fig(b). The compactness of the source on the other hand, is stable between 95% and 100% even when the core flux density falls, except in early 2007 where it reaches a low of 83%. After this, the compactness returns to between 95% and 100%. This source is one of the benchmark sources in the establishment of a high precision radio/optical celestial reference frames (Costa & Loyola, 1992). Shen et al. (1997) fit a single Gaussian component with a flux density of 2.6 Jy to this source, observed in November 1992. The mean core flux density is 1.26 Jy. The flux density standard deviation is 0.29 Jy giving a flux density variability index of 0.23. The compactness mean is 96.26%, standard deviation is 4% giving a variability index of 0.04. The unweighted radial extent standard deviation is 17.13 mas giving a variability index of 2.18. The mean is 7.84 mas. The mean of the weighted radial extent is 0.94 mas, the standard deviation is 1.24 mas giving a variability index of 1.33. This source has been classified as a **class C source**.

4.2.3 0238-084

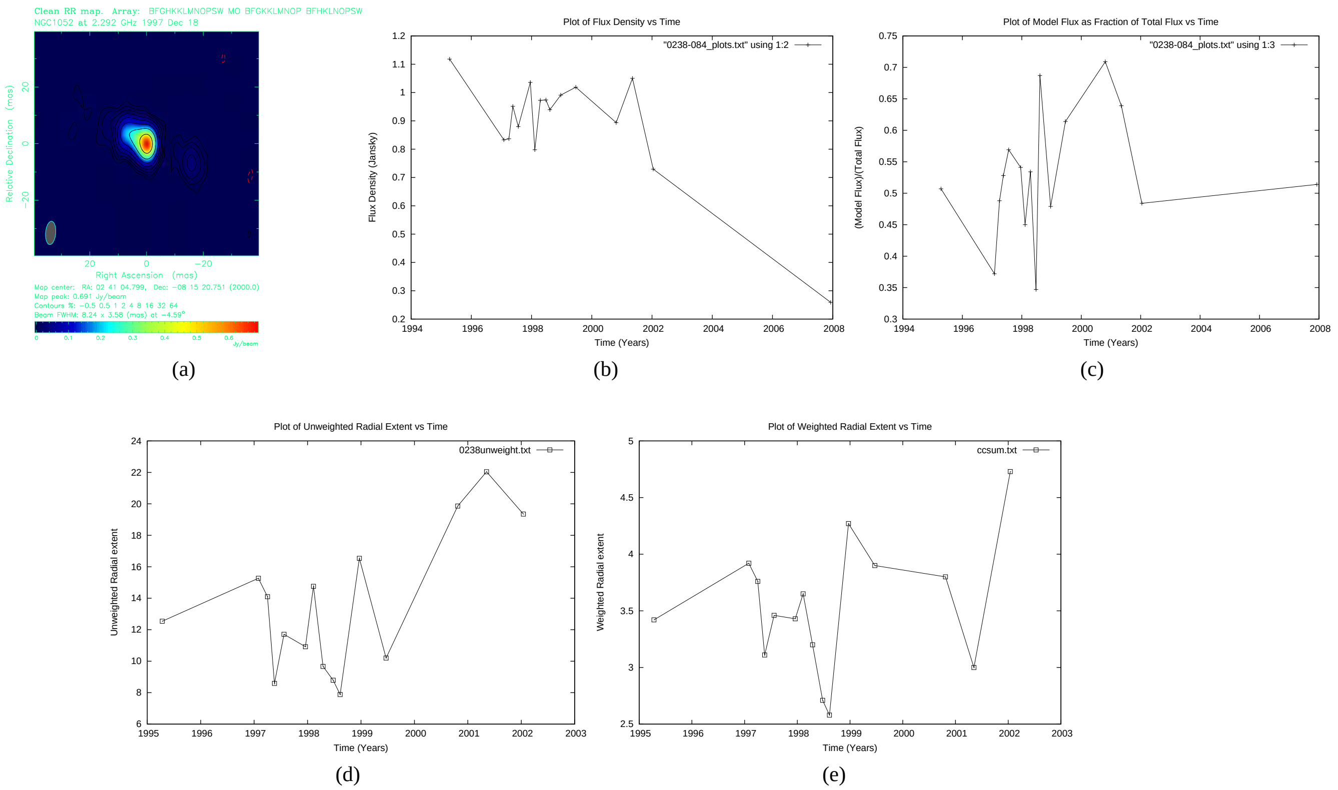

Figure 4.3: (a):Source image:0238-084. (b):Plot of Flux Density Variation. (c):Source Compactness. (d): Unweighted radial extent. (e): Weighted radial extent

Also known as NGC1052, 0238-084 is a nearby LINER galaxy at a redshift of 0.005.

Kadler et al. (2004b) used the VLBA to resolve the core into twin jets at four different frequencies. This work at 2.3 GHz also shows the source to be a double jet source. The twin radio jets reaches to kilo-parsec scales but is still embodied within the optical galaxy (Kadler et al., 2004a). The flux density in the core varies between 1.1 Jy and 0.7 Jy from 1995 to 2002. Kadler et al. (2004b) using MERLIN at 1.4 GHz in November 1995 measure the core to have a flux density of 1.01 Jy. After 2002, the flux density falls to a low of 0.26 Jy in December 2007.

The flux density standard deviation is 0.20 mas giving a flux density variability index of 0.22. The compactness standard deviation is 10% giving a variability index of 0.19. The unweighted radial extent standard deviation is 16.13 giving a variability index of 0.93. The weighted radial extent standard deviation is 0.10 mas giving a variability index of 0.27. The compactness of the core varies significantly between 37% and 70% with a mean of 52%. Both the weighted and unweighted radial extents also vary quite significantly, and this source is a double sided source, making it unsuitable for use as a calibrator.

This is a **class D source**.

4.2.4 0336-019

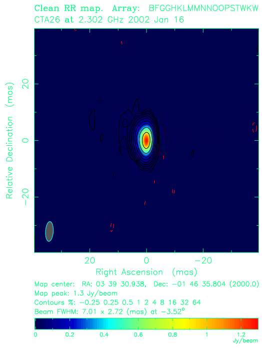

(a)

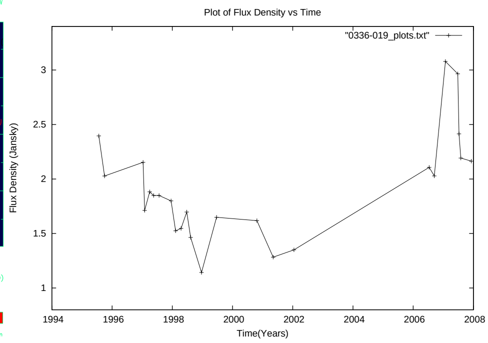

(b)

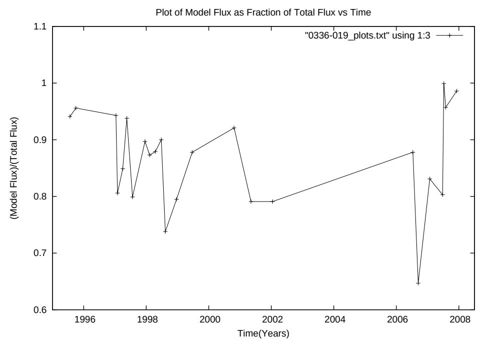

(c)

(d)

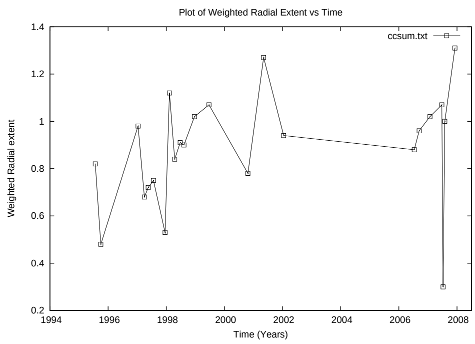

(e)

Figure 4.4: (a):Source image:0336-019. (b):Plot of Flux Density Variation. (c):Source Compactness. (d): Unweighted radial extent. (e): Weighted radial extent

0336-019 is a quasar at a redshift of 0.85. This source has been fitted with up to 3 other components after the core component. The image shows the source to be extended in the north-east direction, fig(a). The core flux density is 2.40 Jy in mid-1995 and gradually falls to 1.14 Jy in December 1998. The flux density then increases slightly and the falls again. It then increases gradually to 3.1 Jy in early 2007 and then falls to 2.16 Jy in early 2008, fig(b). The source compactness on the other hand does not vary as much as the core flux density, varying between 65% and 100%, fig(c). The unweighted radial extent within which 95% of the total flux density is contained also varies between 1.8 mas and 3.78 mas, fig(d). The weighted radial extent also varies, but in a different range, 0.3 mas and 1.3 mas, fig(e) .

The flux density standard deviation is 0.48 Jy giving a flux density variability index of 0.25. The compactness standard deviation is 8% giving a variability index of 0.10. The unweighted radial extent standard deviation is 2.32 mas giving a variability index of 0.76. The weighted radial extent standard deviation is 0.64 mas giving a variability index of 0.64. While 87% of the flux density is in the core, a flux density index of 0.25 shows a 25% variation in the flux density. The radial extent also varies to a large extent.

This is a **class C source**.

4.2.5 0402-362

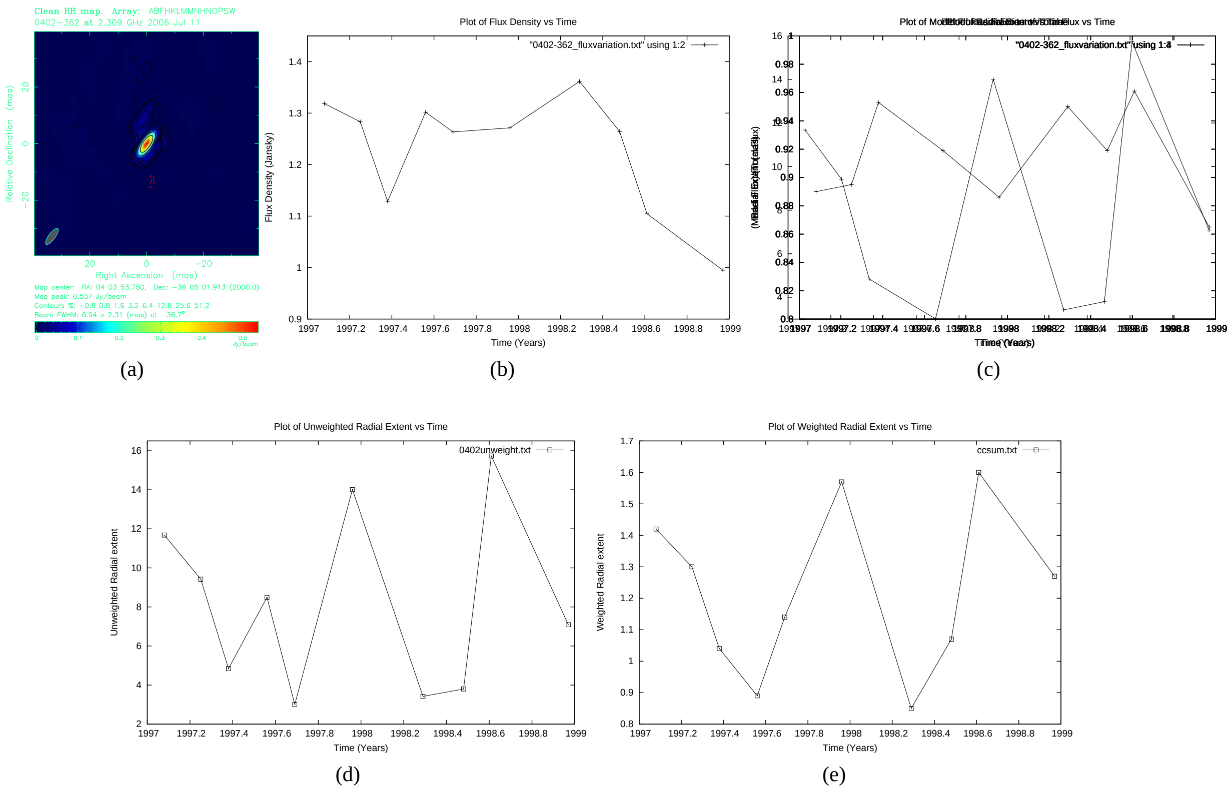

Figure 4.5: (a):Source image:0402-362. (b):Plot of Flux Density Variation. (c):Source Compactness. (d): Unweighted radial extent. (e): Weighted radial extent

This source is at a redshift of 1.42 and has been identified as a quasar. Modelfits show the presence of 2 components other than the core for most of the epochs. The source image suggests the presence of components on both sides of the core, fig(a). The flux density varies between 1 Jy and 1.4 Jy over 2 years, fig(b). The compactness is between 87% and 96%, meaning that this source is quite compact, fig(c). The unweighted radial extent however varies over a wide range, 3 to 16 mas fig(d) . The weighted radial extent varies between 0.85 to 1.60 mas .

The flux density standard deviation is 0.11 Jy from a mean of 1.23 Jy giving a flux density variability index of 0.09. The compactness standard deviation is 0.03% from a mean of 91.54% giving a variability index of 0.03. The unweighted radial extent standard deviation is 4.54 mas giving a variability index of 0.56. The weighted radial extent standard deviation is 0.26 mas giving a variability index of 0.22.

The source is very compact and with little variation in the both the flux density and the compactness. Although modelfits show the presence of components, 92% of the total flux density is in the core. The radial extent also does not varies significantly. This is a **class A source**

4.2.6 0454-234

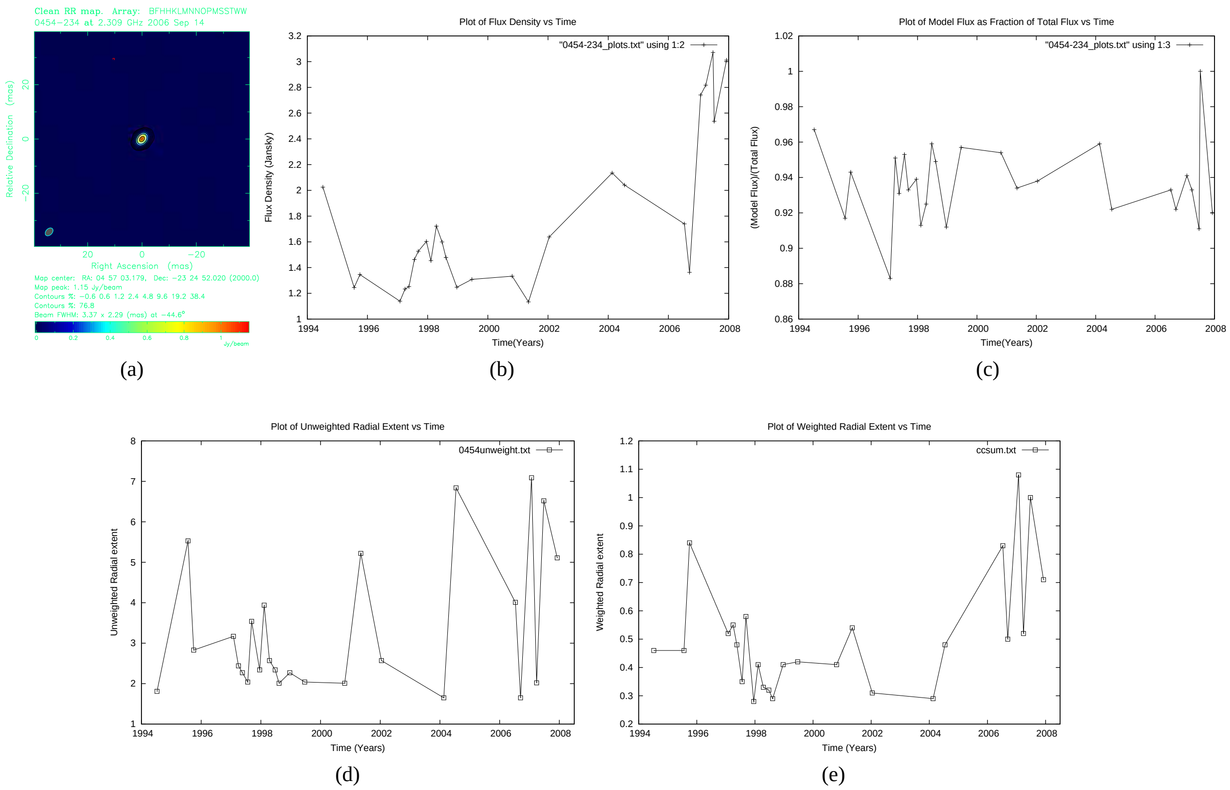

Figure 4.6: (a):Source image:0454-234. (b):Plot of Flux Density Variation. (c):Source Compactness. (d): Unweighted radial extent. (e): Weighted radial extent

Components were fitted for all epochs for this quasar. It is at a redshift of 1.00.

Between 1994 and 2006, the flux density varies between 1.1 and 2.1 Jy, fig(b). The flux density shoots up to 2.7 Jy in in early 2007, to 3.1 Jy in mid-2007 and decreases slightly to 3.0 Jy in 2008. On the other hand, the source is very compact, with the model core flux density ranging from about 90% to 100% of the total source flux density, fig(c). The unweighted radial extent varies between 2 and 7 mas, fig(d) and the weighted radial extent between about 0.3 and 1.1 mas fig(e).

The flux density standard deviation is 0.59 Jy giving a flux density variability index of 0.34. This shows a very high variation. The compactness standard deviation is 2% giving a variability index of 0.02. The mean of the compactness is 93.70%, making this source one of the most compact in this sample. The unweighted radial extent standard deviation is 1.78 mas giving an index of 0.56. The weighted radial extent standard deviation is 0.31 giving a variability index of 0.67.

Although it is very compact, the high variation in flux density and radial extent however disqualifies this source from being a class A source. This is a **class B source**.

4.2.7 0458-020

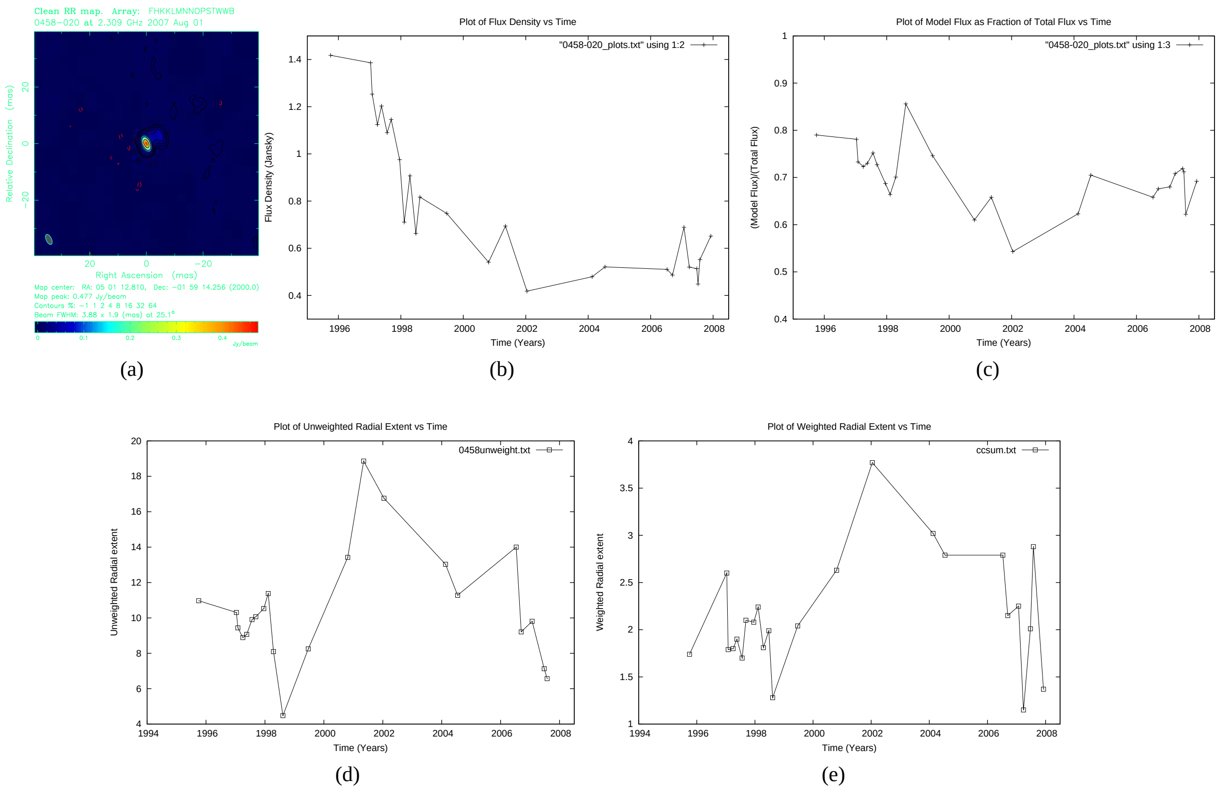

Figure 4.7: (a):Source image:0458-020. (b):Plot of Flux Density Variation. (c):Source Compactness. (d): Unweighted radial extent. (e): Weighted radial extent

0458-020 has been detected by EGRET as a high energy γ-ray source (von Montigny et al., 1995). It is a quasar at a redshift of 2.29.

The image shows a slight extension to the west, fig(a). The flux density falls gradually from 1.4 Jy in early 2000 to 0.4 Jy in 2002, fig(b). From 2002 to 2008, the flux density varies between 0.4 and about 0.7 Jy. The compactness mostly falls in the range 60% and 86% except for the epoch January 2002 where it falls to 54%, fig(c). The unweighted radial extent varies widely. The least value of 4.48 mas in 1998 (fig(d)) corresponds to the point when the source is most compact but not brightest. The weighted radial extent varies but on a smaller scale, between 1.3 mas and 3.8 mas, fig(e).

The flux density standard deviation is 0.31 Jy giving a flux density variability index of 0.40. The compactness standard deviation is 15% from a mean of 67.29% giving a variability index of 0.22. The unweighted radial extent standard deviation is 17.93 mas giving a variability index of 1.10. The weighted radial extent standard deviation is 1.02 mas giving a variability index of 0.46.

This source shows variation in all the measured parameters. It is a **class D source**.

4.2.8 0727-115

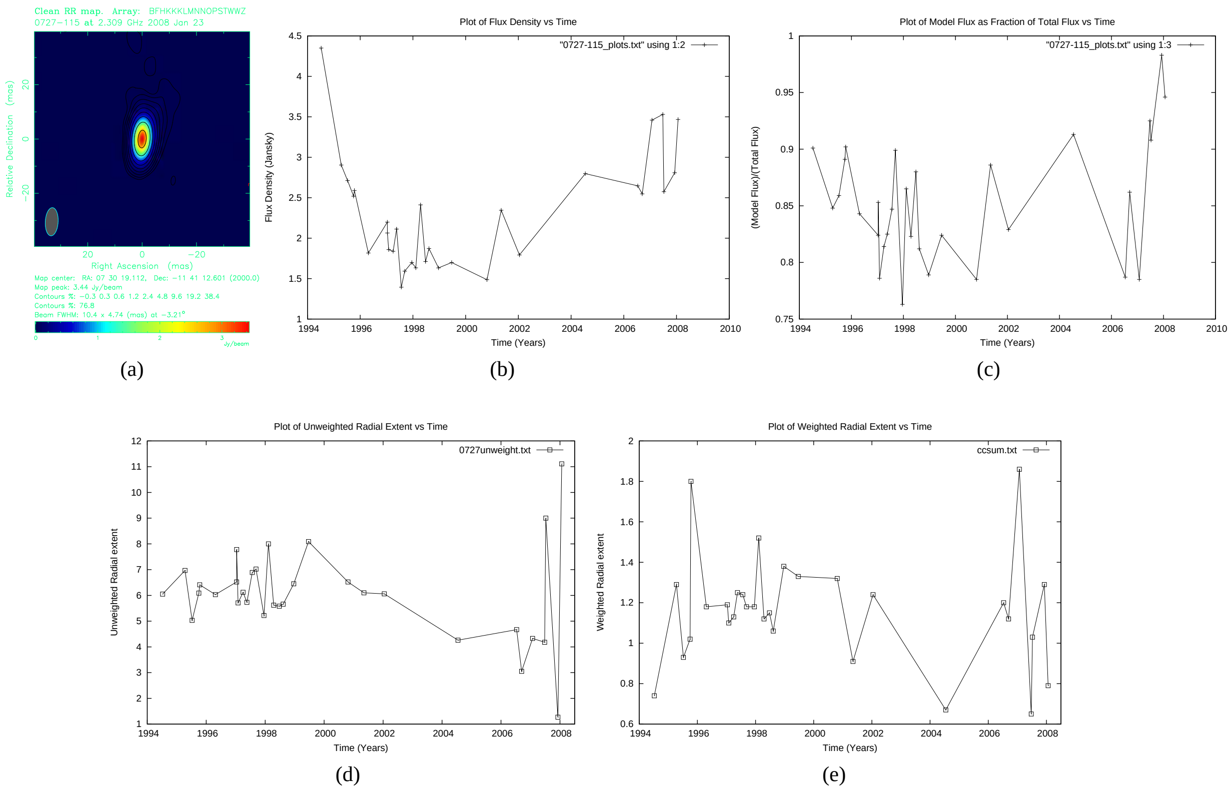

Figure 4.8: (a):Source image:0727-115. (b):Plot of Flux Density Variation. (c):Source Compactness. (d): Unweighted radial extent. (e): Weighted radial extent

This source was observed at all 32 epochs. It is a quasar at a redshift of 1.59.

The core flux density is 4.4 Jy in mid-1994 but this goes down sharply to 2.9 Jy in early 1995 and continues to fall until 1996. Thereafter it peaks and falls between 1.4 Jy and 2.4 Jy for the period January 1997 to January 2002. The core flux density raises gradually to 3.5 Jy from early 2002 to late 2007. At its brightest (4.4 Jy in mid-1994), the source only has 90% of the total flux density in the core, but is most compact (98%) in late 2007 when the core flux density is 3.5 Jy. The unweighted radial extent varies between 5 and 8 mas for most epochs but varies significantly for the last 3 epochs. The weighted radial extent is not as erratic as the unweighted radial extent. It varies for all epochs, between about 0.7 mas and 1.9 mas. This means the core is very compact and most of the flux density is in the core component.

The flux density standard deviation is 0.71 Jy from a mean of 2.32 Jy giving a flux density variability index of 0.30. The compactness standard deviation is 5% from a mean of 85.35% giving a variability index of 0.06. The unweighted radial extent standard deviation is 1.77 mas giving a variability index of 0.29. The weighted radial extent standard deviation is 0.30 mas giving a variability index of 0.26.

This is a **class B source**.

4.2.9 0919-260

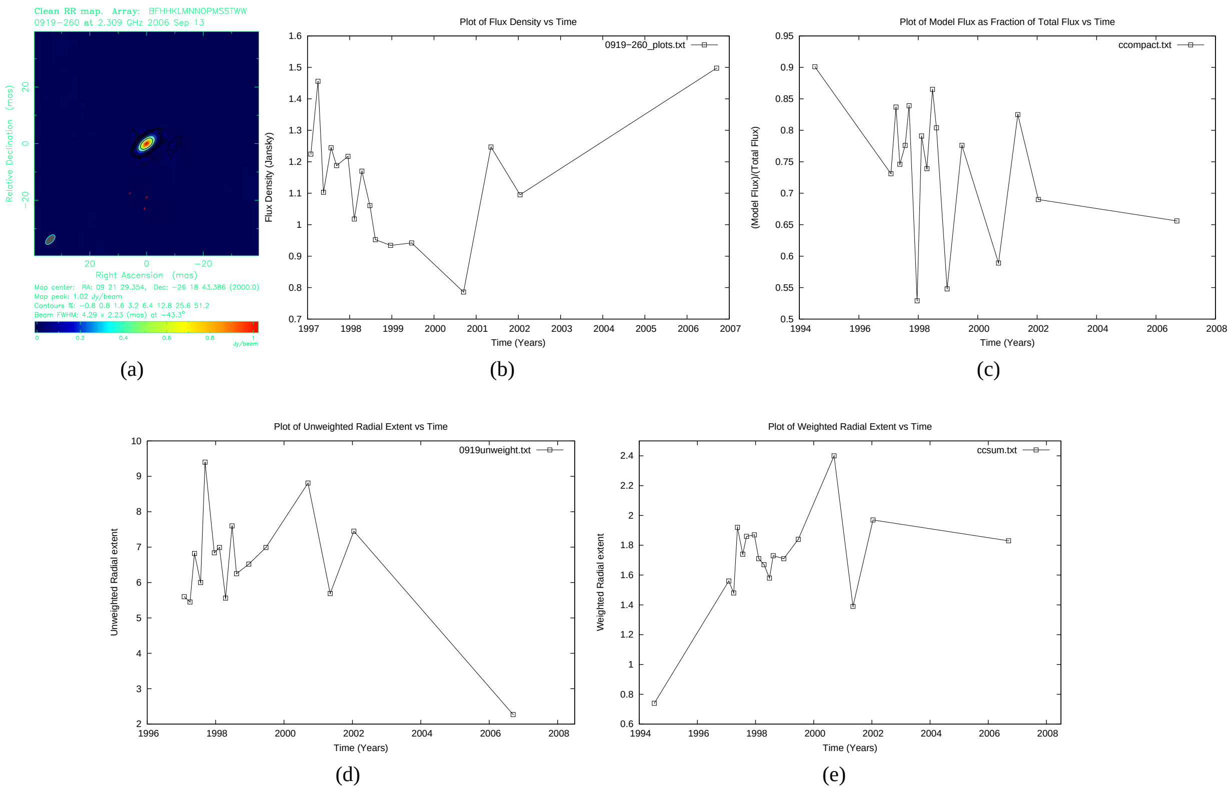

Figure 4.9: (a):Source image:0919-260. (b):Plot of Flux Density Variation. (c):Source Compactness. (d): Unweighted radial extent. (e): Weighted radial extent

0919-260 has been optically identified as a quasar at a redshift of 2.30.

This source has been fit for almost all epochs with the core and a single component. The image shows a component to the west of the core, fig(a). On the whole, the core flux density falls between 0.8 and 1.5 Jy, fig(b). Between 1997 and 2001, the flux density is on a downward trend, falling from about 1.5 Jy to about 0.8 Jy. This could be due a component ejection. After 2001, the flux density rises eventually going back to 1.5 Jy.

The compactness is highest at 87% and lowest at 53%, fig(c) while the mean is 74.40%. The unweighted radial extent ranges from 2 mas to about 9 mas with a mean on 6.49 mas but the weighted radial extent varies from about 1.4 mas to about 2.4 mas with a mean of 1.71 mas. The flux density standard deviation is 0.83 Jy, the mean is 1.33 Jy giving a flux density variability index of 0.63. The compactness standard deviation is 11% giving a variability index of 0.15. The unweighted radial extent standard deviation is 1.55 mas giving an index of 0.24. The weighted radial extent standard deviation is 0.34 mas giving an index of 0.20.

The core flux density does not vary to large extent but the radial extent is slightly variable. This is a **class B source**.

4.2.10 0920-397

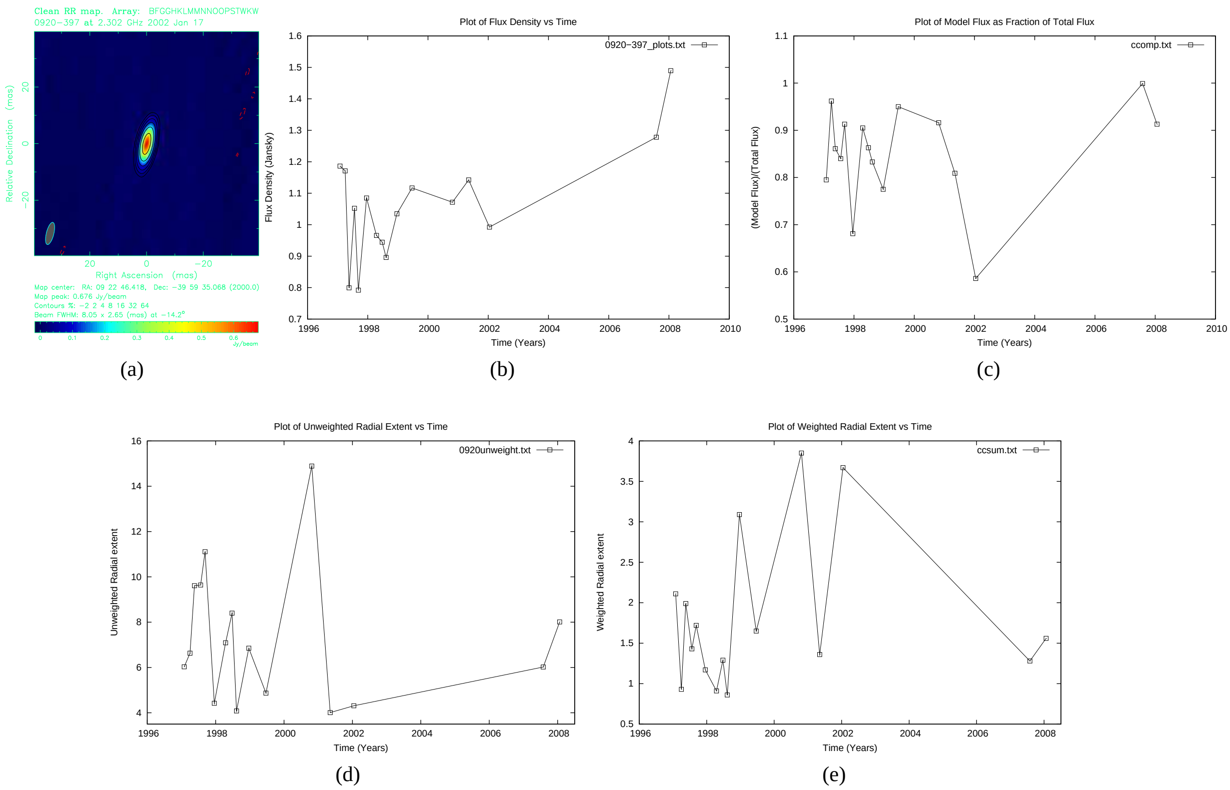

Figure 4.10: (a):Source image:0920-397. (b):Plot of Flux Density Variation. (c):Source Compactness. (d): Unweighted radial extent. (e): Weighted radial extent

This source shows hint of a component to the east as can be seen from the image, fig(a). A single component after the core was fitted for most epochs. It has been identified as a quasar at a redshift of 0.59.

The core flux density falls between 0.8 Jy and 1.5 Jy with a mean of 1.06 Jy. The compactness varies between 60% and 99% with a mean of 85%. The unweighted radial extent varies significantly but the weighted radial extent varies on a smaller scale, between 1 mas and 3.9 mas.

The flux density standard deviation is 0.18 Jy giving a flux density variability index of 0.17. The compactness standard deviation is 11% giving a variability index of 0.12. The unweighted radial extent standard deviation is 2.98 mas giving an index of 0.41. The weighted radial extent standard deviation is 0.94 mas giving a variability index of 0.52.

This is a **class B source**. It is very compact and the flux density and unweighted radial extent do not vary significantly.

4.2.11 1034-293

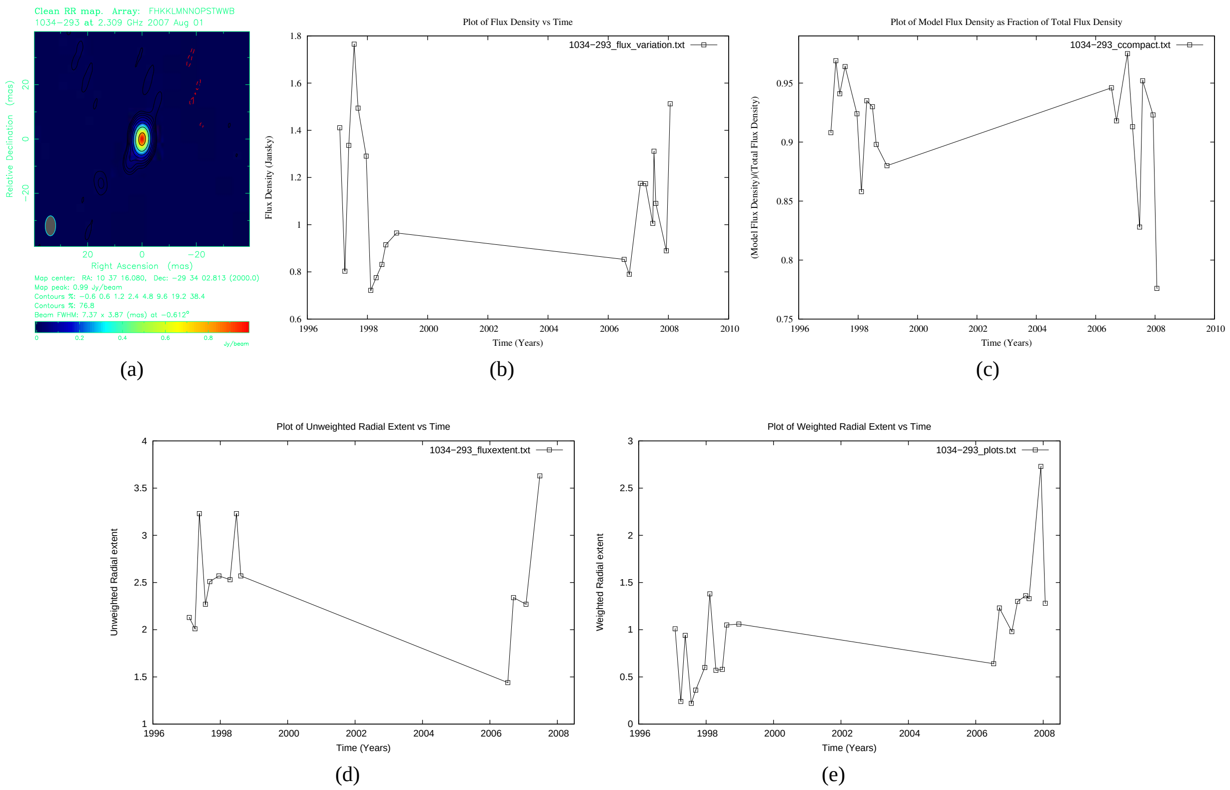

Figure 4.11: (a):Source image:1034-293. (b):Plot of Flux Density Variation. (c):Source Compactness. (d): Unweighted radial extent. (e): Weighted radial extent

The source is extended in the south-east direction as can be seen from the image, fig(a). It has been identified as a quasar at a redshift of 0.31.

The source has been fitted with up to 2 components for most epochs. The flux density varies between 1.8 Jy and about 0.7 Jy. The mean flux density is 1.11 Jy. The mean compactness is 87.20%, showing 87% of the total flux is contained in the core component. The unweighted radial extent lies between 1.5 mas and 3.5 mas.

The flux density standard deviation is 0.30 Jy giving a flux density variability index of 0.27. The compactness standard deviation is 21% giving a variability index of 0.24. The unweighted radial extent standard deviation is 8.22 mas giving a variability index of 1.41. The weighted radial extent standard deviation is 0.68 mas giving a variability index of 0.75. This shows a very high variation in the radial extent although the source is very compact.

This is a **class C source**.

4.2.12 1124-186

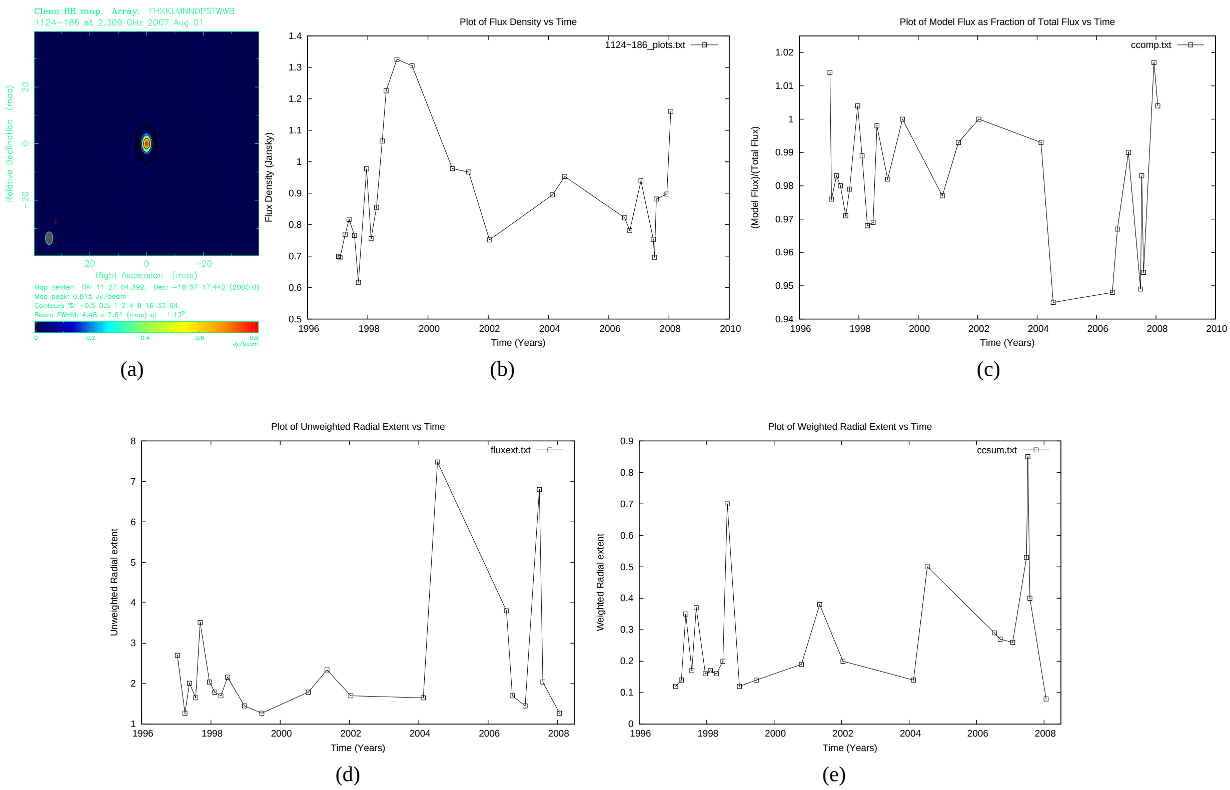

Figure 4.12: (a):Source image:1124-186. (b):Plot of Flux Density Variation. (c):Source Compactness. (d): Unweighted radial extent. (e): Weighted radial extent

The image shows this source be a point source, fig(a). With 26 epochs, it is one of the most observed sources in this sample. It is a quasar at a redshift of 1.05 according to the Véron-Cetty & Véron Catalogue.

The flux density increases from about 0.7 Jy to about 1.3 Jy in mid-1999 and falls to 0.75 Jy in 2002, fig(b). This could be due to a component ejection. Thereafter, the flux density rises and falls between 0.8 Jy and 1.2 Jy. The compactness however lies between about 95% and 100%, fig(c). The mean of the compactness is 98.20%. This means this a compact source, as 98% of the total flux density is in the core component. The unweighted radial extent, is mostly between 1 mas and 4 mas, fig(d) while the weighted radial extent is between 0.1 mas and 0.9 mas, fig(e).

The flux density standard deviation is 0.19 Jy giving a flux density variability index of 0.21. The compactness standard deviation is 2% giving a variability index of 0.02. The unweighted radial extent standard deviation is 16.50 mas giving a variability index of 2.40. The weighted radial extent standard deviation is 0.29 mas giving a variability index of 1.18.

This is a very compact source but with a high variability in the flux extent. This is a **class B source**.

4.2.13 1144-379

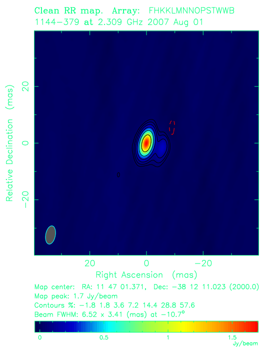

(a)

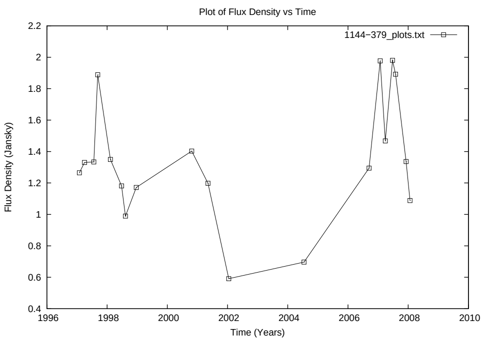

(b)

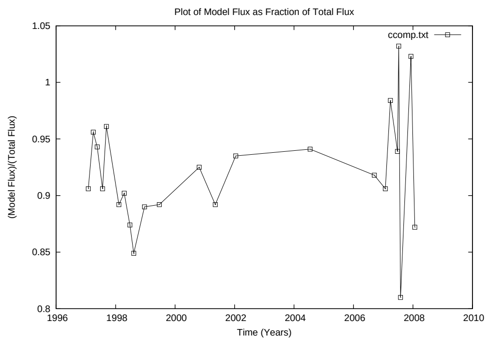

(c)

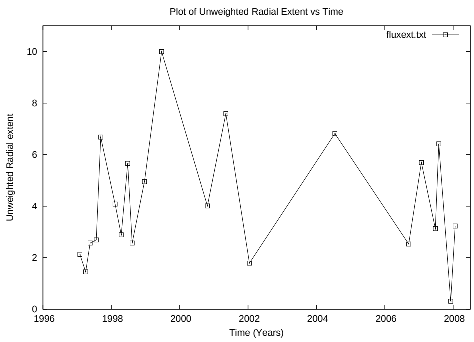

(d)

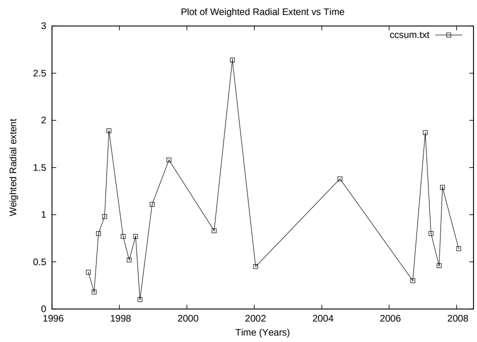

(e)

Figure 4.13: (a):Source image:1144-379. (b):Plot of Flux Density Variation. (c):Source Compactness. (d): Unweighted radial extent. (e): Weighted radial extent

This source is slightly extended to the west. It is listed in the Véron-Cetty & Véron Catalogue as a quasar. Impey & Tapia (1988) classified it as a blazar, considering its highly variable optical emission. Modelfits show two components in addition to the core. The flux density mostly varies between 1 and 2 Jy but Shen et al. (1997) recorded a flux density of 4.6 Jy from measurements taken in 1995 at 5 GHz. It is thought the source was is an active phase then.

The compactness is between 80% and 100%, with most points falling between 85% and 95%, making this source, one of the most compact sources in the sample. The mean compactness is 91.95%. The unweighted radial extent varies between 1 and 10 mas with two outliers at 34 mas and 99 mas. The mean is 9.60 mas. The weighted radial extent varies between 0.2 and 2.6 mas.

The flux density standard deviation is 0.39 mas giving a flux density variability index of 0.29. The compactness standard deviation is 5% giving a variability index of 0.06. The unweighted radial extent standard deviation is 20.66 mas giving a variability index of 2.15. The weighted radial extent standard deviation is 1.79 mas giving a variability index of 4.10.

This is a **class C source**, it is very compact but both the radial extents varies quite significantly.

4.2.14 1145-071

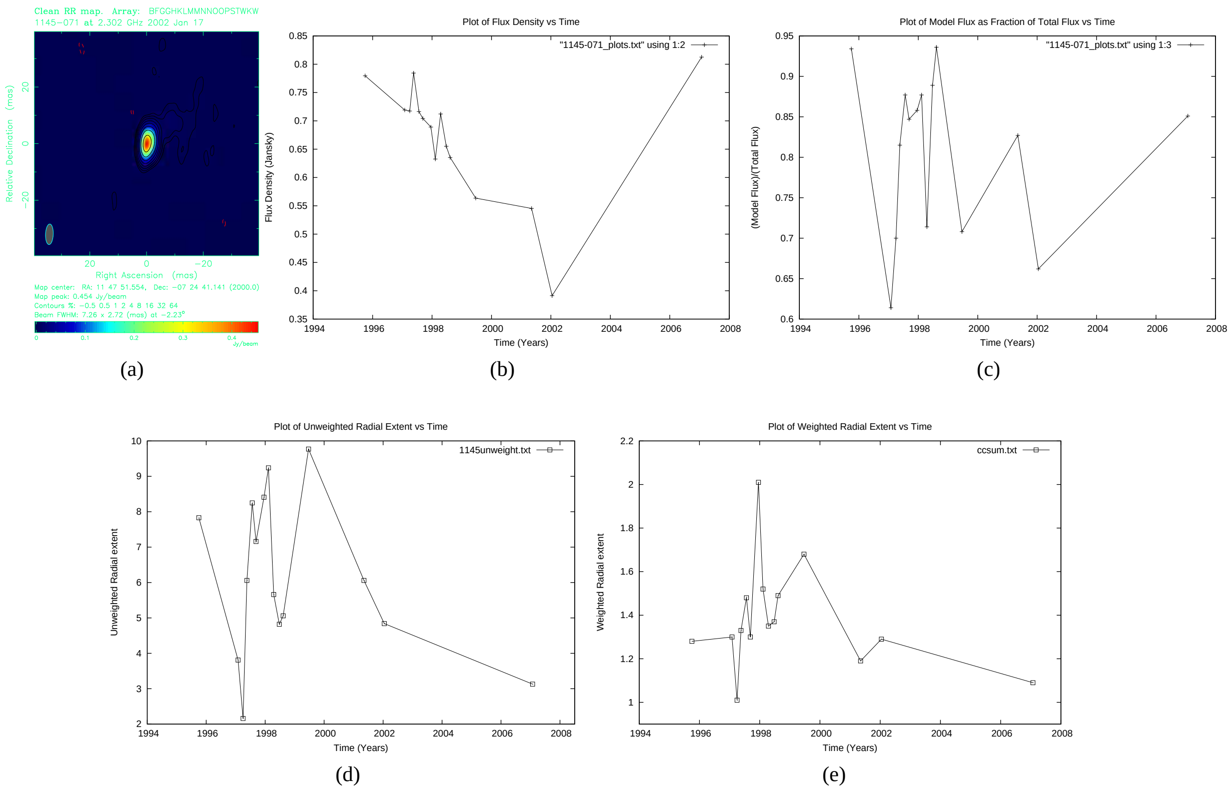

Figure 4.14: (a):Source image:1145-071. (b):Plot of Flux Density Variation. (c):Source Compactness. (d): Unweighted radial extent. (e): Weighted radial extent

1145-071 is binary quasar at a redshift of 1.34. It was discovered to be a binary quasar by Djorgovski (1987) but only one of the quasars is bright at radio wavelengths.

The source is extended in the north-west direction, fig(a). It has been fitted with 2 components, other than the central core component. The flux density of the source generally decreases from about 0.8 Jy to 0.4 Jy in the period 1995 to 2002, then shoots back to 0.8 Jy in early 2007. This is most likely due to ejection of a component. The compactness varies erratically between 60% and 95% with a mean of 80%. The unweighted radial extent also varies erratically between 2 and 10 mas with a mean of 6.15 mas. The weighted radial extent is less erratic and varies between 1 and 2 mas with a mean of 1.38 mas.

The flux density standard deviation is 0.11 Jy giving a flux density variability index of 0.16. The compactness standard deviation is 10% giving a variability index of 0.13. The unweighted radial extent standard deviation is 2.26 mas giving a variability index of 0.37. The weighted radial extent standard deviation is 0.24 giving a variability index of 0.18.

This is a **class A source**. It is compact with little variation in all the measured parameters.

4.2.15 1253-055

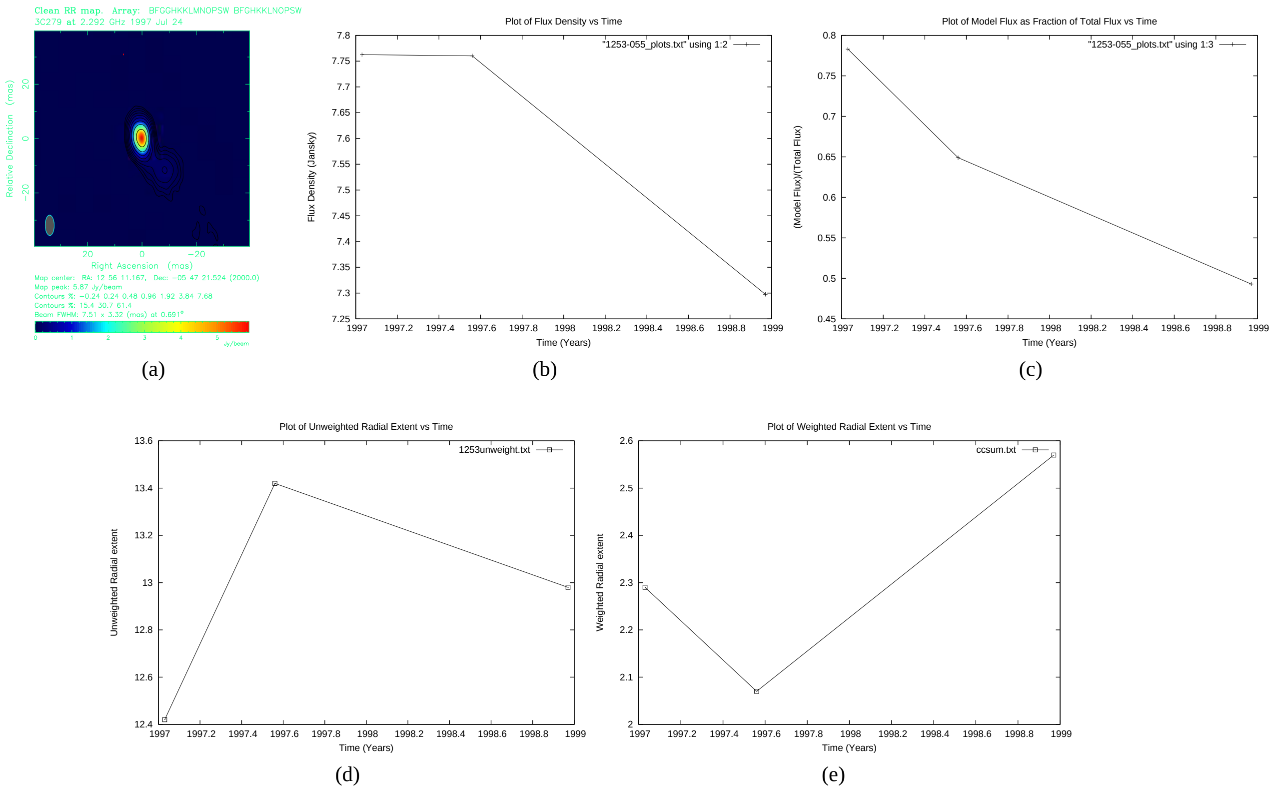

Figure 4.15: (a):Source image:1253-055. (b):Plot of Flux Density Variation. (c):Source Compactness. (d): Unweighted radial extent. (e): Weighted radial extent

With only 3 epochs, this is the least observed source in the sample. This source is also known as source number 279 in the Third Cambridge Catalogue (3C279) and is at a redshift of 0.54. This source was excluded from the ATCA intraday variability sample because of extended structure (Kedziora-Chudczer et al., 2001) and this can be seen in the image, fig(a). The flux density falls between 7.3 and 7.8 Jy, fig(b). This source is one of the brightest and most variable at radio wavelengths (Lindfors et al., 2006). The compactness falls between 50% and 80% with a mean of 64%. The unweighted radial extent is between 12.4 and 13.4 mas and the weighted radial extent is between 2.1 and 2.6 mas. Although extended, the source core seems to be very stable. It is known to exhibit superluminal motion of components that “appear to be ejected from a presumably stationary core.” (Jorstad et al., 2004). It has been described as the archetypical superluminal radio sources (Cotton et al., 1979). It is a good candidate for further studies on superlunimal motion at 2.3 GHz. The flux density standard deviation is 0.27 Jy giving a flux density variability index of 0.20. The compactness standard deviation is 15% giving an index variability is 0.23. The unweighted radial extent standard deviation is 0.50 mas giving a variability index of 0.04. The weighted radial extent standard deviation is 0.25 mas giving a variability index of 0.11. Its classified as a **class B source**.

4.2.16 1255-316

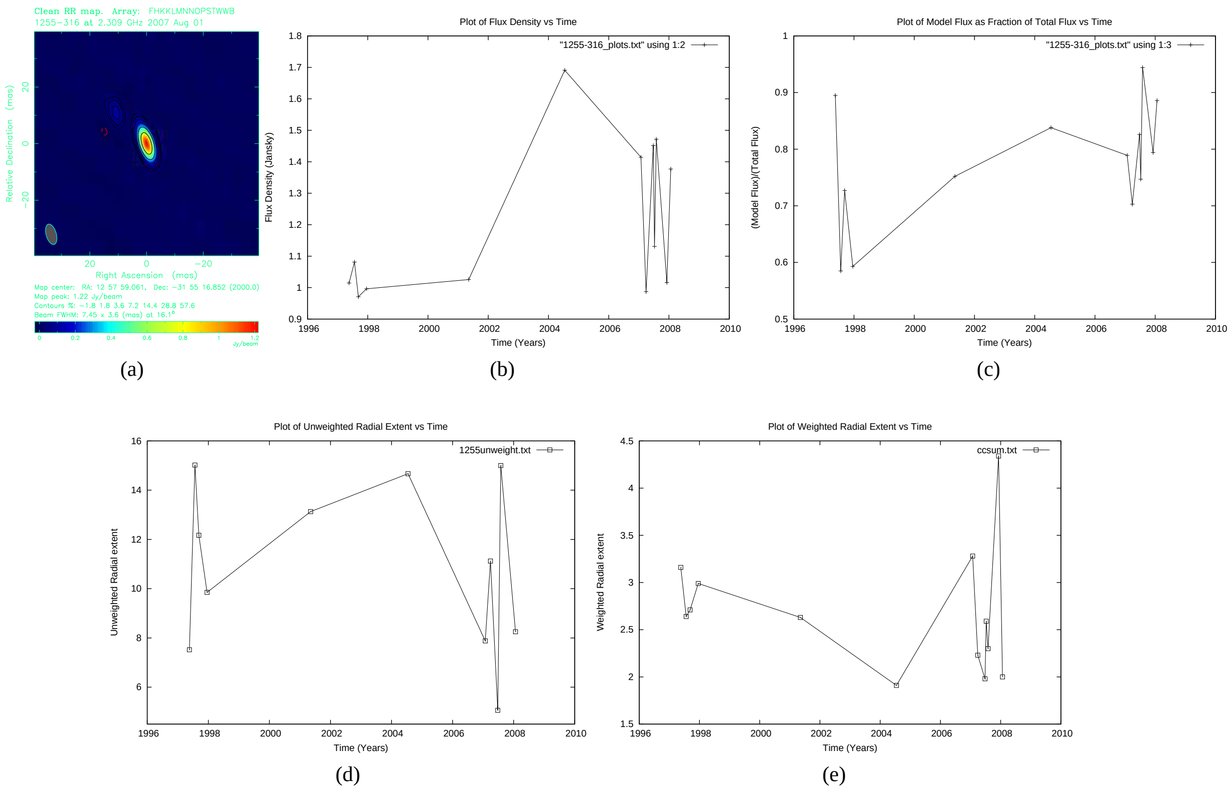

Figure 4.16: (a):Source image:1255-316. (b):Plot of Flux Density Variation. (c):Source Compactness. (d): Unweighted radial extent. (e): Weighted radial extent

A quasar at a redshift of 1.92, this is source has multi-components as shown in the image (fig(a)) and the modelfits.

The flux density varies between about 1 Jy and 1.7 Jy. It starts off around 1 Jy from 1997 to 2001 but raises sharply to about 1.7 Jy in 2004, fig(b), a 70% increase in the flux density. It is possible that it was active during this period. The compactness is between 60% (in earlier epochs), and 95% (in later epochs), fig(c). The mean compactness is 77.53%. The unweighted radial extent is between 4 and 15 mas with a mean of 14.17 mas. The weighted radial extent is between 2 and 4.5 mas with a mean of 2.67 mas.

The flux density standard deviation is 0.24 Jy giving a flux density variability index of 0.20. The compactness standard deviation is 11% giving a variability index of 0.14. The unweighted radial extent standard deviation is 11.86 mas giving an index of 0.84. The weighted radial extent standard deviation is 0.67 giving an index of 0.25.

This source is not very compact and an unweighted radial extent variability index of 0.84 shows a large variation in the radial extent. This is a **class C source**.

4.2.17 1313-333

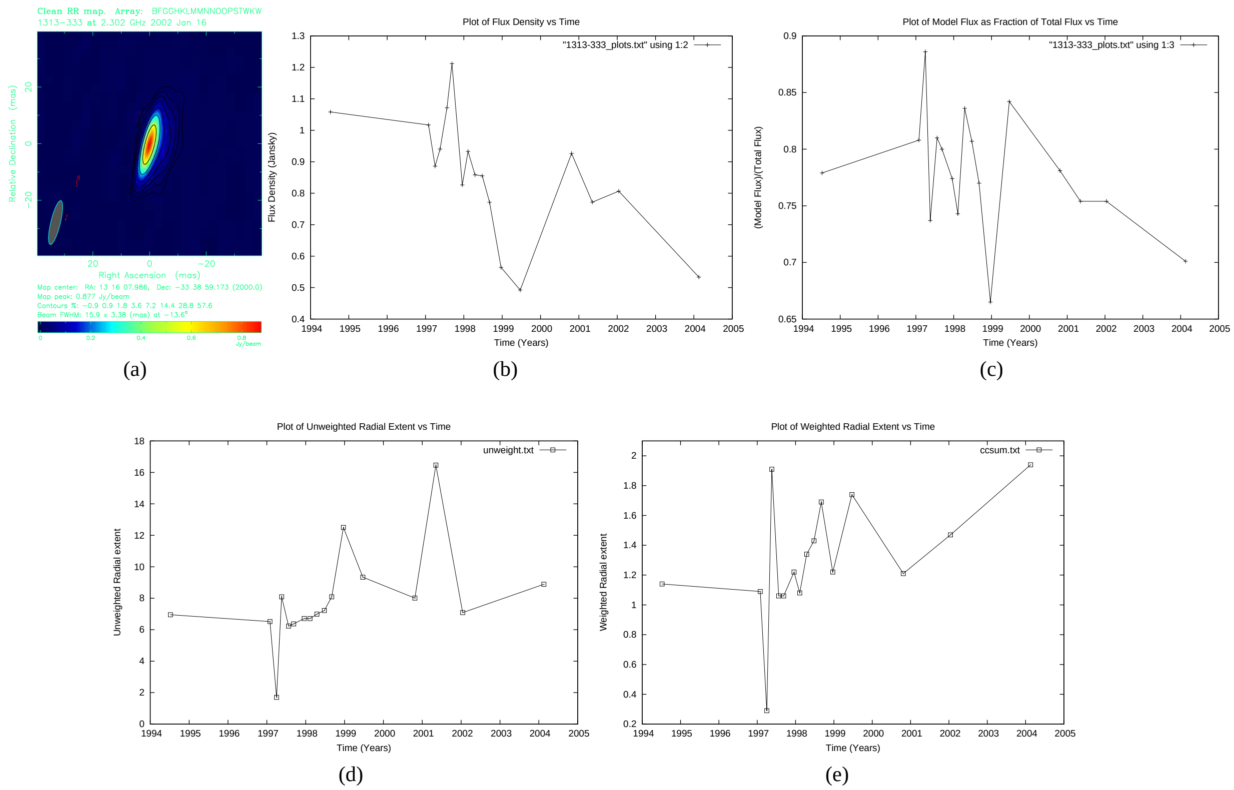

Figure 4.17: (a):Source image:1313-333. (b):Plot of Flux Density Variation. (c):Source Compactness. (d): Unweighted radial extent. (e): Weighted radial extent

This source is a quasar at a redshift of 1.21.

From the image, fig(a), this source is extended in the eastern direction. It has been fitted for all epochs with at least one component. In earlier epochs, this source is brighter than in later epochs where the flux density drops to as low as 0.5 Jy from 1.2 Jy, fig(b). This could be due to component ejection around 1999. After 1999, the flux density raises and falls again in 2004. The compactness varies from 67% to 89% with a mean of 77.92%. Except for two points, the unweighted radial extent falls between 6 and 10 mas. The weighted flux density radial extent varies between 1 and 2 mas.

The flux density standard deviation is 0.28 Jy giving a flux density variability index of 0.35. The compactness standard deviation is 5% giving a variability index of 0.07. The unweighted radial extent standard deviation is 3.05 mas giving a variability index of 0.39. The weighted radial extent standard deviation is 0.40 mas giving a variability index of 0.31

This source has been classified as a **class B source**.

4.2.18 1334-127

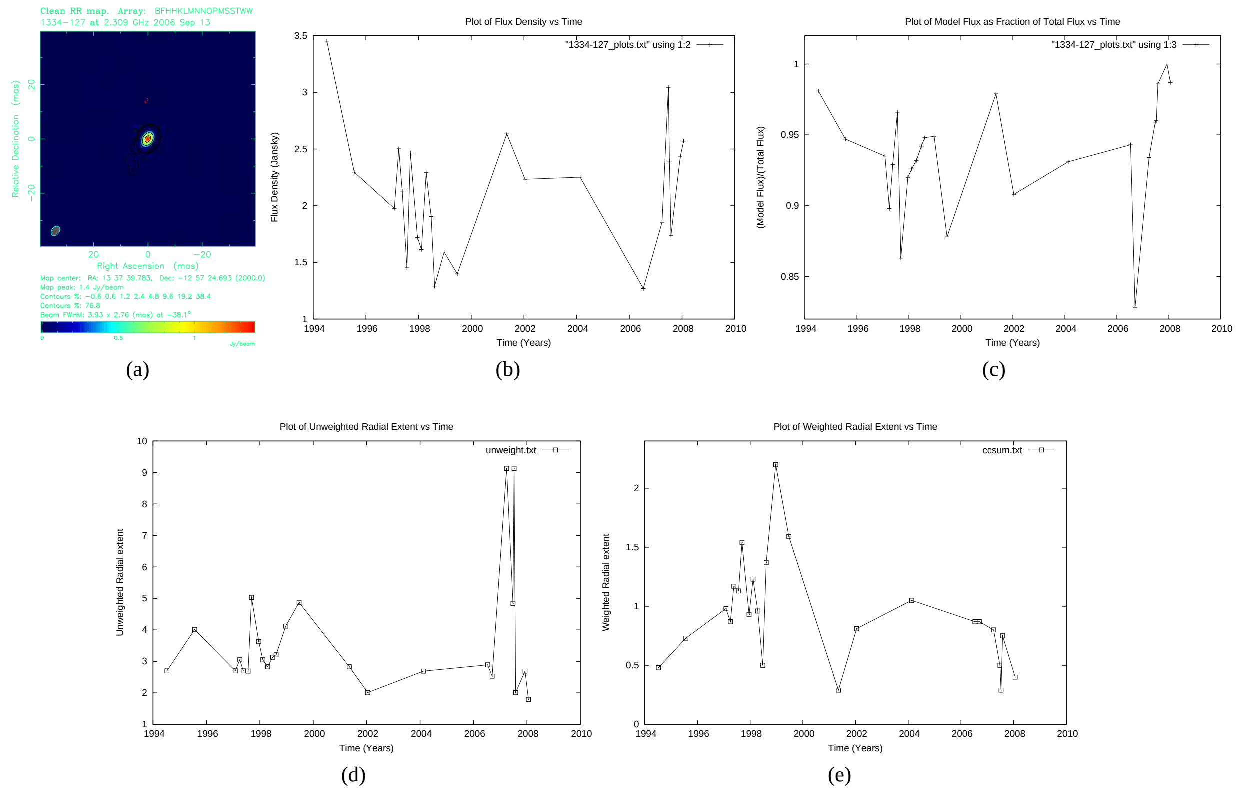

Figure 4.18: (a):Source image:1334-127. (b):Plot of Flux Density Variation. (c):Source Compactness. (d): Unweighted radial extent. (e): Weighted radial extent

A highly polarised quasar (Impey & Tapia, 1988) at a redshift of 0.54, this source has been fitted with more than 2 components in most epochs.

At its brightest, the source has a flux density of 3.5 Jy but the flux density mostly falls between 2.5 Jy and 1.5 Jy for most epochs, fig(b). The compactness is between 82% and 100%, making this source one of the most compact in the sample, fig(c). The unweighted radial extent varies between 1.8 and 4.9 mas, fig(d). The weighted radial extent varies between 0.4 and 2.2 mas, fig(e). This source has been named as a superluminal candidate by Shen et al. (1997) and we can certainly investigate further as we have 17 epochs of observations. It is also known to have been active and underwent an outburst (Wehrle et al., 1992).

The flux density standard deviation is 0.55 Jy from a mean of 2.10 Jy giving a flux density variability index of 0.26. The compactness standard deviation is 4 % from a mean of 93.72% giving a variability index of 0.04. The unweighted radial extent standard deviation is 1.87 mas giving a variability index of 0.52. The weighted radial extent standard deviation is 0.62 mas giving a variability index of 0.74.

The source is very compact but shows some variation in the radial extent. This is a **class B source**.

4.2.19 1351-018

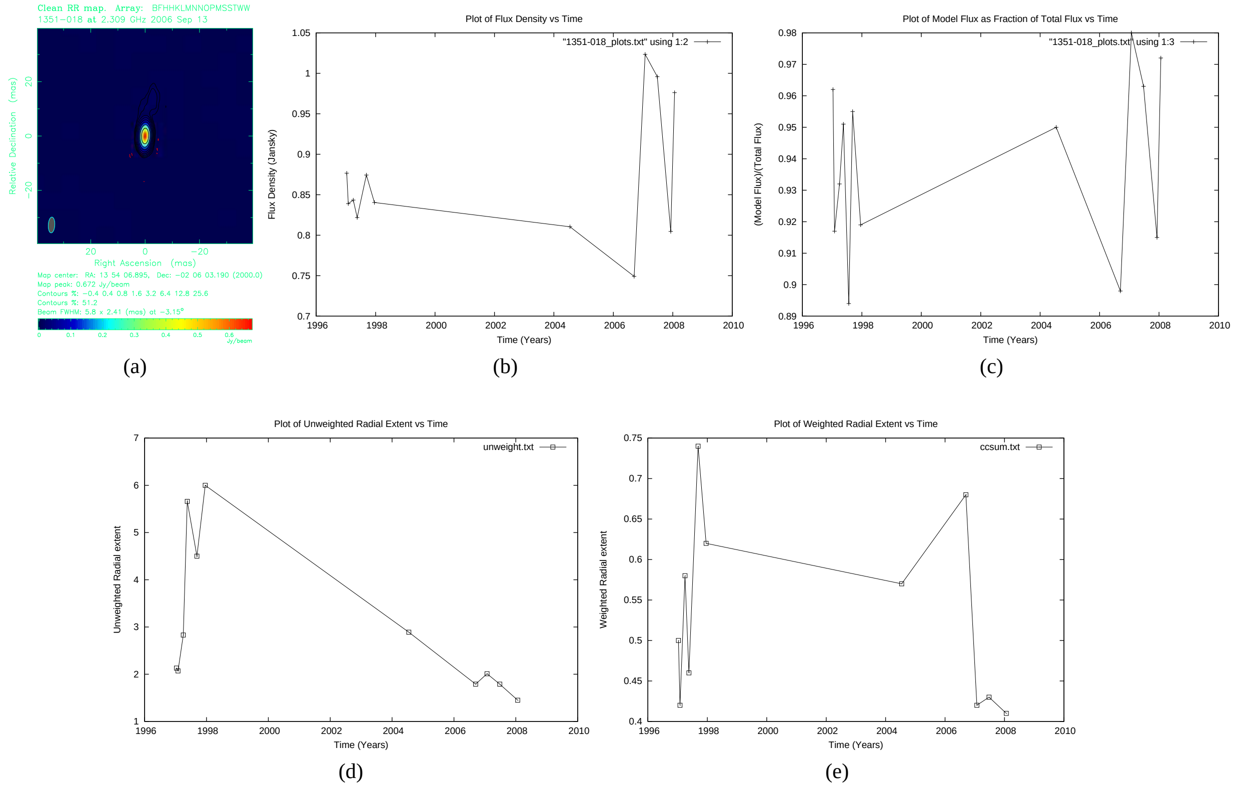

Figure 4.19: (a):Source image:1351-018. (b):Plot of Flux Density Variation. (c):Source Compactness. (d): Unweighted radial extent. (e): Weighted radial extent

At a redshift of 3.71, this source has the highest redshift in the sample.

It has been fitted for all epochs with one component in addition to the core component. The image shows the source to be extended in the northern direction, fig(a). Frey et al. (1997) find a dominant core and a weak extension in the same direction as the above image. Neff & Hutchings (1990) found the source to be unresolved by the VLA. The flux density of this source does not vary much, it falls between 0.75 and 1 Jy with a mean of 0.80 Jy. 9 out of 12 epochs have flux density in the range 0.75 and 0.87 Jy. The compactness varies between 89% and 100% with a mean of 93.90%. This is a very compact source with about 94% of the total flux density in the core. The unweighted radial extent is between 2 and 8 mas, fig(d) with a mean of 2.55 mas. It falls to about 2 mas in 2008 from 6 mas in 1999. It is possible a component was ejected during the period 2000 and 2007. The weighted radial extent is between 0.4 and 0.7 mas, fig(e).

The flux density standard deviation is 0.25 Jy giving a flux density variability index of 0.32. The compactness standard deviation is 3% giving a variability index of 0.03. The unweighted radial extent standard deviation is 1.86 mas giving a variability index of 0.73. The weighted radial extent standard deviation is 2.93 mas giving a variability index of 1.94. This is a **class B source**.

4.2.20 1424-418

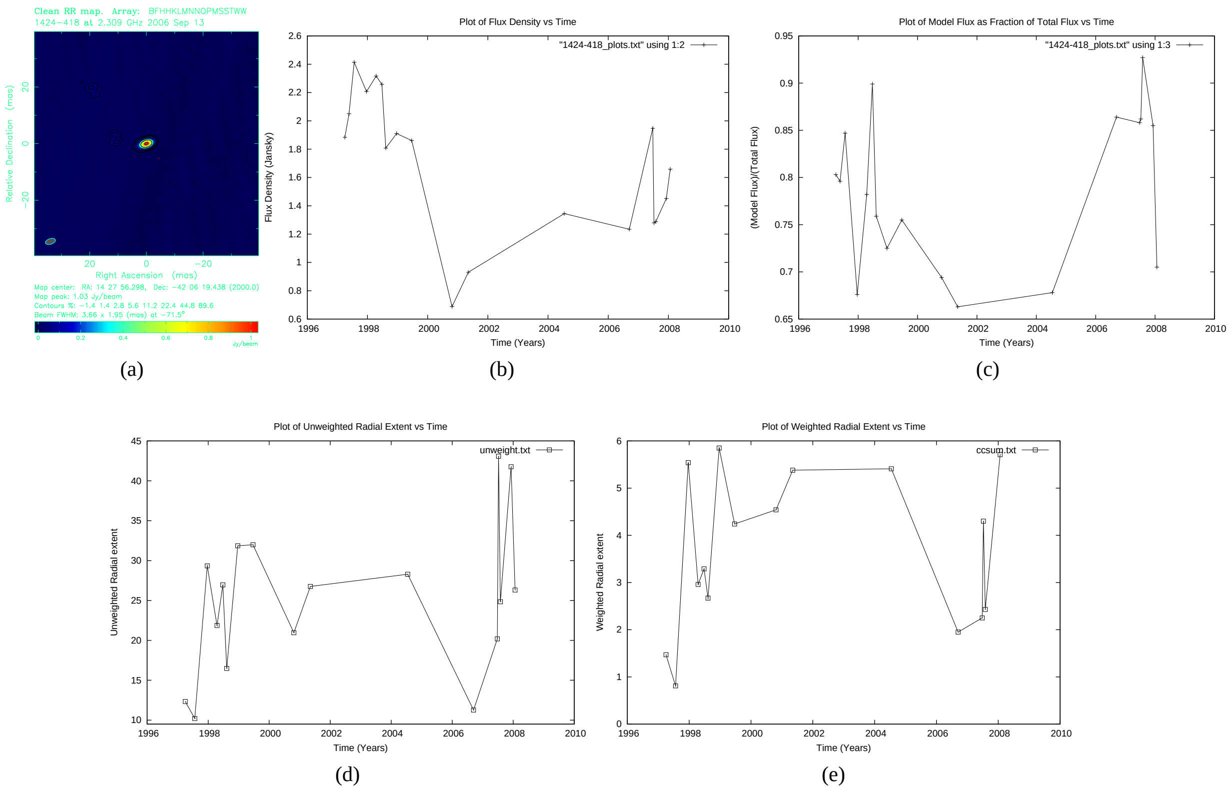

Figure 4.20: (a):Source image:1424-418. (b):Plot of Flux Density Variation. (c):Source Compactness. (d): Unweighted radial extent. (e): Weighted radial extent

The source is extended in the north-eastern direction, fig(a) and has been fitted with components for all epochs. It is a relatively bright source and has been identified as a quasar at a redshift of 1.52.

For earlier epochs, the flux density is above 1.8 Jy but falls to 0.6 Jy towards the end of the year 2000, fig(b). The flux density rises gradually thereafter by does not go back to previous levels, reaching a high of 1.94 Jy compared to 2.4 Jy before. It is possible a component was ejected around 2000 but there is nothing in the literature to support this. The compactness varies between 65% and 95%, fig(c). The compactness mean is 78.6%. The unweighted radial extent rises to 45 mas from 10 mas. The weighted radial extent rises to 6 mas from 1 mas.

The flux density standard deviation is 0.49 Jy giving a flux density variability index of 0.29. The compactness standard deviation is 8% giving a variability index of 0.11. The unweighted radial extent standard deviation is 11.07 mas giving a variability index of 0.47. The weighted radial extent standard deviation is 1.88 mas giving a variability index of 0.55.

This is a **class C source**.

4.2.21 1451-375

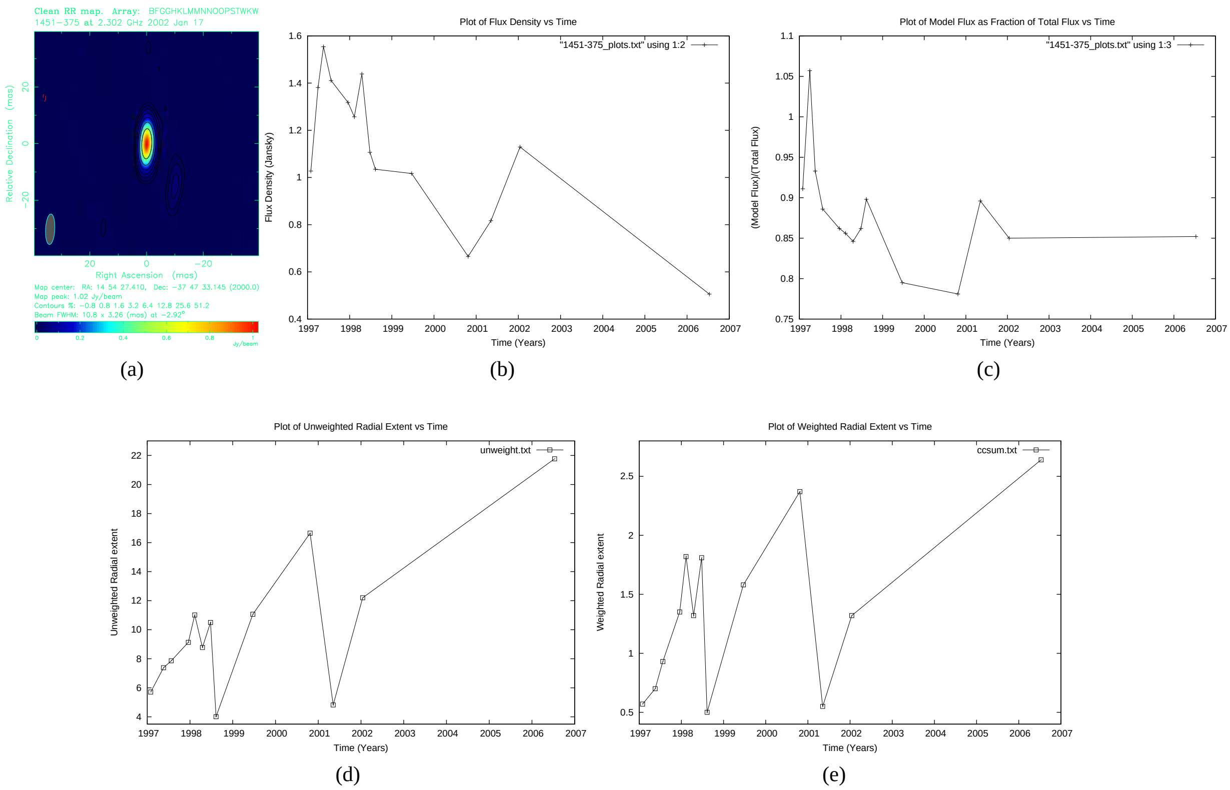

Figure 4.21: (a):Source image:1451-375. (b):Plot of Flux Density Variation. (c):Source Compactness. (d): Unweighted radial extent. (e): Weighted radial extent

The image of this source clearly shows it to have at least 2 components, fig(a) and this is confirmed by the modelfits which show up to 3 components. The source is a quasar at a redshift of 0.31.

The flux density varies but is on a general downward trend from around 1.6 Jy in the early epochs to 0.5 Jy in the last observed epoch, fig(b). It is possible it was active in earlier epochs and went back to it quiescent state in later epochs. The compactness is between 80% and 100% for all but one epoch, fig(c), with a mean of 87.75%. The unweighted radial extent within which 95% of the flux density is contained ranges between 4 and 22 mas with a mean of 9.35 mas. The weighted radial extent varies between 0.5 mas and 2.5 mas.

The flux density standard deviation is 0.30 Jy giving a flux density variability index of 0.27. The compactness standard deviation is 7% giving a variability index of 0.08. The unweighted radial extent standard deviation is 5.40 mas giving a variability index of 0.58. The weighted radial extent standard deviation is 3.71 mas giving a variability index of 10.08.

This is a **class C source**. It is clearly extended and its radial extent varies significantly but it has a fairly compact core.

4.2.22 1514-241

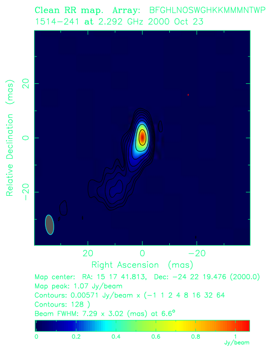

(a)

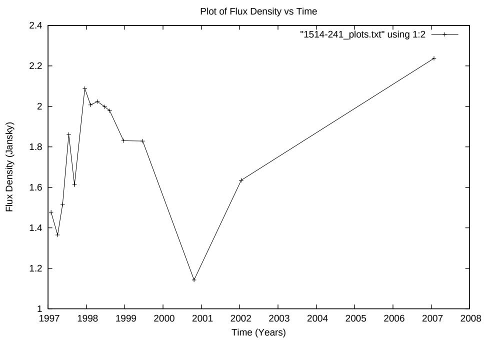

(b)

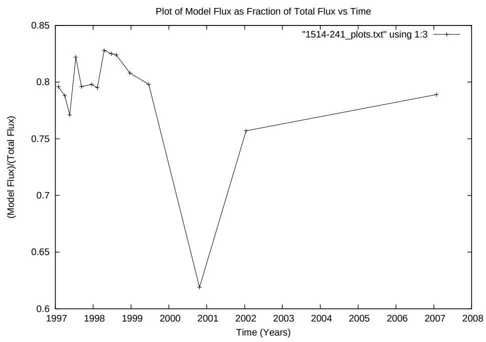

(c)

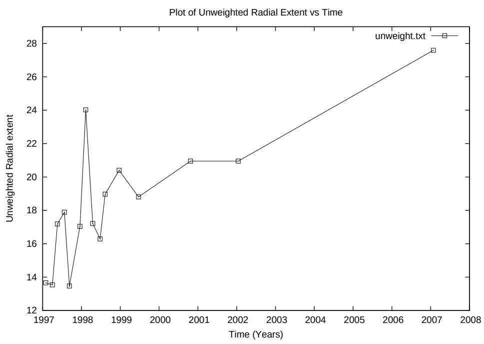

(d)

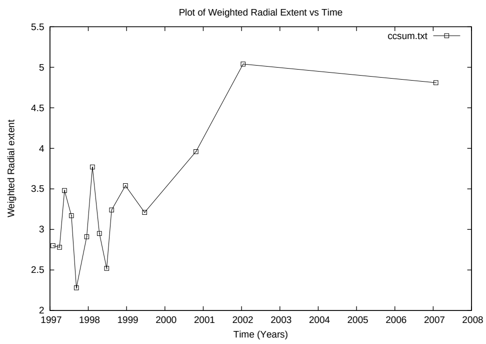

(e)

Figure 4.22: (a):Source image:1514-241. (b):Plot of Flux Density Variation. (c):Source Compactness. (d): Unweighted radial extent. (e): Weighted radial extent

This source is a BL Lac object at a redshift of 0.05.

The image shows it is extended in the south-east directions, fig(a). Modelfits show up to five different components. The flux variation shows a major dip in the flux density in October 2000. The compactness ranges between 76% and 83% except in October 2000 when it drops to 62%. The mean compactness is 78.76%. The unweighted radial extent also increases after this epoch. The weighted radial extent varies slightly before October 2000 but also increases after this epoch. It is possible a component was ejected between 1998 and 2001, leading to a drop in flux density and compactness of the source, and an increase in the radial extent.

The flux density standard deviation is 0.30 Jy giving a flux density index of 0.17. The compactness standard deviation is 5% giving a variability index of 0.11. The unweighted radial extent standard deviation is 3.90 mas giving a variability index of 0.21. The weighted radial extent standard deviation is 0.78 mas giving a variability index of 0.23.

This is a **class B source**.

4.2.23 1622-253

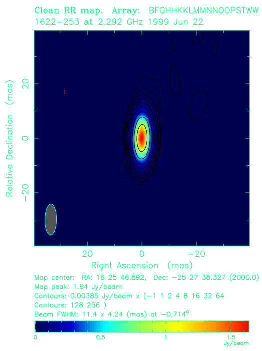

(a)

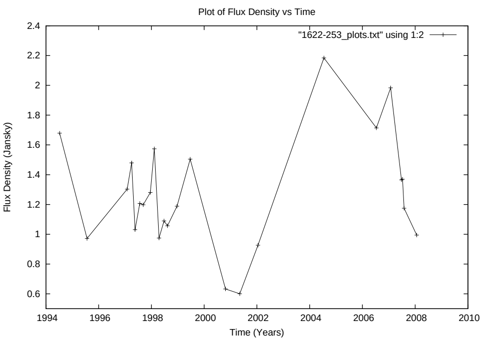

(b)

(c)

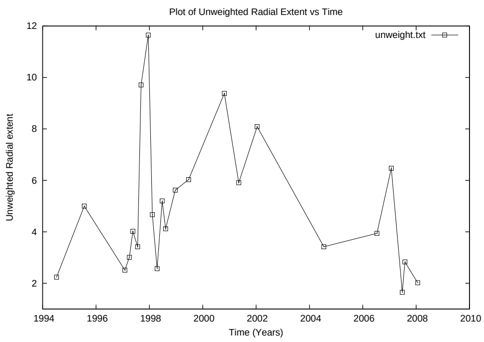

(d)

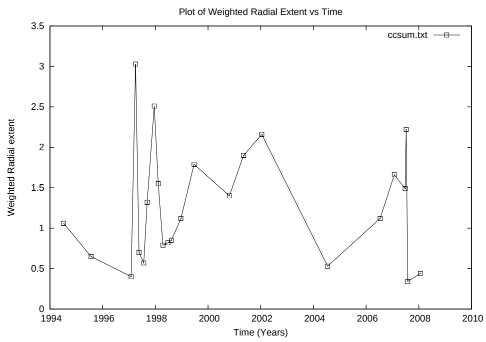

(e)

Figure 4.23: (a):Source image:1622-253. (b):Plot of Flux Density Variation. (c):Source Compactness. (d): Unweighted radial extent. (e): Weighted radial extent

1622-253 is described by Punsly et al. (2005) as a triple radio source with a superluminal radio core and powerful FRII radio lobes. It is a quasar at a redshift of 0.79 and has been fitted with multiple components, (see Appendix A). It is extended and is known to be variable (Tingay et al., 2003).

The flux density varies between 0.6 Jy and 2.2 Jy with a mean of 1.27 Jy. This source is in the top 10% of 185 sources in the ATCA (Australia Telescope Compact Array) monitoring program when ranked by source variability at 4.8 GHz (Tingay et al., 2003). The compactness varies between 78% and 98% with a mean of 90%. The unweighted radial extent is between 2 and 12 mas. The unweighted radial extent is between 0.5 and 3 mas.

The flux density standard deviation is 0.38 Jy giving a flux density variability index of 0.30. The compactness standard deviation is 7% giving a variability index of 0.06. The unweighted radial extent standard deviation is 7.37 mas giving a variability index of 1.16. The weighted radial extent standard deviation is 0.72 mas giving a variability index of 0.57.

This is a **class B source**. Although the flux density and radial extent variability indices show the source to be variable, its core is very compact.

4.2.24 1741-038

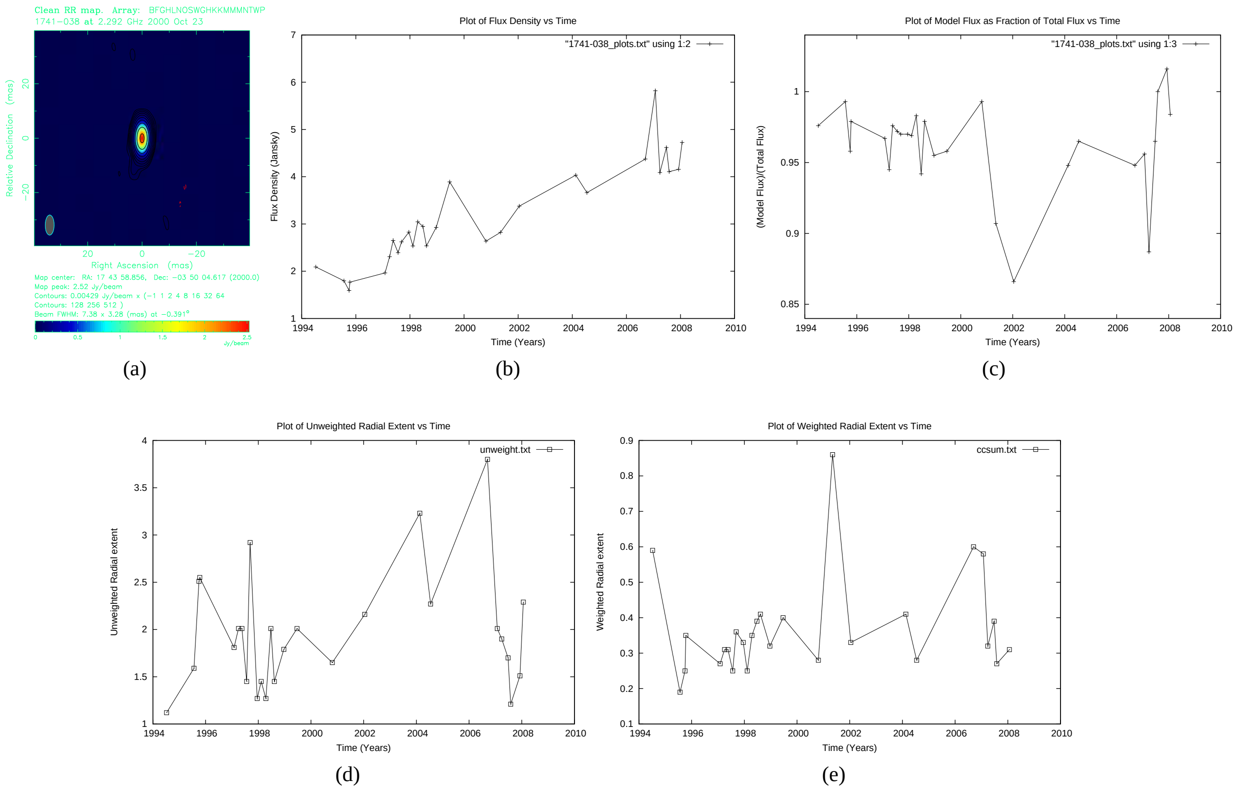

Figure 4.24: (a):Source image:1741-038. (b):Plot of Flux Density Variation. (c):Source Compactness. (d): Unweighted radial extent. (e): Weighted radial extent

1741-038 has been optically identified as a quasar at a redshift of 1.05.

It is one of the best observed sources in this sample and shows a gradual increase in the flux density from the first epoch to the last, fig(b). When first observed in mid-1994, it has a flux density of about 2 Jy and this increases to 5.8 Jy by early 2007. Flux-density fluctuation in this source have been reported in some monitoring programs (Fiedler et al., 1987; Hjellming & Narayan, 1986). The source is also a known intra-day variable (Quirrenbach et al., 1992). The compactness is between 95% and 100% for most epochs, making this source a very compact source. The unweighted radial extent is between 1 and 4 mas. The weighted radial extent is between 0.2 and 0.9 mas.

The flux density standard deviation is 1.05 Jy giving a flux density variability index of 0.33. The compactness standard deviation is 3% , the mean is 96.17% giving a variability index of 0.3. The unweighted radial extent standard deviation is 7.37 mas giving a variability index of 1.16. The weighted radial extent standard deviation is 0.72 mas giving a variability index of 0.57.

This is **class B source**.

4.2.25 1908-201

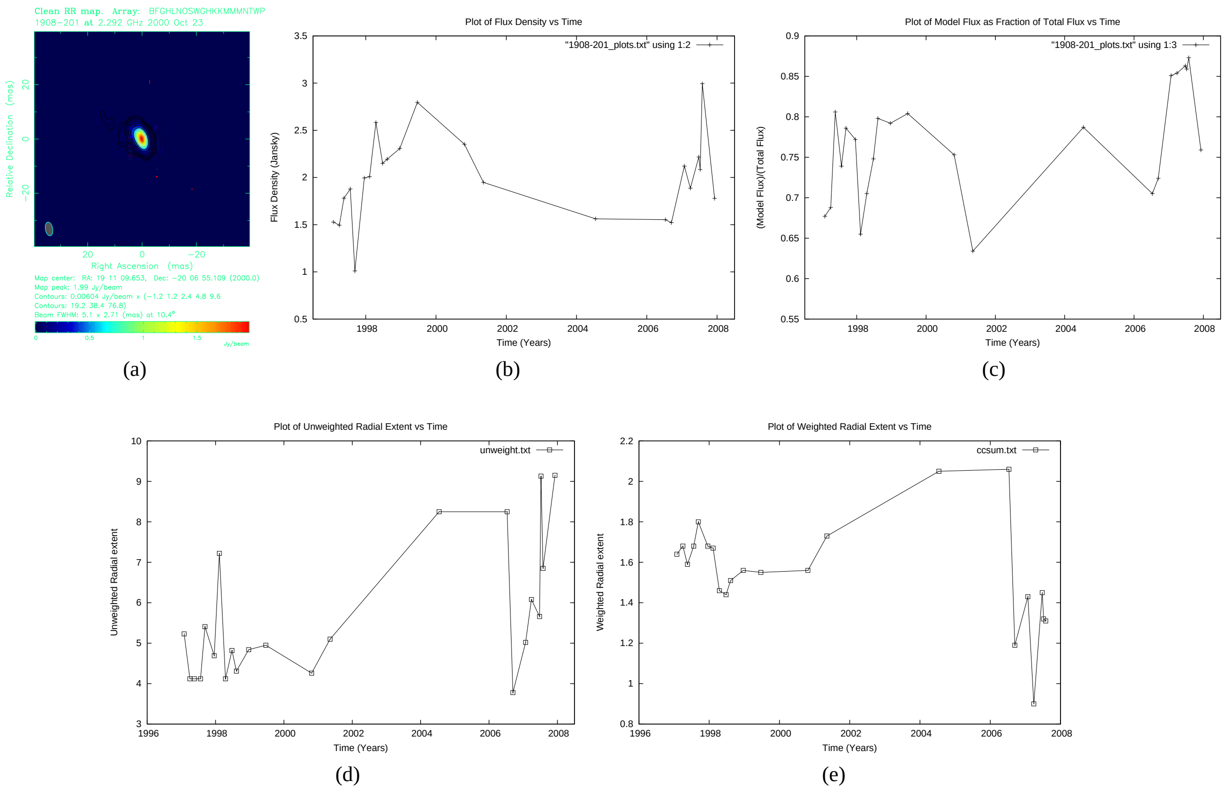

(a) (b) (c) (d) (e)

Figure 4.25: (a):Source image:1908-201. (b):Plot of Flux Density Variation. (c):Source Compactness. (d): Unweighted radial extent. (e): Weighted radial extent

This source is a quasar at a redshift of 1.12.

It has been fitted with multiple components for all epochs. The flux density falls between 1 Jy and 3 Jy with a mean of 1.99 Jy. The compactness is between 63% and 87% with a mean of 76.66%. The unweighted radial extent varies between 4 mas and 9 mas. The weighted radial extent falls between 1 mas and 2 mas .

The flux density standard deviation is 0.45 Jy giving a flux density variability index of 0.23. The compactness standard deviation is 7% giving a variability index of 0.09. The unweighted radial extent standard deviation is 1.68 mas giving a variability index of 0.30. The weighted radial extent standard deviation is 0.45 mas giving a variability index of 0.30. The variability index for the compactness shows there is little variation in the compactness. The variability indices for the radial extent show significant variation as does the flux density variability index.

This is a **class B source**.

4.2.26 1921-293

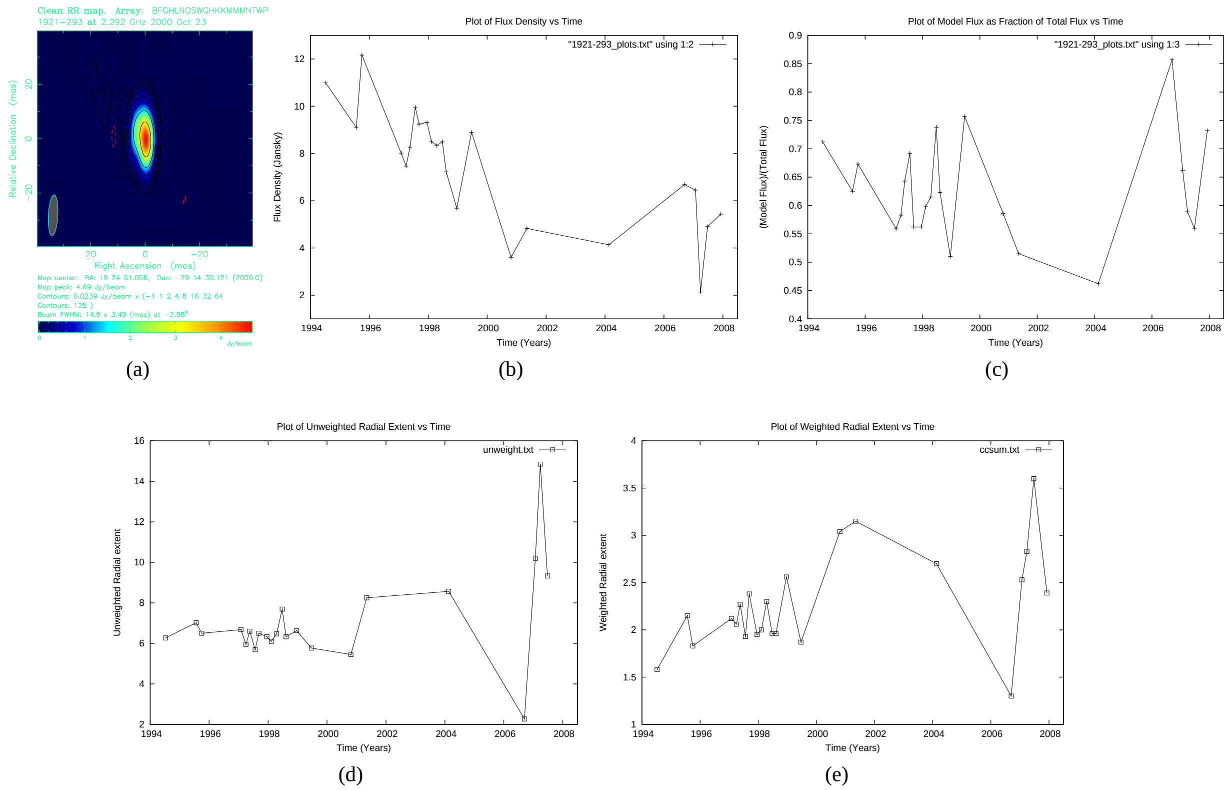

Figure 4.26: (a):Source image:1921-293. (b):Plot of Flux Density Variation. (c):Source Compactness. (d): Unweighted radial extent. (e): Weighted radial extent

This is the brightest source in the sample. It is a quasar at a redshift of 0.35. It has been imaged at 5 GHz and has a strong compact core with a flux density of 11.1 Jy (Shen et al., 1997). It is unresolved by the VLA (de Pater et al., 1985) at 5 GHz and at 1.4 GHz by the same instrument (Perley, 1982) but slightly resolved at 2.3 GHz on baselines to Australia (Preston et al., 1989).

From our observations, the source has a core flux density of 11 Jy in mid-1994. The image shows a slight component to the north-east, fig(a). Modelfits show 2 components for almost all epochs. The flux density falls slightly to 9 Jy and rises to a high of 12.16 Jy in October 1995, fig(b). After this, the core flux density in on a general downward trend, falling to 4.8 Jy on early 2001. The compactness varies a significantly, fig(c) with a mean of 62.7%. The unweighted radial extent varies very little between 1994 and 2004. Between 2004 and 2007, it falls to around 2 mas from around 8 mas and then it rises sharply to around 15 mas, fig(d). The weighted radial extent is also variable, fig(e). The flux density standard deviation is 2.45 Jy giving a flux density variability index of 0.33. The compactness standard deviation is 9% giving a variability index of 0.15. The unweighted radial extent standard deviation is 8.17 mas giving a variability index of 0.93. The weighted radial extent standard deviation is 0.53 mas giving a variability index of 0.23. This is a **class C source**.

4.2.27 1954-388

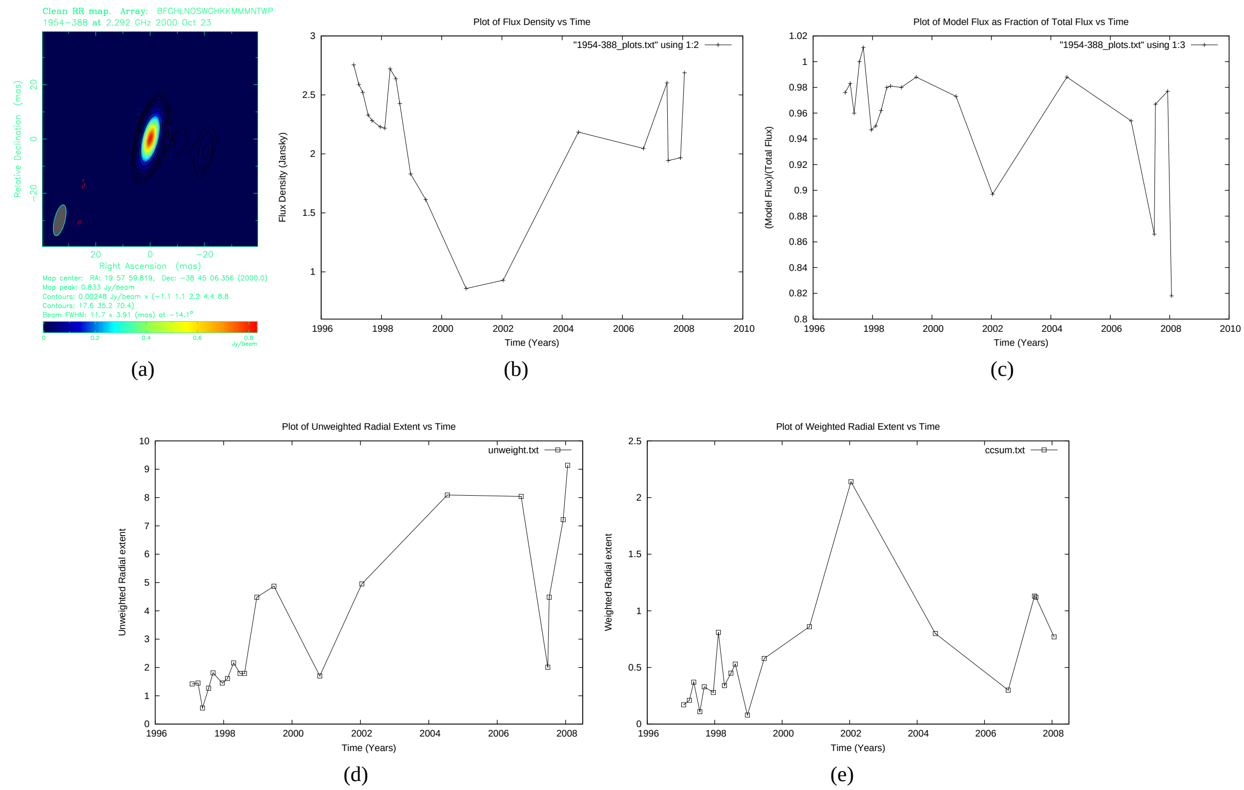

Figure 4.27: (a):Source image:1954-388. (b):Plot of Flux Density Variation. (c):Source Compactness. (d): Unweighted radial extent. (e): Weighted radial extent

This source is a quasar at a redshift of 0.63.

The image shows a component to the west, fig(a). Preston et al. (1985) show in a previous VLBI observation at 2.3 GHz, the presence of a very compact core. Shen et al. (1998b) also show a compact core with a flux density of 1.9 Jy at 5 GHz. The flux density in early 1997 is about 2.8 Jy but begins to fall in 1999 until it reaches a low of 0.85 Jy in late 2000, fig(b). After 2002, the flux density begin to go up and returns to previous levels above 2 Jy. It is very likely a component was ejected between 1998 and 2002 as the core compactness decreases during this period and the weighted radial extent goes up.

The flux density standard deviation is 0.54 Jy giving a flux density variability index of 0.25. The compactness mean is 95.79% with a standard deviation of 5% giving a variability index of 0.05. The unweighted radial extent standard deviation is 2.17 mas giving a variability index of 0.77. The weighted radial extent standard deviation is 0.52 mas giving a variability index of 0.93.

This source is a **class B source**. Its core is very compact but there is variation in the flux density and the radial extent.

4.2.28 1958-179

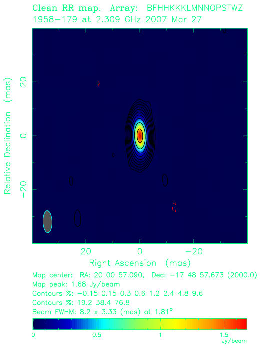

(a)

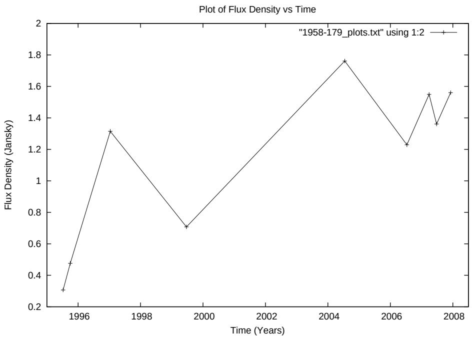

(b)

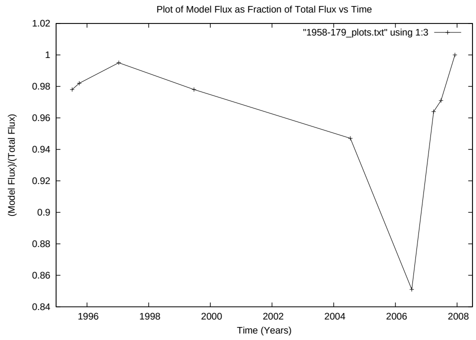

(c)

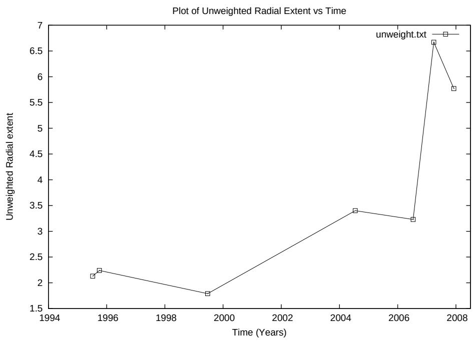

(d)

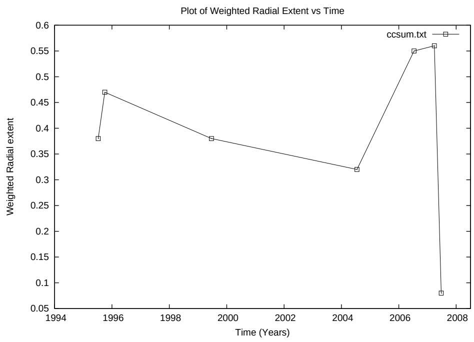

(e)

Figure 4.28: (a):Source image. (b):Plot of Flux Density Variation. (c):Source Compactness. (d): Unweighted radial extent. (e): Weighted radial extent

This source is a quasar at a redshift of 0.65. It is one of the least observed with only 9 epochs.

The flux density is on a general upward trend from 1998 to 2008, fig(b), peaking in 2004. The compactness is quite stable between 96% and 100% except for one point at 85% in 2006. The mean is 96.28%. The unweighted radial extent is also stable between 2 and 3 mas from 1995 to late 2006 but shoots up to 6.5 mas in early 2007.

The flux density standard deviation is 0.52 Jy giving a flux density variability index of 0.45. The compactness standard deviation is 4% giving a variability index of 0.05. The unweighted radial extent standard deviation is 2.29 mas giving a variability index of 0.82. The weighted radial extent standard deviation is 0.56 mas giving a variability index of 3.29.

This source is very compact but both the radial extents vary. It is **class B source**.

4.2.29 2052-474

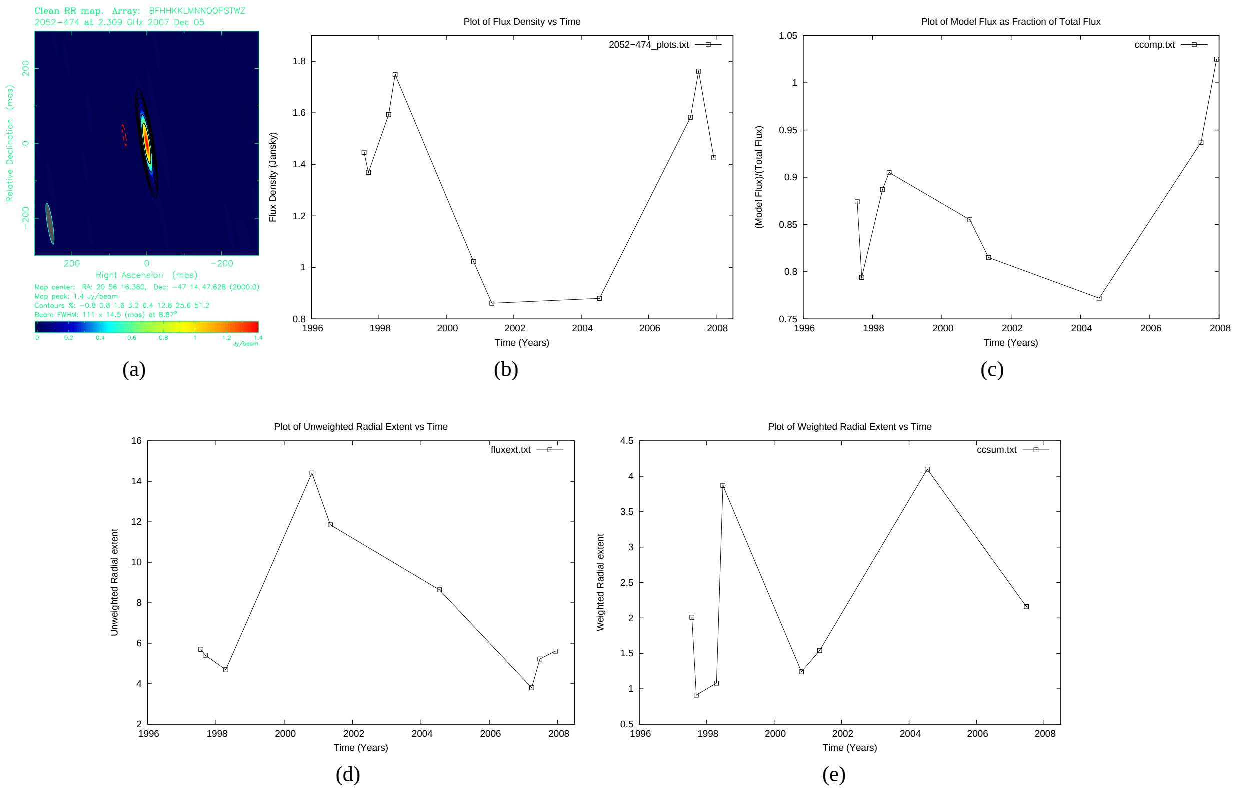

Figure 4.29: (a):Source image:2052-474. (b):Plot of Flux Density Variation. (c):Source Compactness. (d): Unweighted radial extent. (e): Weighted radial extent

2052-474 is the southern most source in the sample. It is a quasar at a redshift of 1.49. The beam is elongated in the north-south direction, fig(a), and this makes it difficult to resolve components in this direction. The source was observed in only 10 epochs.

Its flux density falls between 0.8 Jy and 1.7 Jy, fig(b), with a mean value of 1.37 Jy. The sources' highest value for radial extent coincides with its lowest value for flux density. It is very possible that a component was eject around this time (2001). The compactness varies between 75% and 100%, with a mean of 78.64%. This source was excluded from the ATCA intraday variability sample because of extended structure (Kedziora-Chudczer et al., 2001).

The flux density standard deviation is 0.34 Jy giving a flux density variability index of 0.25. The compactness standard deviation is 2.9% giving a variability index of 0.36. The unweighted radial extent standard deviation is 10.66 mas giving a variability index of 1.02. An index of 1.02 shows high variability. The weighted radial extent standard deviation is 2.09 mas giving a variability index of 1.56, showing very high variability in the radial extent. This source shows very high variability in the radial extent. It is relatively compact but the flux density also varies significantly. This is a **class D source**.

4.2.30 2243-123

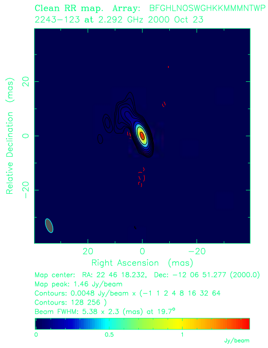

(a)

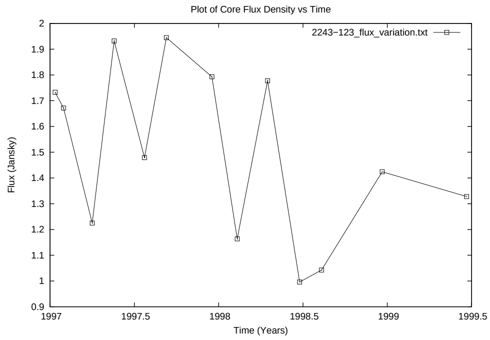

(b)

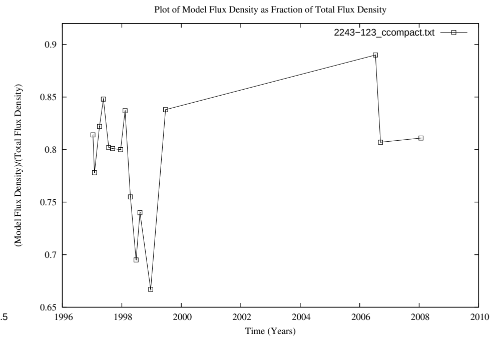

(c)

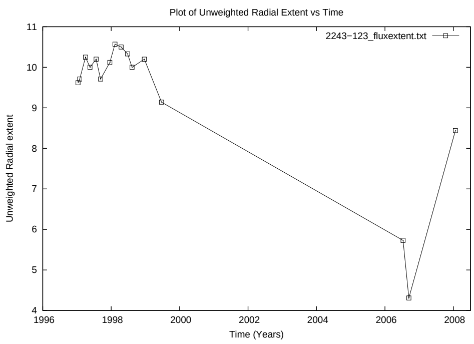

(d)

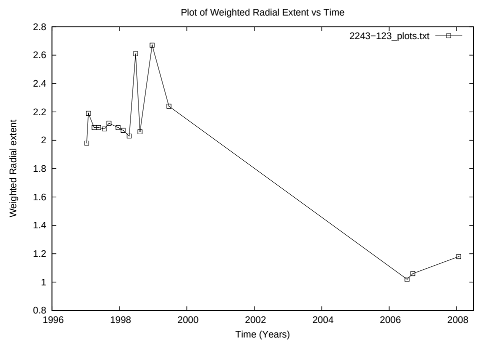

(e)

Figure 4.30: (a):Source image:2243-123. (b):Plot of Flux Density Variation. (c):Source Compactness. (d): Unweighted radial extent. (e): Weighted radial extent

2243-123 was named as a superluminal candidate by Hong et al. (1999) and has been detected in the X-ray and γ-ray (Maisack et al., 1994; Fichtel et al., 1994). It is a quasar at a redshift of 0.63.

It is quite extended in the north-east direction, fig(a). It is resolved with the VLA showing an extended component at 4" from the core (Morganti et al., 1993). The flux density varies between 1 Jy and 2 Jy, fig(b), with a mean of 1.5 Jy. The core compactness varies between about 65% and 90%, (fig(c)) with a mean of 79.40%. The unweighted radial extent is quite high in earlier epochs (around 10 mas) but begins to fall in 2000, falling to about 4 mas by late 2006, fig(d). Although the numbers are different, the trend is the same for the weighted radial extent, fig(e).

The flux density standard deviation is 0.33 Jy giving a flux density index of 0.22. The compactness standard deviation is 6% giving a variability index of 0.07. The unweighted radial extent standard deviation is 1.77 mas giving an index of 0.19. The weighted radial extent standard deviation is 0.48 mas giving an index of 0.24.

This is a **class B source**.

4.2.31 2255-282

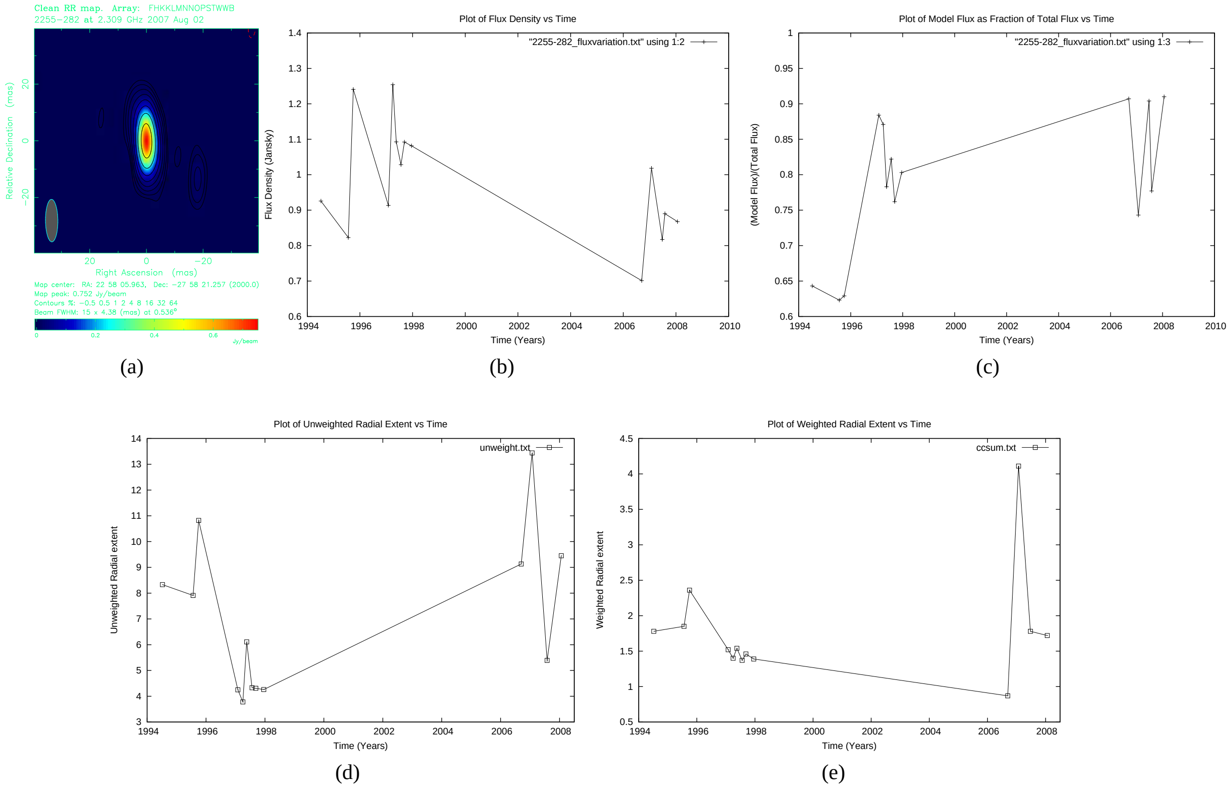

Figure 4.31: (a):Source image:2255-282. (b):Plot of Flux Density Variation. (c):Source Compactness. (d): Unweighted radial extent. (e): Weighted radial extent.

2255-282 is a quasar at a redshift of 0.93. It has a component to the south-west, fig(a). Modelfits show 2 components for most epochs (see Appendix A). A γ-ray flare was detected from this source by EGRET in early January 1998 (Macomb et al., 1999). Prior to this flare, this source did not receive much attention. It had no prominent radio or optical bursts recorded in the literature and was classified as a low-priority source in an AGN monitoring program undertaken by Tornikoski et al. (1996). The flux density falls between 0.7 Jy and 1.25 Jy, fig (b). In mid-1994, the source has a core flux density of about 0.93 Jy which drops to 0.82 Jy in mid-1995 then it peaks to 1.24 Jy. It falls again to 0.91 Jy and peaks in early 1997 to a high of 1.25 Jy but falls just before the flare (December 1997). In April 1997, this source was observed to have a flux density of 8 Jy at 90 GHz, which was about twice the flux density which had been observed about a year earlier (Tornikoski et al., 1999). Our observations on 31 March 1997 gives the highest core flux density for all epochs and it is possible there was a wave outburst around this time which resulted in an increase in the flux density and coincides with the flare in the millimeter regime. The compactness ranges from about 62% to 90% with a mean of 79%, fig (c). The standard deviation is 10% and the compactness index of 0.13. The unweighted radial extent mean is 6.54 mas with a standard deviation of 3.49 mas and an index of 0.53. The weighted radial extent mean is

2.29 mas with a standard deviation of 2.05 mas and an index of 0.89. This source is not very compact, has a component and is quite active, it is a **class D source**.

4.3 Summary of Results

Results and figures for all sources discussed above are summarised in Table 4.4

Table 4.4: Results of variability analysis in the flux density, compactness and radial extent.

Source Name	Core Flux Density		Compactness		Unweighted Radial Extent		Weighted Radial Extent	
	σ_{core}	$\sigma_{core}/\bar{S}$	σ_C	$\sigma_C/\bar{C}$	$\sigma_{R_{UW}}$	$\sigma_{R_{UW}}/\bar{R}_{UW}$	σ_{R_W}	$\sigma_{R_W}/\bar{R}_W$
0003-066	0.31	0.20	0.07	0.11	2.22	0.36	0.40	0.24
0104-408	0.29	0.23	0.04	0.04	17.13	2.18	1.24	1.33
0238-084	0.20	0.22	0.10	0.19	16.13	0.93	0.10	0.27
0336-019	0.48	0.25	0.08	0.10	2.32	0.76	0.64	0.64
0402-362	0.11	0.09	0.03	0.03	4.54	0.56	0.26	0.22
0454-234	0.59	0.34	0.02	0.02	1.78	0.56	0.31	0.67
0458-020	0.31	0.40	0.15	0.22	17.93	1.10	1.02	0.46
0537-441	0.74	0.24	0.21	0.23	18.23	2.29	4.09	2.38
0727-115	0.71	0.30	0.05	0.06	1.77	0.29	0.30	0.26
0919-260	0.83	0.63	0.11	0.15	1.55	0.24	0.34	0.20
0920-397	0.18	0.17	0.11	0.12	2.98	0.41	0.94	0.52
1034-293	0.30	0.27	0.21	0.24	8.22	1.41	0.68	0.75
1124-186	0.19	0.21	0.02	0.02	16.50	2.40	0.29	1.18
1144-379	0.39	0.29	0.05	0.06	20.66	2.15	1.79	4.10
1145-071	0.11	0.16	0.10	0.13	2.26	0.37	0.24	0.18
1253-055	0.27	0.04	0.15	0.23	0.50	0.04	0.25	0.11
1255-316	0.24	0.20	0.11	0.14	11.86	0.84	0.67	0.25
1313-333	0.28	0.35	0.05	0.07	3.05	0.39	0.40	0.31
1334-127	0.55	0.26	0.04	0.04	1.87	0.52	0.62	0.74
1351-018	0.25	0.32	0.03	0.03	1.86	0.73	2.93	1.94
1424-418	0.49	0.29	0.08	0.11	11.07	0.47	1.88	0.55
1451-375	0.30	0.27	0.07	0.08	5.40	0.58	3.71	10.08
1514-241	0.30	0.17	0.05	0.06	3.90	0.21	0.78	0.23
1622-253	0.38	0.30	0.05	0.06	7.37	1.16	0.72	0.57
1741-038	1.05	0.33	0.03	0.03	1.24	0.57	0.22	0.66
1908-201	0.45	0.23	0.07	0.09	1.68	0.30	0.45	0.30
1921-293	2.45	0.33	0.09	0.15	8.17	0.93	0.53	0.23
1954-388	0.54	0.25	0.05	0.05	2.71	0.77	0.52	0.93
1958-179	0.52	0.45	0.04	0.05	2.29	0.82	0.56	3.29
2052-474	0.34	0.25	0.29	0.36	10.66	1.02	2.09	1.56
2243-123	0.33	0.22	0.06	0.07	1.77	0.19	0.48	0.24
2255-282	1.11	1.17	0.10	0.13	3.49	0.53	2.05	0.89

Table 4.5: Classification of the Sources.

Source Name	Core Flux Density $\sigma_{core}/\bar{S}$	W	Compactness mean μ	W	Unweighted R.E $\sigma_{R_{UW}}/\bar{R}_{UW}$	W	Weighted R.E $\sigma_{R_W}/\bar{R}_W$	W	Image %	Sum of Weights (%)	Class
0003-066	0.20	10	68	10	0.36	16	0.24	16	8	60	C
0104-408	0.23	8	96	40	2.18	2	1.33	2	8	60	C
0238-084	0.22	8	52	0	0.93	4	0.27	16	2	30	D
0336-019	0.25	8	87	30	0.76	8	0.64	8	6	60	C
0402-362	0.09	10	92	40	0.56	12	0.22	16	4	82	A
0454-234	0.34	8	94	40	0.56	12	0.67	8	10	78	B
0458-020	0.40	8	67	10	1.10	2	0.46	12	4	36	D
0727-115	0.30	8	85	30	0.29	16	0.26	16	6	76	B
0919-260	0.63	4	74	20	0.24	16	0.20	20	6	66	B
0920-397	0.17	10	85	30	0.41	12	0.52	12	10	74	B
1034-293	0.27	8	87	30	1.41	2	0.75	8	8	56	C
1124-186	0.21	8	98	40	2.40	2	1.18	2	10	62	B
1144-379	0.29	8	92	40	2.15	2	4.10	2	8	60	C
1145-071	0.16	10	80	30	0.37	16	0.18	20	6	82	A
1253-055	0.04	10	64	10	0.04	20	0.11	20	2	62	B
1255-316	0.20	10	78	20	0.84	4	0.25	16	6	56	C
1313-333	0.35	8	78	20	0.39	16	0.31	16	4	64	B
1334-127	0.26	8	94	40	0.52	12	0.74	8	8	76	B
1351-018	0.32	8	94	40	0.73	8	1.94	2	6	64	B
1424-418	0.29	8	79	20	0.47	12	0.55	12	6	58	C
1451-375	0.27	8	88	30	0.58	12	10.08	2	6	58	C
1514-241	0.17	10	79	20	0.21	16	0.23	16	2	64	B
1622-253	0.30	8	90	40	1.16	2	0.57	12	6	68	B
1741-038	0.33	8	96	40	0.57	12	0.66	8	8	76	B
1908-201	0.23	8	77	20	0.30	16	0.30	16	6	66	B
1921-293	0.33	8	63	10	0.93	4	0.23	16	4	42	C
1954-388	0.25	8	96	40	0.77	8	0.93	4	4	64	B
1958-179	0.45	6	96	40	0.82	4	3.29	2	10	62	B
2052-474	0.25	8	79	20	1.02	2	1.56	2	8	40	D
2243-123	0.22	8	79	20	0.19	20	0.24	16	4	68	B
2255-282	1.17	2	79	20	0.53	12	0.89	4	4	42	D

Chapter 5

Discussion

5.1 Discussion

The 31 sources in this thesis are a subset of sources in the the RRFID Kinematic survey. While the Kinematic survey looks more at proper motion in the sources at 8.4 GHz, this thesis concentrates on the calibrator properties of the sources at 2.3 GHz, with the goal of developing a way to quantify how good a source is as a calibrator. A calibrator should ideally be compact, unresolved, bright and the flux density should be stable. Unfortunately, there is no such thing as a perfect calibrator. Most calibrator sources are AGN and these are known to vary at almost all wavelengths at which they have been observed. They are also known to show structure down to milliarcsecond scales. It is therefore necessary to monitor calibrators at different frequencies and resolutions and tailor them for a particular application. The sources in this thesis can be used for medium to long baselines. These sources have been observed at some of the longest baselines possible with very high resolution, milliarcsecond scale, and so are resolved. For telescopes like meerKAT, ASKAP and SKA, most of these sources can be used as calibrators as they are unlikely to be resolved by these telescopes.

The sources were observed using the technique of VLBI, with the VLBA as the core of all observations together with a global array of telescopes. They are part of the RRFID, which is a result of the USNO's ongoing program to image the radio reference frame sources on a regular basis. The observation epochs are from July 1994 to January 2008, giving a total of 32 epochs and an average of 20 epochs for the 31 sources. Observations were made in dual frequency bandwidth synthesis mode, allowing imaging at both frequency bands (2.3 and 8.4 GHz). The data were correlated at the Array Operations Center in Socorro, New Mexico. The data were calibrated using AIPS. System temperature tables and gain curves generated during observations were used to calibrate the amplitudes. Imaging was done in interactive mode in Difmap due due poor u-v coverage. Models were fit to the visibility data in Difmap. Modelfitting is used to parameterize characteristics of the sources, in particular to determine component location and flux density.

To analyse the data, I used a combination of the source image, the core flux density, the compactness, the unweighted radial extent and the weighted radial extent. The image gives an idea of the source morphology. The core flux density was determined using the Gaussian component I fit to the core. This was done for all epochs at which each source was observed. A plot of core flux density against time was then made for each source. The compactness gives an indication of how point like a source is and is calculated by dividing the core flux density by the total flux density. The unweighted radial extent provides a measure of how extended a source is. It is the radius within which 95% of the flux density is contained. The weighted radial extent gives another measure of core-dominance. The presence and magnitude of proper motion is an important additional criteria that can be used to analyse and categorise the sources as calibrators.

From the above criteria, the standard deviation and a variability index was calculated for each parameter for each source. The mean compactness for all the source is 82.77% with a standard deviation of 11.54%. All sources have a mean compactness variability index below 0.40. 27 sources have a variability index between 0 and 0.2 and the remaining 4 between 0.21 and 0.40, see Figure 5.1. An index of 0.0 shows no variation at all. In general, the southern sample sources are very compact with little variation.

90% of the sources have a core flux density variability index below 0.4, with 29% of these having a variability index below 0.2, see Figure 5.1. This also shows these sources generally have stable core flux densities. The unweighted radial extent variability index of more widely distributed. 6% of the sources have an index below 0.2, 23% have an index between 0.21 and 0.40 while 26% have an index between 0.41 and 0.60. About 10% have an index between 0.61 and 0.80 while 35% have an index greater than 0.80, showing very high variability in the unweighted radial extent. The weighted radial extent is also widely distributed with 10% of the sources having an index between 0 and 0.2, showing minimal variation in the weighted radial extent. 32% of the sources have an index between 0.21 and 0.40 while 13% have an index between 0.41 and 0.60. 16% of the sources have an index between 0.61 and 0.80 giving a rest (29%) have an index greater than 0.81. Again, this shows a very high degree of variability in the weighted radial extent.

The source image, variability indices and the mean compactness were given each a score whose total determined which calibrator class an image would fall into. The mean compactness has a weight of 40%, the source image 10%, the core variability index 10% and the weighted and unweighted radial extent 20% each. A source falls into class A if its overall score is between 80 and 100%, class B if the score is between 60 and 80%, class C is if scores between 40 and 60% and class D for any score below 40%. From our classification scheme, we have 2 class A sources, 16 class B sources, 9 class C sources and 4 class D sources.

We have developed a multi-parameter method to judge and classify sources into different calibrator categories. This classification scheme is by no way complete but provides a good starting point. All the sources in this sample are relatively bright with $S_{\mu} > 300$ mJy. One source, 0238-084 has a double-jets structure. The rest of the sources have been noted to have a core-jet structure on mas scales and some might exhibit superluminal motion as can be seen from the modelfits.

This work is also useful for the ICRF which suffers from a deficit of southern sources with an average of one source per 8x8 degrees on the sky (Charlot et al., 2000), VSOP-2 (VLBI Space Observatory Programme-2) which will observe with both northern and southern telescopes, and any other VLBI observations involving telescopes in the southern hemisphere.

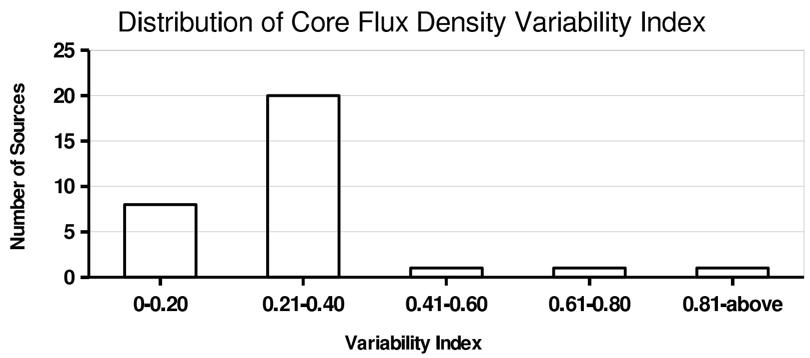

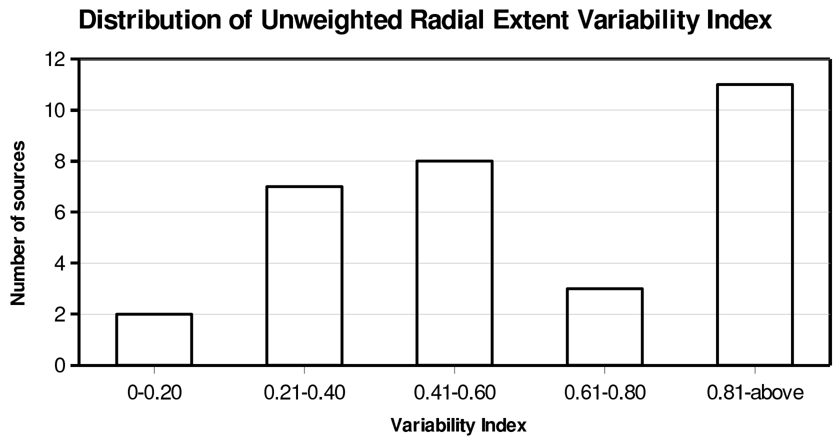

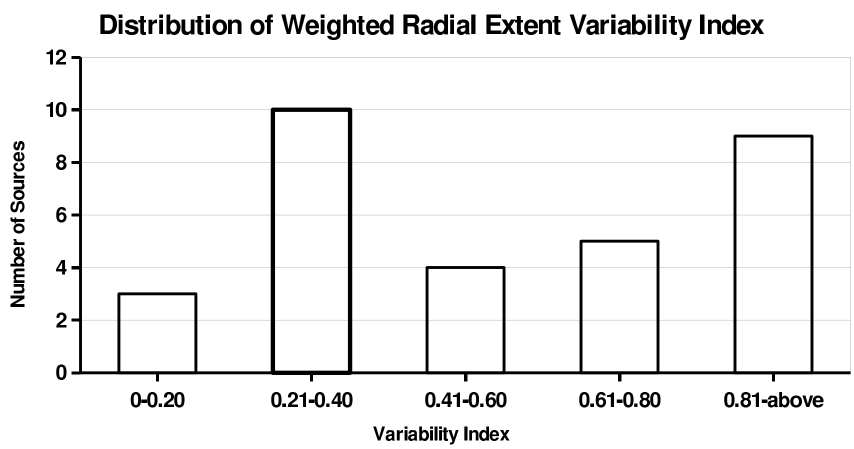

Figure 5.1: Distribution of the Variability Indices for the Measured Parameters

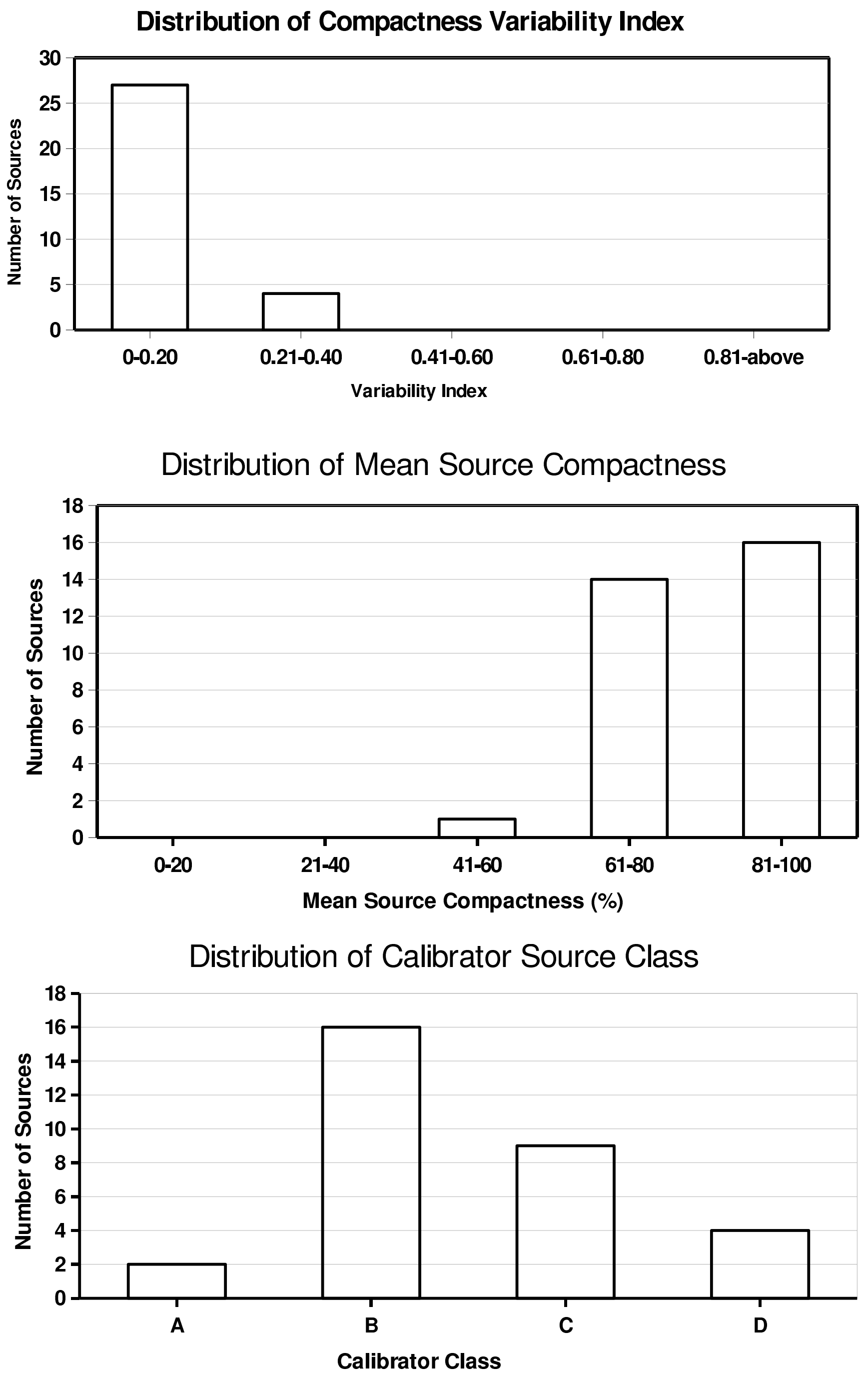

Figure 5.2: Distribution of the Variability Indices for the Measured Parameters

5.2 Conclusions and Future Work

We have developed a multi-parameter method to classify sources as calibrators. This was achieved by fitting Gaussian models to the visibility data of the sources. From this, the core flux density and source compactness was determined. The weighted and unweighted radial extent were also determined and together with the source image, these parameters were used to classify the sources. This classification scheme yielded 2 class A sources (6%), 16 class B sources (52%), 9 class C sources (29%) and 4 class D sources (13%).

This classification scheme can be improved on by looking at the presence and magnitude of proper motion in the sources. This will be used as an additional criteria to classify the sources. The modelfits have already been done but this is beyond the scope of this thesis but will be included in future work. Sources 1334-127 and 2243-123 are named as superluminal candidates in the literature and it is worthwhile to investigate further to see if these sources exhibit superluminal motion at 2.3 GHz. 1253-055 is a confirmed superluminal source and it is worthwhile to determine the apparent speed at 2.3 GHz and compare it with the published data. It is also worthwhile to follow up on sources that have been fitted with more that one component at other frequencies to see if the same components are fitted at the same position angle and radius from the phase centre. This can help answer questions on the nature of AGN jets.

Sources 1334-127 and 2255-282 are known to have undergone flares in 1992 and 1998 respectively. We have a number of epochs of radio data for the source 2255-282 prior and around the time of the flare. It is worthwhile to investigate if a radio flare occurred before or after the γ-ray flare. This will help in the understanding of the energetics of outbursts

Finally, I also intend to observe and analyze more sources in order to densify the southern hemisphere calibrator grid and to gather and measure improved positions for these and potential calibrator sources.

Bibliography

Alfvén, H. & Herlofson, N. 1950, Physical Review, 78, 616

Beasley, A. J., Gordon, D., Peck, A. B., Petrov, L., MacMillan, D. S., Fomalont, E. B., & Ma, C. 2002, ApJS, 141, 13

Begelman, M. C., Blandford, R. D., & Rees, M. J. 1984, Reviews of Modern Physics, 56, 255

Blandford, R. D. 1990, in Active Galactic Nuclei, ed. R. D. Blandford, H. Netzer, L. Woltjer, T. J.-L. Courvoisier, & M. Mayor, 161–275

Bridle, A. H., Hough, D. H., Lonsdale, C. J., Burns, J. O., & Laing, R. A. 1994, AJ, 108, 766

Carilli, C. L. & Rawlings, S. 2004, New Astronomy Review, 48, 979

Charlot, P., Viateau, B., Baudry, A., Ma, C., Fey, A., Eubanks, M., Jacobs, C., & Sovers, O. 2000, in International VLBI Service for Geodesy and Astrometry: 2000 General Meeting Proceedings, p. 168, ed. F. Takahashi, 168–+

Cohen, M. H., Cannon, W., Purcell, G. H., Shaffer, D. B., Broderick, J. J., Kellermann, K. I., & Jauncey, D. L. 1971, ApJ, 170, 207

Cordes, J. 2009, Astronomy, 2010, 56

Costa, E. & Loyola, P. 1992, Astron. Astrophys. Suppl. Ser., 96, 183

Cotton, W. D., Counselman, III, C. C., Geller, R. B., Shapiro, I. I., Wittels, J. J., Hinteregger, H. F., Knight, C. A., Rogers, A. E. E., Whitney, A. R., & Clark, T. A. 1979, ApJL, 229, L115

Curran, S. J., Aalto, S., & Booth, R. S. 2000, Astron. Astrophys. Suppl. Ser., 141, 193

de Pater, I., Schloerb, F. P., & Johnson, A. H. 1985, AJ, 90, 846

Diamond, P. J. 1995, in Astronomical Society of the Pacific Conference Series, Vol. 82, Very Long Baseline Interferometry and the VLBA, ed. J. A. Zensus, P. J. Diamond, & P. J. Napier, 227–+

Djorgovski, S. G. 1987, Sky & Telescope, 74, 237

Fanaroff, B. L. & Riley, J. M. 1974, MNRAS, 167, 31P

Fey, A. & Charlot, P. 1996, in Bulletin of the American Astronomical Society, Vol. 28, Bulletin of the American Astronomical Society, 1292–+

Fey, A. L. & Charlot, P. 1997, ApJS, 111, 95

—. 2000, ApJS, 128, 17

Fichtel, C. E., Bertsch, D. L., Chiang, J., Dingus, B. L., Esposito, J. A., Fierro, J. M., Hartman, R. C., Hunter, S. D., Kanbach, G., Kniffen, D. A., Kwok, P. W., Lin, Y. C., Mattox, J. R., Mayer-Hasselwander, H. A., McDonald, L., Michelson, P. F., von Montigny, C., Nolan, P. L., Pinkau, K., Radecke, H.-D., Rothermel, H., Sreekumar, P., Sommer, M., Schneid, E. J., Thompson, D. J., & Willis, T. 1994, ApJS, 94, 551

Fiedler, R. L., Waltman, E. B., Spencer, J. H., Johnston, K. J., Angerhofer, P. E., Florkowski, D. R., Josties, F. J., Klepczynski, W. J., McCarthy, D. D., & Matsakis, D. N. 1987, ApJS, 65, 319

Fomalont, E. B., Petrov, L., MacMillan, D. S., Gordon, D., & Ma, C. 2003, AJ, 126, 2562

Frey, S., Gurvits, L. I., Kellermann, K. I., Schilizzi, R. T., & Pauliny-Toth, I. I. K. 1997, Astron. Astrophys., 325, 511

Greenstein, J. L. 1963, Nat, 197, 1041

Hjellming, R. M. & Narayan, R. 1986, ApJ, 310, 768

Hong, X. Y., Venturi, T., Wan, T. S., Jiang, D. R., Shen, Z.-Q., Liu, X., Nicolson, G., & Umana, G. 1999, Astron. Astrophys. Suppl. Ser., 134, 201

Impey, C. D. & Tapia, S. 1988, ApJ, 333, 666

Jonas, J. 2007, in From Planets to Dark Energy: the Modern Radio Universe. October 1-5 2007, The University of Manchester, UK. Published online at SISSA, Proceedings of Science, p.7

Jorstad, S. G., Marscher, A. P., Lister, M. L., Stirling, A. M., Cawthorne, T. V., Gómez, J.-L., & Gear, W. K. 2004, AJ, 127, 3115

Kadler, M., Kerp, J., Ros, E., Falcke, H., Pogge, R. W., & Zensus, J. A. 2004a, Astron. Astrophys., 420, 467

Kadler, M., Ros, E., Lobanov, A. P., Falcke, H., & Zensus, J. A. 2004b, Astron. Astrophys., 426, 481

Kedziora-Chudczer, L. L., Jauncey, D. L., Wieringa, M. H., Tzioumis, A. K., & Reynolds, J. E. 2001, MNRAS, 325, 1411

Kellermann, K. 2009, Astronomy, 2010, 154

Khachikian, E. Y. & Weedman, D. W. 1974, ApJ, 192, 581

Knight, C. A., Robertson, D. S., Rogers, A. E. E., Shapiro, I. I., Whitney, A. R., Clark, T. A., Goldstein, R. M., Marandino, G. E., & Vandenberg, N. R. 1971, Science, 172, 52

Kovalev, Y. Y., Petrov, L., Fomalont, E. B., & Gordon, D. 2007, AJ, 133, 1236

Laing, R. A. & Bridle, A. H. 1987, MNRAS, 228, 557

Lazio, J. 2009, Astronomy, 2010, 176

Lindfors, E. J., Türler, M., Valtaoja, E., Aller, H., Aller, M., Mazin, D., Raiteri, C. M., Stevens, J. A., Tornikoski, M., Tosti, G., & Villata, M. 2006, Astron. Astrophys., 456, 895

Macomb, D. J., Gehrels, N., & Shrader, C. R. 1999, ApJ, 513, 652

Maisack, M., Wood, K. S., & Gruber, D. E. 1994, Astron. Astrophys., 284, 28

Morganti, R., Killeen, N. E. B., & Tadhunter, C. N. 1993, MNRAS, 263, 1023

Myers, S. T. 2009, Astronomy, 2010, 219

Napier, P. J. 1995, in Astronomical Society of the Pacific Conference Series, Vol. 82, Very Long Baseline Interferometry and the VLBA, ed. J. A. Zensus, P. J. Diamond, & P. J. Napier, 59–+

Neff, S. G. & Hutchings, J. B. 1990, AJ, 100, 1441

Ojha, R., Fey, A. L., Charlot, P., Jauncey, D. L., Johnston, K. J., Reynolds, J. E., Tzioumis, A. K., Quick, J. F. H., Nicolson, G. D., Ellingsen, S. P., McCulloch, P. M., & Koyama, Y. 2005, AJ, 130, 2529

Ojha, R., Fey, A. L., Johnston, K. J., Jauncey, D. L., Reynolds, J. E., Tzioumis, A. K., Quick, J. F. H., Nicolson, G. D., Ellingsen, S. P., Dodson, R. G., & McCulloch, P. M. 2004, AJ, 127, 3609

Oke, J. B. 1963, Nat, 197, 1040

Perley, R. A. 1982, AJ, 87, 859

Petrov, L., Kovalev, Y. Y., Fomalont, E., & Gordon, D. 2005, AJ, 129, 1163

Petrov, L., Kovalev, Y. Y., Fomalont, E. B., & Gordon, D. 2006, AJ, 131, 1872

—. 2008, AJ, 136, 580

Phinney, E. S. 1985, in Astrophysics of Active Galaxies and Quasi-Stellar Objects, ed. J. S. Miller, 453–496

Piner, B. G., Mahmud, M., Fey, A. L., & Gospodinova, K. 2007, AJ, 133, 2357

Preston, R. A., Jauncey, D. L., Meier, D. L., Tzioumis, A. K., Ables, J., Batchelor, R., Faulkner, J., Gates, J., Greene, B., Hamilton, P. A., Harvey, B. R., Haynes, R. F., Johnson, B., Lambeck, K., Louie, A. P., McCulloch, P., Moorey, G., Morabito, D. D., Nicolson, G. D., Niell, A. E., Robertson, J. G., Royle, G. R., Skjerve, L., Slade, M. A., Slee, O. B., Stolz, A., Watkinson, A., Wehrle, A. E., & Wright, A. E. 1989, AJ, 98, 1

Preston, R. A., Morabito, D. D., Williams, J. G., Faulkner, J., Jauncey, D. L., & Nicolson, G. 1985, AJ, 90, 1599

Punsly, B., Rodríguez, L. F., Tingay, S. J., & Cellone, S. A. 2005, ApJL, 633, L93

Putman, M. E. 2009, Astronomy, 2010, 241

Quirrenbach, A., Witzel, A., Kirchbaum, T. P., Hummel, C. A., Wegner, R., Schalinski, C. J., Ott, M., Alberdi, A., & Rioja, M. 1992, Astron. Astrophys., 258, 279

Schmidt, M. 1963, Nat, 197, 1040

Seyfert, C. K. 1943, ApJ, 97, 28

Shen, Z.-Q., Wan, T.-S., Moran, J. M., Jauncey, D. L., Reynolds, J. E., Tzioumis, A. K., Gough, R. G., Ferris, R. H., Sinclair, M. W., Jiang, D.-R., Hong, X.-Y., Liang, S.-G., Costa, M. E., Tingay, S. J., McCulloch, P. M., Lovell, J. E. J., King, E. A., Nicolson, G. D., Murphy, D. W., Meier, D. L., van Ommen, R. D., Edwards, P. G., & White, G. L. 1997, AJ, 114, 1999

Shen, Z.-Q., Wan, T.-S., Moran, J. M., Jauncey, D. L., Reynolds, J. E., Tzioumis, A. K., Gough, R. G., Ferris, R. H., Sinclair, M. W., Jiang, D.-R., Hong, X.-Y., Liang, S.-G., Edwards, P. G., Costa, M. E., Tingay, S. J., McCulloch, P. M., Lovell, J. E. J., King, E. A., Nicolson, G. D., Murphy, D. W., Meier, D. L., van Ommen, T. D., & White, G. L. 1998a, AJ, 115, 1357

—. 1998b, AJ, 115, 1357

Tingay, S. J., Jauncey, D. L., King, E. A., Tzioumis, A. K., Lovell, J. E. J., & Edwards, P. G. 2003, PASJ, 55, 351

Tornikoski, M., Tingay, S. J., Mücke, A., Chen, A., Connaughton, V., Jauncey, D. L., Johnston-Hollitt, M., Kemp, J., King, E. A., McGee, P., Rantakyrö, F., Rayner, D., Reimer, O., & Tzioumis, A. K. 1999, AJ, 118, 1161

Tornikoski, M., Valtaoja, E., Teraesranta, H., Karlamaa, K., Lainela, M., Nilsson, K., Kotilainen, J., Laine, S., Laehteenmaeki, A., Knee, L. B. G., & Botti, L. C. L. 1996, Astron. Astrophys. Suppl. Ser., 116, 157

Véron-Cetty, M.-P. & Véron, P. 2003, Astron. Astrophys., 412, 399

von Montigny, C., Bertsch, D. L., Chiang, J., Dingus, B. L., Esposito, J. A., Fichtel, C. E., Fierro, J. M., Hartman, R. C., Hunter, S. D., Kanbach, G., Kniffen, D. A., Lin, Y. C., Mattox, J. R., Mayer-Hasselwander, H. A., Michelson, P. F., Nolan, P. L., Radecke, H. D., Schneid, E., Sreekumar, P., Thompson, D. J., & Willis, T. 1995, ApJ, 440, 525

Wardle, J. F. C., Homan, D. C., Ojha, R., & Roberts, D. H. 1998, Nat, 395, 457

Wehrle, A. E., Cohen, M. H., Unwin, S. C., Aller, H. D., Aller, M. F., & Nicolson, G. 1992, ApJ, 391, 589

Wehrle, A. E., Piner, B. G., Unwin, S. C., Zook, A. C., Xu, W., Marscher, A. P., Teräsranta, H., & Valtaoja, E. 2001, ApJS, 133, 297

Whitney, A. R., Shapiro, I. I., Rogers, A. E. E., Robertson, D. S., Knight, C. A., Clark, T. A., Goldstein, R. M., Marandino, G. E., & Vandenberg, N. R. 1971, Science, 173, 225

Appendix A

Modelfits

The models fitted to the visibility data are of Gaussian form with flux density S and FWHM major axis a, with major axis in position angle ϕ (measured north through east). Components are separated from the (arbitrary) origin of the image by an amount r in position angle θ, which is the position angle (measured north through east) of a line joining the components with the origin. The source name is derived from B1950 co-ordinates. The components are assigned a number, 0 representing the core component. 99 represents unidentified components that could not be linked to components in other epochs.

These are raw results from the model-fitting algorithm hence the variation in significant figures. Some components have $r = 0$ and this is only a result of the model-fitting process and has no physical meaning.

Table A.1: Derived parameters of sources in sample.

Source Name	*Epoch*	*Component*	S (Jy)	a (mas)	ϕ (deg)	*Axial Ratio*	r (mas)	θ (deg)
$0003-066$	1995.78	0	2.2884	0.260	128.67	1.00000	1.224	-30.440
	1995.78	1	0.5290	3.941	-71.76	1.00000	3.330	-10.567
	1997.08	0	1.4763	0.227	134.34	1.00000	1.516	-11.083
	1997.08	1	0.6710	2.928	-73.36	1.00000	4.236	15.828
	1997.25	0	1.4594	0.235	135.87	1.00000	1.551	2.670
	1997.25	1	0.6374	3.034	-72.72	1.00000	3.842	9.666
	1997.38	0	1.4645	0.291	119.25	1.00000	1.305	16.374
	1997.38	1	0.7847	2.718	-74.28	1.00000	4.024	26.091
	1997.56	0	1.4111	0.301	113.29	1.00000	1.399	0.000
	1997.56	1	0.7174	2.912	-74.00	1.00000	3.925	15.219
	1997.69	0	1.5232	0.371	135.07	1.00000	1.569	-15.219
	1997.69	1	0.6735	3.083	-73.08	1.00000	3.858	-30.059
	1997.96	0	1.4642	0.345	125.22	1.00000	1.390	-10.097
	1997.96	1	0.7512	2.932	-73.72	1.00000	3.748	-4.002
	1998.11	0	1.2724	0.248	126.81	1.00000	1.331	-9.806
	1998.11	1	0.7387	2.932	-72.03	1.00000	3.827	-26.091
	1998.29	0	1.3181	0.296	126.36	1.00000	1.239	-108.796
	1998.29	1	0.7671	2.836	-74.23	1.00000	3.929	0.000
	1998.48	0	1.2266	0.303	116.73	1.00000	1.183	0.000
	1998.48	1	0.8329	2.735	-70.35	1.00000	4.402	-26.091
	1998.61	0	1.2581	0.283	134.63	1.00000	1.099	0.000
	1998.61	1	0.8308	2.643	-74.89	1.00000	4.198	-9.271
	1998.97	0	1.4314	0.269	90.05	1.00000	1.690	0.000
	1998.97	1	0.5733	3.382	-74.34	1.00000	3.539	-149.560
	2006.53	0	1.4669	0.094	41.50	0.602167	1.783	-67.579
	2006.53	1	0.5307	6.012	-82.11	1.00000	1.499	-4.666
	2006.70	0	2.0304	0.179	72.70	0.540124	3.621	33.674
	2006.70	1	0.6451	5.905	-76.09	1.00000	2.132	-6.980
	2007.07	0	1.9609	0.358	163.29	0.00000	2.036	-77.598
	2007.07	1	0.6084	5.566	-81.74	1.00000	1.689	-3.736
	2007.48	0	2.0587	0.154	-136.42	0.693757	1.950	87.280
	2007.48	1	0.6443	6.046	-80.25	1.00000	2.057	-13.758
	2007.58	0	1.4642	0.052	-20.15	0.367055	1.447	74.515
	2007.58	1	0.3568	6.446	-78.31	1.00000	0.347	15.633
	2007.93	1	0.4250	6.190	-85.51	1.00000	0.916	-30.661
	2007.93	0	1.6711	0.041	-17.48	1.00000	1.933	-86.502
	2008.06	0	1.7860	0.123	171.34	1.00000	2.131	89.748
	2008.06	1	0.5245	5.600	-80.05	1.00000	2.317	-8.357
$0104-408$	1997.08	0	1.4146	0.014	-3.21	3.14912e-09	0.819	24.225
	1997.08	1	0.0298	6.682	23.74	1.00000	2.697	4.002

continue on next page...

...continued from previous page

Source Name	*Epoch*	*Component*	S (Jy)	a (mas)	ϕ (deg)	*Axial Ratio*	r (mas)	θ (deg)
	1997.25	0	1.3128	0.012	-164.94	0.151410	1.112	28.286
	1997.38	0	1.5216	0.005	50.76	1.00000	0.506	0.000
	1997.38	1	0.0224	7.448	21.76	1.00000	0.153	-13.758
	1997.56	0	1.5026	0.028	-14.19	1.25086e-09	1.372	44.859
	1997.56	1	0.0213	12.306	85.91	1.00000	3.457	9.271
	1997.96	0	1.4747	0.013	-3.64	0.00000	1.041	19.198
	1997.96	1	0.0216	3.084	40.51	1.00000	1.000	-90.000
	1998.11	0	1.3614	0.095	4.80	1.00000	0.428	-74.960
	1998.11	1	0.0105	9.025	26.09	1.00000	0.397	-69.965
	1998.29	0	1.6564	0.014	-107.89	0.00000	0.747	44.315
	1998.29	1	0.0485	2.313	49.12	1.00000	1.000	-34.975
	1998.48	0	1.4023	0.005	70.90	0.545372	1.171	5.598
	1998.48	1	0.0123	8.564	88.39	1.00000	1.000	-90.000
	1998.61	0	1.3996	0.005	117.92	4.68679e-09	0.394	46.704
	1998.97	0	1.2689	0.003	-82.50	2.34431e-09	0.900	37.301
	1998.97	1	0.0183	2.716	60.21	1.00000	1.000	-5.594
	1999.47	0	1.5293	0.001	-40.34	1.00000	1.077	-51.545
	2000.81	0	1.2722	0.020	-2.97	0.155092	3.029	0.987
	2001.35	0	1.5242	0.021	144.17	1.00000	0.950	-6.211
	2002.04	0	1.1073	0.007	157.22	0.209670	1.218	31.831
	2002.04	1	0.0231	8.475	80.28	1.00000	1.000	-13.758
	2004.54	0	0.7162	0.019	159.54	0.619280	1.305	-4.488
	2007.07	0	0.9514	0.036	-1.74	0.109563	19.169	-16.033
	2007.24	0	0.8104	0.023	170.33	1.00000	0.631	-159.833
	2007.48	0	1.1035	0.066	178.83	0.149887	3.763	0.169
	2007.52	0	0.6537	0.067	9.86	5.87314e-09	9.072	10.269
	2007.93	0	0.9485	0.010	122.98	1.00000	1.549	-19.603
	2008.06	0	1.5153	0.103	2.12	0.00000	5.886	1.024
$0238-084$	1995.28	0	1.1182	0.178	-124.68	4.02624e-09	4.404	63.894
	1995.28	1	0.2923	6.205	64.98	1.00000	2.408	0.000
	1995.28	3	0.0441	17.362	-115.59	1.00000	0.000	10.097
	1995.28	2	0.0434	12.718	65.35	1.00000	3.848	-29.233
	1997.08	0	0.8330	0.162	47.31	0.00000	5.085	63.656
	1997.08	1	0.3056	7.099	60.89	1.00000	4.156	0.000
	1997.08	3	0.0476	17.498	-113.90	1.00000	2.571	-33.141
	1997.08	2	0.0254	15.715	62.07	1.00000	0.545	-53.896
	1997.25	0	0.8366	0.079	26.31	0.175274	4.630	64.039
	1997.25	1	0.3342	6.927	59.89	1.00000	4.348	38.079
	1997.25	3	0.0431	17.666	-113.80	1.00000	1.663	-9.271
	1997.25	2	0.0164	15.781	66.25	1.00000	0.000	180.000
	1997.38	0	0.9513	0.128	62.06	3.77201e-09	4.670	63.968
	1997.38	1	0.3181	6.795	61.32	1.00000	3.245	21.393
	1997.38	3	0.0380	17.559	-113.35	1.00000	1.860	0.000

continue on next page...

...continued from previous page								
Source Name	*Epoch*	*Component*	S (Jy)	a (mas)	ϕ (deg)	*Axial Ratio*	*r* (mas)	θ (deg)
	1997.38	2	0.0166	12.910	55.37	1.00000	0.000	4.666
	1997.56	0	0.8798	0.125	-33.04	0.00000	4.132	68.136
	1997.56	1	0.3334	6.790	59.61	1.00000	3.710	36.299
	1997.56	3	0.0482	17.741	-112.34	1.00000	3.596	26.091
	1997.56	2	0.0224	13.205	62.94	1.00000	3.101	0.000
	1997.96	0	1.0356	0.106	165.56	0.00000	4.486	64.001
	1997.96	1	0.3796	7.053	60.66	1.00000	4.280	73.319
	1997.96	3	0.0592	17.470	-112.93	1.00000	3.150	-5.594
	1998.11	0	0.7979	0.201	-125.21	3.41215e-09	3.798	70.714
	1998.11	1	0.3637	6.635	58.27	1.00000	5.230	36.299
	1998.11	3	0.0333	17.524	-113.37	1.00000	1.400	0.000
	1998.29	0	0.9726	0.077	110.54	0.0952791	3.846	70.791
	1998.29	1	0.3551	7.030	59.89	1.00000	4.699	26.091
	1998.29	3	0.0450	18.313	-116.19	1.00000	3.920	0.000
	1998.48	0	0.9737	0.226	-119.40	0.00000	3.982	72.837
	1998.48	1	0.2435	6.993	57.14	1.00000	4.482	-9.271
	1998.61	0	0.9393	0.134	-166.60	0.308484	2.923	67.835
	1998.61	1	0.3202	6.998	62.69	1.00000	3.417	-20.641
	1998.97	0	0.9910	0.165	-132.09	0.0893961	3.913	71.328
	1998.97	1	0.3278	7.061	59.48	1.00000	4.661	-5.594
	1998.97	3	0.0561	18.889	-114.78	1.00000	4.828	-36.299
	1999.47	0	1.0189	0.109	-147.42	2.74694e-09	3.994	73.198
	1999.47	1	0.2562	6.747	59.27	1.00000	3.970	31.471
	1999.47	3	0.0311	19.258	-112.09	1.00000	3.198	40.013
	2000.81	0	0.8938	0.170	-110.13	0.338381	4.121	65.842
	2000.81	1	0.2260	6.850	60.03	1.00000	3.720	14.955
	2000.81	3	0.0666	20.814	-110.81	1.00000	4.293	-13.758
	2000.81	2	0.0350	15.528	64.36	1.00000	8.190	22.770
	2001.35	0	1.0502	0.030	107.20	0.689749	4.261	72.158
	2001.35	3	0.0909	21.662	-105.40	1.00000	3.122	-44.403
	2002.04	0	0.7294	0.202	1.64	0.601297	3.353	71.926
	2002.04	1	0.2609	5.803	54.77	1.00000	3.851	-7.965
	2002.04	2	0.0995	14.498	-112.88	1.00000	4.750	0.000
	2007.93	0	0.2591	0.105	-92.34	1.00000	0.000	-18.080
	2007.93	1	0.2410	10.990	66.38	1.00000	8.204	62.955
	2007.93	3	0.0512	23.064	-114.87	1.00000	1.647	-22.770
$0336-019$	1995.56	0	2.3954	0.039	-107.07	3.47728e-09	1.405	64.343
	1995.56	1	0.1375	2.389	64.95	1.00000	1.000	-12.736
	1995.56	2	0.0461	7.221	59.89	1.00000	3.057	26.091
	1995.75	0	2.0276	0.085	-126.89	0.921757	1.189	21.779
	1995.75	1	0.2291	1.987	52.97	1.00000	2.078	11.083
	1997.03	0	2.1530	0.045	-96.06	0.517211	1.507	68.819
	1997.03	1	0.1012	2.128	64.34	1.00000	1.606	11.083

continue on next page...

...continued from previous page								
Source Name	*Epoch*	*Component*	S (Jy)	a (mas)	ϕ (deg)	*Axial Ratio*	r (mas)	θ (deg)
	1997.03	2	0.0406	6.621	56.27	1.00000	2.093	12.278
	1997.08	0	1.7118	0.089	-135.47	0.426342	1.607	63.932
	1997.08	1	0.2141	1.500	51.56	1.00000	2.228	13.758
	1997.08	2	0.0395	5.418	59.61	1.00000	3.080	7.965
	1997.25	0	1.8819	0.031	-92.01	0.530323	1.803	60.428
	1997.25	1	0.0853	2.572	63.15	1.00000	2.184	6.211
	1997.25	2	0.0288	6.594	60.50	1.00000	2.953	44.403
	1997.38	0	1.8489	0.025	-106.54	0.482242	1.809	59.698
	1997.38	1	0.0845	2.450	68.94	1.00000	1.843	26.091
	1997.38	2	0.0484	7.527	64.85	1.00000	7.173	-11.083
	1997.56	0	1.8489	0.025	-106.54	0.482242	1.809	59.698
	1997.56	1	0.0845	2.450	68.94	1.00000	1.843	26.091
	1997.56	2	0.0484	7.527	64.85	1.00000	7.173	-11.083
	1997.96	0	1.7993	0.035	-124.20	0.282106	1.953	60.354
	1997.96	1	0.0876	3.508	61.91	1.00000	2.289	7.965
	1997.96	3	0.0133	12.844	78.47	1.00000	4.253	-164.367
	1998.11	0	1.5242	0.151	-108.59	0.373872	1.745	64.738
	1998.11	1	0.2686	1.706	63.34	1.00000	1.046	13.758
	1998.11	2	0.0434	6.680	59.32	1.00000	3.968	82.727
	1998.29	0	1.5464	0.257	-119.37	0.420547	1.603	68.969
	1998.29	1	0.4638	1.563	59.93	1.00000	1.803	3.736
	1998.29	3	0.0240	13.753	65.55	1.00000	4.406	20.167
	1998.48	0	1.6969	0.232	-114.75	0.593405	1.605	47.699
	1998.48	1	0.4571	1.684	65.55	1.00000	1.534	6.980
	1998.48	2	0.0556	5.859	63.37	1.00000	4.869	-159.359
	1998.61	0	1.4634	0.111	-94.11	0.423325	1.568	60.836
	1998.61	1	0.3624	1.871	62.60	1.00000	1.000	11.083
	1998.61	2	0.0316	8.341	55.38	1.00000	3.014	28.112
	1999.47	0	1.6485	0.322	-119.13	0.519061	1.968	43.685
	1999.47	2	0.0196	6.277	62.30	1.00000	3.266	44.403
	2000.81	0	1.6177	0.173	-111.26	0.435486	1.838	57.417
	2000.81	1	0.2487	2.723	63.92	1.00000	1.607	48.808
	2001.35	0	1.2826	0.231	-135.54	0.428253	1.521	60.005
	2001.35	1	0.4448	2.000	63.35	1.00000	2.503	0.000
	2002.04	0	1.3500	0.149	-122.91	0.714293	1.440	56.874
	2002.04	1	0.3963	2.182	62.36	1.00000	1.977	0.000
	2007.58	0	2.1921	0.112	174.52	0.639274	1.845	14.499
	2007.58	2	0.0781	6.412	47.74	1.00000	1.388	52.556
$0402-362$	1997.08	0	1.3185	0.008	-106.69	0.00000	2.018	25.561
	1997.08	1	0.0550	10.736	10.97	1.00000	2.323	0.000
	1997.08	2	0.0454	21.561	-0.90	1.00000	4.039	-5.088
	1997.25	0	1.2834	0.012	62.63	0.289032	1.518	22.392
	1997.25	1	0.0430	5.701	15.20	1.00000	0.772	-23.997

continue on next page...

...continued from previous page

Source Name	*Epoch*	*Component*	S (Jy)	a (mas)	ϕ (deg)	*Axial Ratio*	r (mas)	θ (deg)
	1997.25	2	0.0796	16.976	4.34	1.00000	5.368	-26.091
	1997.38	0	1.1287	0.112	-178.92	1.00000	0.699	180.000
	1997.38	1	0.1054	6.318	10.23	1.00000	3.098	0.000
	1997.56	0	1.3019	0.141	-176.90	1.00000	0.696	176.264
	1997.56	1	0.1039	10.690	8.91	1.00000	2.337	0.000
	1997.69	0	1.2636	0.011	0.54	1.00000	1.244	0.000
	1997.69	2	0.0481	22.037	4.85	1.00000	6.581	-15.633
	1997.96	0	1.2714	0.040	170.31	0.00000	2.570	13.952
	1997.96	1	0.0770	7.839	18.83	1.00000	1.403	-5.088
	1998.29	0	1.3615	0.050	-4.63	0.286372	1.981	17.384
	1998.29	1	0.0393	16.633	9.63	1.00000	0.965	-12.549
	1998.48	0	1.2642	0.013	-101.62	0.429430	2.008	8.314
	1998.48	1	0.0522	14.560	6.05	1.00000	1.219	-30.440
	1998.61	0	1.1046	0.002	19.64	1.00000	0.704	8.569
	1998.97	0	0.9948	0.248	-168.13	1.00000	0.411	-3.736
	1998.97	1	0.1464	3.115	17.90	1.00000	1.435	-3.114
	1998.97	2	0.0556	19.122	3.91	1.00000	3.177	-3.114
$0454-234$	1994.52	0	2.0250	0.014	100.40	0.373468	1.538	52.577
	1994.52	1	0.0678	4.796	-123.87	1.00000	2.529	44.403
	1995.56	0	1.2446	0.032	87.82	0.678257	1.649	38.947
	1995.56	1	0.0882	2.849	-126.48	1.00000	4.054	6.980
	1995.75	0	1.3455	0.054	129.27	0.538309	2.436	-11.993
	1995.75	1	0.0472	3.028	-113.44	1.00000	1.001	-4.666
	1997.08	0	1.1388	0.034	144.14	0.598121	1.311	-20.321
	1997.08	1	0.0570	2.752	-112.15	1.00000	1.902	-29.233
	1997.08	2	0.0223	8.547	-143.93	1.00000	3.098	-20.167
	1997.25	0	1.2336	0.017	87.08	0.569688	1.549	-10.978
	1997.25	1	0.0278	2.938	-103.28	1.00000	1.199	-6.980
	1997.25	2	0.0276	9.844	-142.54	1.00000	4.918	4.002
	1997.38	0	1.2522	0.032	155.26	0.411741	1.581	-19.185
	1997.38	1	0.0303	2.778	-97.06	1.00000	1.807	10.097
	1997.38	2	0.0202	8.046	-139.27	1.00000	1.618	180.000
	1997.56	0	1.4623	0.030	148.82	0.453386	1.273	-21.902
	1997.56	1	0.0410	2.998	-118.50	1.00000	1.070	-26.091
	1997.56	2	0.0202	7.067	-145.01	1.00000	1.000	0.000
	1997.69	0	1.5270	0.077	158.93	0.323645	2.390	-12.718
	1997.69	2	0.0096	9.476	-137.51	1.00000	1.000	-5.088
	1997.69	1	0.0676	2.837	-140.30	1.00000	1.927	0.000
	1997.96	0	1.6028	0.020	55.04	0.616176	1.042	2.294
	1997.96	1	0.1147	2.529	-136.80	1.00000	4.431	-13.758
	1998.11	0	1.4538	0.056	172.38	0.466312	1.573	-7.512
	1998.11	1	0.0485	3.346	-128.85	1.00000	1.080	-6.980
	1998.11	2	0.0087	6.604	-108.80	1.00000	1.120	-174.912

continue on next page...

...continued from previous page

Source Name	*Epoch*	*Component*	S (Jy)	a (mas)	ϕ (deg)	*Axial Ratio*	r (mas)	θ (deg)
	1998.29	0	1.7221	0.022	161.77	0.473446	1.317	2.312
	1998.29	1	0.0496	3.019	-121.72	1.00000	1.039	5.088
	1998.29	2	0.0156	6.810	-131.04	1.00000	1.000	-4.308
	1998.61	0	1.4780	0.022	118.46	1.00000	0.662	0.000
	1998.61	1	0.0442	3.211	-122.73	1.00000	1.000	0.000
	1999.47	0	30852.0	0.018	160.99	0.537975	1.709	-0.257
	1999.47	1	0.0320	2.802	-103.46	1.00000	1.010	-174.912
	2000.81	0	1.3329	0.022	142.42	0.560632	1.346	5.011
	2000.81	1	0.0436	3.915	-123.70	1.00000	2.094	-18.080
	2001.35	0	1.1337	0.010	174.62	0.645232	1.262	3.523
	2001.35	2	0.0947	5.319	-132.24	1.00000	3.742	0.000
	2002.04	0	1.6379	0.028	170.79	0.461680	1.432	25.214
	2002.04	1	0.0331	3.845	-125.03	1.00000	1.000	33.141
	2004.13	0	2.1350	0.009	148.66	0.756969	0.879	12.081
	2004.13	1	0.0284	3.160	-108.47	1.00000	1.636	0.000
	2004.13	2	0.0190	7.787	-143.32	1.00000	0.705	4.308
	2004.54	0	2.0414	0.009	161.16	0.609262	0.862	-15.170
	2004.54	2	0.0691	5.798	-143.33	1.00000	2.867	180.000
	2007.24	0	2.8174	0.021	174.16	0.412951	1.935	19.938
	2007.24	1	0.0343	4.029	-120.79	1.00000	0.588	-18.080
	2007.93	0	3.0121	0.034	107.62	0.405911	1.971	81.271
	2007.93	2	0.1033	6.256	-124.24	1.00000	2.459	13.758
$0458-020$	1995.75	0	1.4178	0.174	116.57	1.00000	0.953	-42.554
	1995.75	1	0.2968	3.074	-51.24	1.00000	2.492	21.393
	1995.75	3	0.1090	10.146	-60.72	1.00000	5.908	59.738
	1997.03	0	1.3859	0.197	146.15	5.17347e-09	1.920	-43.268
	1997.03	1	0.2144	3.316	-60.64	1.00000	1.679	26.091
	1997.03	3	0.1657	11.250	-59.18	1.00000	10.089	6.980
	1997.08	0	1.2534	0.233	130.83	0.341891	1.523	-44.271
	1997.08	1	0.2024	2.482	-60.60	1.00000	1.417	12.278
	1997.08	2	0.1191	5.392	-54.64	1.00000	3.029	0.000
	1997.08	3	0.0659	13.620	-59.78	1.00000	4.473	16.374
	1997.25	0	1.1240	0.152	128.58	0.341305	1.654	-47.090
	1997.25	1	0.1766	2.639	-65.97	1.00000	1.511	-121.493
	1997.25	2	0.1268	5.447	-50.79	1.00000	4.085	0.000
	1997.25	3	0.0862	14.134	-61.32	1.00000	7.958	59.738
	1997.38	0	1.2028	0.169	144.10	0.243802	1.657	-38.617
	1997.38	1	0.2234	2.731	-61.76	1.00000	1.737	0.000
	1997.38	2	0.0972	5.800	-51.94	1.00000	3.041	0.000
	1997.38	3	0.0810	14.145	-60.29	1.00000	6.809	-5.088
	1997.56	0	1.0897	0.160	111.40	0.351855	1.661	-46.269
	1997.56	1	0.2347	3.234	-60.31	1.00000	2.676	-5.594
	1997.56	3	0.0386	16.477	-65.27	1.00000	4.160	0.000

continue on next page...

...continued from previous page								
Source Name	*Epoch*	*Component*	S (Jy)	a (mas)	ϕ (deg)	*Axial Ratio*	r (mas)	θ (deg)
	1997.56	2	0.0908	8.411	-53.10	1.00000	6.795	0.000
	1997.69	0	1.1458	0.169	136.44	0.514744	2.389	-24.938
	1997.69	1	0.2117	3.741	-57.40	1.00000	1.510	15.633
	1997.69	2	0.0522	9.224	-54.31	1.00000	2.816	-11.083
	1997.69	3	0.0610	15.621	-60.64	1.00000	4.070	-14.955
	1997.96	0	0.9754	0.209	142.98	0.224016	1.673	-51.074
	1997.96	1	0.2134	3.038	-61.03	1.00000	1.649	29.233
	1997.96	2	0.1047	6.982	-55.29	1.00000	5.657	7.965
	1997.96	3	0.0705	16.159	-61.19	1.00000	6.729	0.000
	1998.11	0	0.7107	0.624	133.48	1.00000	0.327	-9.271
	1998.11	1	0.3934	1.683	-56.92	1.00000	1.803	-12.278
	1998.11	2	0.0948	5.405	-52.58	1.00000	2.343	-18.080
	1998.11	3	0.1110	13.125	-61.77	1.00000	10.330	14.955
	1998.29	0	0.9070	0.148	135.75	0.192891	1.537	-57.250
	1998.29	1	0.2027	2.615	-64.31	1.00000	1.642	-26.091
	1998.29	2	0.1028	5.126	-52.05	1.00000	3.032	-161.920
	1998.29	3	0.0546	12.936	-62.63	1.00000	4.498	69.048
	1998.48	0	0.6632	0.589	131.25	1.00000	0.886	-168.917
	1998.48	1	0.3110	2.064	-55.04	1.00000	2.270	14.955
	1998.48	2	0.0611	6.173	-48.56	1.00000	2.441	0.000
	1998.48	3	0.0788	13.666	-64.18	1.00000	8.651	-6.211
	1998.61	0	0.8170	0.328	116.06	0.364592	2.285	-56.937
	1998.61	1	0.1912	3.751	-58.26	1.00000	2.978	0.000
	1998.61	3	0.0142	12.101	-80.22	1.00000	2.050	-8.569
	1999.47	0	0.7476	0.455	156.17	0.404500	2.458	-65.022
	1999.47	1	0.1865	4.438	-53.50	1.00000	4.613	49.606
	2000.81	0	0.5409	0.193	122.16	3.72686e-09	1.349	-76.147
	2000.81	1	0.2252	3.573	-55.82	1.00000	2.148	164.367
	2000.81	2	0.0814	11.569	-55.95	1.00000	11.252	18.080
	2002.04	0	0.4182	0.261	111.49	0.454991	1.514	-39.612
	2002.04	1	0.1584	3.016	-56.03	1.00000	1.778	12.278
	2002.04	2	0.0844	5.251	-51.54	1.00000	1.603	0.000
	2002.04	3	0.0968	13.342	-59.25	1.00000	9.959	50.757
	2004.13	0	0.4794	0.160	38.41	0.443653	1.557	-33.929
	2004.13	1	0.1789	4.334	-55.86	1.00000	1.815	-47.699
	2004.13	3	0.0964	12.248	-55.66	1.00000	10.500	18.080
	2004.54	0	0.5212	0.455	103.89	1.00000	2.190	-45.725
	2004.54	1	0.1937	4.408	-55.07	1.00000	3.061	-12.278
	2004.54	3	0.0414	16.181	-57.49	1.00000	6.577	-4.666
	2006.53	0	0.5107	0.147	123.72	0.327577	1.442	-62.897
	2006.53	1	0.1381	4.982	-58.58	1.00000	2.145	10.097
	2006.53	3	0.0631	12.618	-59.31	1.00000	10.472	0.000
	2006.70	0	0.4863	0.103	130.55	0.357480	0.932	-67.355
								continue on next page...

...continued from previous page

Source Name	Epoch	Component	S (Jy)	a (mas)	ϕ (deg)	Axial Ratio	r (mas)	θ (deg)
	2006.70	1	0.1606	4.786	-55.83	1.00000	2.138	-9.271
	2006.70	3	0.0385	11.301	-71.33	1.00000	5.000	-44.403
	2007.07	0	0.6890	0.075	142.52	1.00000	1.031	-41.791
	2007.07	2	0.1903	6.307	-50.18	1.00000	2.406	4.666
	2007.24	0	0.5202	0.080	109.90	1.00000	0.583	-124.243
	2007.24	2	0.1570	4.707	-56.71	1.00000	2.345	-18.080
	2007.24	3	0.0666	12.588	-59.92	1.00000	10.096	-33.141
	2007.48	0	0.5137	0.222	124.81	0.00000	1.074	-70.359
	2007.48	2	0.1785	4.855	-54.63	1.00000	1.944	-5.594
	2007.48	3	0.0455	13.619	-59.86	1.00000	11.852	-13.758
	2007.52	0	0.4486	0.075	47.88	1.00000	0.808	-48.084
	2007.52	2	0.1115	4.551	-56.38	1.00000	1.642	21.393
	2007.52	3	0.0657	10.571	-64.66	1.00000	6.315	18.080
	2007.58	0	0.5516	0.036	57.51	0.726153	1.079	24.592
	2007.58	2	0.1689	4.933	-53.55	1.00000	2.876	12.278
	2007.93	0	0.6516	0.037	89.83	0.509220	1.286	-47.794
	2007.93	2	0.1364	6.696	-54.94	1.00000	2.776	-6.980
	2007.93	3	0.0305	16.708	-63.58	1.00000	0.667	-18.080
$0727-115$	1994.52	0	4.3501	0.074	103.33	0.538033	0.713	68.946
	1994.52	2	0.1093	8.779	-42.44	1.00000	2.096	-34.433
	1994.52	1	0.3162	2.554	-50.24	1.00000	0.614	13.758
	1995.28	0	2.9043	0.189	131.27	0.345261	1.235	43.833
	1995.28	1	0.7584	1.799	-40.81	1.00000	2.067	-38.079
	1995.28	2	0.1190	8.900	-39.79	1.00000	3.019	10.097
	1995.52	0	2.7113	0.104	100.83	0.621084	1.375	21.647
	1995.52	1	0.3701	2.301	-52.53	1.00000	1.134	16.374
	1995.52	2	0.0891	8.577	-43.20	1.00000	4.845	-11.083
	1995.52	5	0.0297	19.014	-60.10	1.00000	7.900	180.000
	1995.75	0	2.5194	0.249	143.84	1.00000	1.075	-38.079
	1995.75	1	0.3775	2.412	-42.72	1.00000	2.598	-11.083
	1995.75	2	0.1825	8.734	-25.48	1.00000	11.698	-21.393
	1995.78	0	2.5893	0.359	151.83	5.09368e-09	1.108	-63.585
	1995.78	1	0.5781	1.829	-37.57	1.00000	3.487	9.271
	1995.78	2	0.1693	9.201	-24.91	1.00000	10.508	-28.112
	1996.31	0	1.8165	0.301	139.62	0.00000	0.686	56.577
	1996.31	1	0.9924	1.153	-42.28	1.00000	2.427	26.091
	1996.31	2	0.1624	9.495	-32.64	1.00000	11.564	22.770
	1997.03	0	2.1988	0.115	106.23	0.701802	1.280	-15.956
	1997.03	1	0.3486	2.626	-46.94	1.00000	1.240	-26.091
	1997.03	2	0.0788	8.727	-46.62	1.00000	2.678	36.299
	1997.03	0	2.0644	0.200	133.39	0.557037	1.217	-26.550
	1997.03	1	0.3881	2.307	-48.34	1.00000	1.374	18.080
	1997.03	3	0.0733	11.830	-6.49	1.00000	5.189	3.736

continue on next page...

...continued from previous page								
Source Name	*Epoch*	*Component*	S (Jy)	a (mas)	ϕ (deg)	*Axial Ratio*	r (mas)	θ (deg)
	1997.03	2	0.0722	7.309	-66.53	1.00000	5.291	15.633
	1997.08	0	1.8579	0.158	109.98	0.628264	1.263	24.970
	1997.08	1	0.3953	2.235	-48.30	1.00000	1.704	28.112
	1997.08	2	0.0958	8.783	-47.24	1.00000	4.797	90.000
	1997.25	0	1.8373	0.247	139.71	3.87436e-09	0.875	46.804
	1997.25	1	0.6669	1.479	-44.13	1.00000	2.314	-33.141
	1997.25	2	0.2016	7.926	-27.59	1.00000	11.582	-11.083
	1997.38	0	2.1121	0.304	151.90	1.00000	0.748	-73.516
	1997.38	1	0.7877	1.652	-33.78	1.00000	2.708	-170.729
	1997.38	2	0.0636	7.631	-57.79	1.00000	3.181	7.965
	1997.38	4	0.0663	14.909	-6.25	1.00000	5.548	7.965
	1997.56	0	1.3944	0.314	152.95	4.34853e-09	0.622	-75.000
	1997.56	1	0.8183	1.401	-26.20	1.00000	3.209	22.770
	1997.56	2	0.0842	9.810	-39.69	1.00000	4.450	28.551
	1997.69	0	1.5927	0.670	158.52	1.00000	0.653	36.393
	1997.69	1	1.0451	1.394	-28.84	1.00000	3.000	-6.980
	1997.69	4	0.0353	14.398	-12.34	1.00000	2.835	13.758
	1997.69	2	0.0496	10.802	-44.00	1.00000	2.746	-20.460
	1997.96	0	1.6988	0.346	158.10	0.727005	0.879	-10.836
	1997.96	1	0.9259	1.467	-31.00	1.00000	2.948	0.000
	1997.96	2	0.0928	8.494	-40.11	1.00000	4.894	0.000
	1997.96	4	0.0271	15.406	-55.00	1.00000	2.909	18.080
	1998.11	0	1.6330	0.261	152.28	1.00000	0.461	0.000
	1998.11	1	0.7592	1.309	-38.12	1.00000	2.666	18.080
	1998.11	99	0.1377	5.844	-32.58	1.00000	7.020	6.210
	1998.11	4	0.0815	14.292	-30.91	1.00000	16.706	-4.666
	1998.29	0	2.4116	0.093	107.52	1.00000	0.980	3.503
	1998.29	1	0.3358	2.536	-49.03	1.00000	2.017	11.083
	1998.29	2	0.0983	10.177	-35.60	1.00000	5.032	13.758
	1998.48	0	1.7118	0.421	153.08	1.00000	0.812	180.000
	1998.48	1	0.8487	1.297	-28.33	1.00000	2.711	0.000
	1998.48	2	0.1366	8.645	-37.79	1.00000	10.877	36.299
	1998.61	0	1.8714	0.217	149.70	1.00000	0.430	-33.141
	1998.61	1	0.6997	1.220	-43.38	1.00000	2.817	21.393
	1998.61	2	0.1790	8.931	-32.79	1.00000	12.103	-13.758
	1998.97	0	1.6323	0.255	149.80	1.00000	0.602	6.211
	1998.97	1	0.6302	1.430	-38.97	1.00000	2.959	38.079
	1998.97	2	0.1660	9.088	-31.30	1.00000	11.870	-4.666
	1999.47	0	1.6992	0.110	116.27	1.00000	0.914	23.997
	1999.47	1	0.2950	2.426	-45.64	1.00000	1.936	-23.997
	1999.47	2	0.1869	7.327	-27.80	1.00000	13.504	-156.477
	2000.81	0	1.4866	0.201	154.47	1.00000	0.455	26.091
	2000.81	1	0.4558	1.720	-40.72	1.00000	2.951	-5.594
								continue on next page...

...continued from previous page								
Source Name	*Epoch*	*Component*	S (Jy)	a (mas)	ϕ (deg)	*Axial Ratio*	r (mas)	θ (deg)
	2000.81	2	0.1414	8.085	-25.63	1.00000	11.432	3.736
	2001.35	0	2.3447	0.074	132.83	1.00000	0.838	-33.141
	2001.35	1	0.2079	2.772	-49.11	1.00000	1.937	-23.194
	2001.35	2	0.1069	7.722	-49.69	1.00000	3.459	9.271
	2002.04	0	1.7921	0.254	164.39	1.00000	0.598	0.000
	2002.04	1	0.4981	2.179	-29.70	1.00000	3.151	33.141
	2002.04	2	0.0940	8.961	-43.96	1.00000	6.608	46.894
	2004.54	0	2.7975	0.035	82.37	1.00000	0.845	14.955
	2004.54	1	0.2031	3.306	-45.67	1.00000	1.541	22.199
	2006.70	0	2.5474	0.039	133.90	0.350984	1.304	-61.377
	2006.70	1	0.2080	3.810	-41.43	1.00000	5.168	67.784
	2007.07	0	3.4588	0.094	167.50	1.00000	1.263	60.436
	2007.07	2	0.2070	7.033	-20.51	1.00000	3.754	49.606
	2007.48	0	3.5299	0.082	155.90	1.00000	1.086	-19.603
	2007.48	99	0.2048	5.892	-43.64	1.00000	3.749	-3.736
	2007.52	0	2.5743	0.163	141.54	1.00000	0.644	4.002
	2007.52	1	0.5182	1.715	-39.57	1.00000	1.861	23.997
	2007.52	2	0.0679	10.089	-38.37	1.00000	2.185	-20.167
	2007.93	0	2.8083	0.095	150.61	0.753046	1.720	-34.401
	2007.93	2	0.1582	7.815	-35.42	1.00000	9.192	0.000
	2008.06	0	3.4663	0.078	156.96	1.00000	1.028	-26.091
	2008.06	99	0.2748	5.369	-32.85	1.00000	5.928	11.083
$0919-260$	1997.08	0	1.2244	0.161	142.46	0.492508	2.878	-78.794
	1997.08	1	0.1371	3.663	-71.36	1.00000	3.443	19.603
	1997.08	2	0.0562	7.759	-52.30	1.00000	5.049	-15.633
	1997.25	0	1.4558	0.070	122.56	0.628415	2.772	-80.699
	1997.25	1	0.1311	5.415	-62.83	1.00000	4.691	0.000
	1997.38	0	1.1028	0.162	110.54	0.788429	3.160	-57.471
	1997.38	1	0.1310	5.542	-59.45	1.00000	3.831	37.298
	1997.38	2	0.0136	14.307	-65.08	1.00000	1.704	-10.097
	1997.56	0	1.2443	0.210	116.25	0.815718	2.979	-69.798
	1997.56	1	0.1567	5.172	-59.56	1.00000	4.487	-135.597
	1997.69	0	1.1878	0.119	38.45	0.403637	6.339	-26.166
	1997.69	1	0.1368	4.598	-77.64	1.00000	4.590	-67.784
	1997.96	0	1.0180	0.226	146.63	0.596420	2.870	-84.336
	1998.11	0	1.2171	0.048	51.53	0.617900	3.051	-81.196
	1998.11	1	0.1242	5.955	-55.22	1.00000	3.055	-11.083
	1998.11	2	0.1222	5.797	-58.42	1.00000	3.450	7.965
	1998.29	0	1.1702	0.097	129.21	0.764626	3.152	-69.881
	1998.29	1	0.1025	5.796	-53.51	1.00000	3.631	22.199
	1998.48	0	1.0607	0.120	105.30	0.732782	3.180	-75.043
	1998.48	1	0.1129	6.500	-53.97	1.00000	4.423	44.403
	1998.61	0	0.9523	0.101	94.79	0.480186	3.107	-73.993

continue on next page...

...continued from previous page

Source Name	*Epoch*	*Component*	S (Jy)	a (mas)	ϕ (deg)	*Axial Ratio*	r (mas)	θ (deg)
	1998.61	1	0.1076	6.234	-52.48	1.00000	3.593	30.440
	1998.97	0	0.9341	0.119	165.34	0.562780	3.268	-83.289
	1998.97	1	0.0852	6.231	-51.68	1.00000	3.338	33.141
	1999.47	0	0.9419	0.192	155.95	0.808868	2.966	-79.603
	1999.47	1	0.1140	5.563	-58.19	1.00000	4.505	11.083
	2000.81	0	0.7859	0.168	-80.71	0.714603	2.988	-79.574
	2000.81	1	0.1760	5.252	-56.58	1.00000	6.280	-172.035
	2001.35	0	1.2468	0.163	163.99	0.566931	2.858	-85.366
	2001.35	1	0.0998	5.822	-56.57	1.00000	2.867	-163.626
	2002.04	0	1.0952	0.187	156.71	0.499977	3.492	87.430
	2002.04	1	0.1147	5.462	-65.20	1.00000	4.166	50.757
	2006.70	0	1.4977	0.091	149.04	1.00000	2.399	104.320
	2006.70	1	0.0608	6.724	-99.15	1.00000	0.277	0.000
$0920-397$	1997.38	0	0.7995	0.178	-0.55	0.270388	5.281	-7.783
	1997.38	1	0.1084	8.161	-174.52	1.00000	5.721	-5.088
	1997.69	0	0.7918	1.165	-2.40	1.00000	1.094	6.211
	1997.69	1	0.2394	6.267	-178.79	1.00000	4.407	-9.271
	2008.06	0	1.4894	0.071	3.51	0.277315	4.228	-7.914
	2008.06	1	0.0756	12.421	-179.46	1.00000	9.431	15.633
$1034-293$	1997.08	0	1.4109	0.102	-49.64	1.00000	0.529	0.000
	1997.08	1	0.1817	1.576	129.89	1.00000	0.980	16.374
	1997.08	2	0.0374	6.162	65.06	1.00000	3.006	11.083
	1997.25	0	0.8029	0.182	-49.89	1.00000	0.219	0.000
	1997.25	1	0.1389	1.581	126.78	1.00000	0.617	-4.666
	1997.38	0	1.3360	0.008	40.51	0.151345	2.335	-34.287
	1997.56	0	1.7652	0.050	-46.69	3.44094e-09	0.606	-65.136
	1997.56	1	0.1298	2.261	137.47	1.00000	1.959	0.000
	1997.69	0	1.4940	0.243	-28.59	1.00000	0.828	-29.584
	1997.69	1	0.1967	2.457	142.49	1.00000	2.301	0.000
	1997.96	0	1.2906	0.042	-93.97	1.00000	0.785	13.758
	1997.96	1	0.0850	2.838	123.13	1.00000	1.675	26.091
	1998.11	0	0.7216	0.109	-27.27	0.00000	0.925	-66.850
	1998.11	1	0.0783	2.840	131.92	1.00000	2.697	6.980
	1998.29	0	0.7753	0.179	-37.88	1.00000	1.031	-5.594
	1998.29	1	0.1565	1.713	134.89	1.00000	3.049	26.091
	1998.48	0	0.8316	0.041	24.16	0.510316	2.239	-51.823
	1998.48	3	0.0216	35.110	139.85	1.00000	2.500	7.965
	1998.61	0	0.9149	0.129	-42.99	0.157583	1.478	-54.983
	1998.61	1	0.0708	2.709	121.51	1.00000	0.824	26.091
	1998.61	2	0.0196	13.371	146.27	1.00000	4.001	3.736
	1998.61	3	0.0103	25.859	133.34	1.00000	2.463	10.097
	1998.97	0	0.9650	0.171	-20.13	1.86644e-09	1.212	-37.065
	1998.97	1	0.1397	1.859	121.92	1.00000	2.619	26.091

continue on next page...

...continued from previous page

Source Name	*Epoch*	*Component*	S	a	ϕ	*Axial Ratio*	r	θ
			(Jy)	(mas)	(deg)		(mas)	(deg)
	2006.53	0	0.8529	0.008	173.57	1.00000	0.515	62.955
	2006.70	0	0.7899	0.017	-18.27	1.00000	0.455	-50.757
	2007.07	0	1.1748	0.038	-22.13	0.00000	2.161	-57.997
	2007.07	3	0.0591	20.861	131.35	1.00000	17.093	0.000
	2007.24	0	1.1736	0.010	124.63	0.148535	2.420	-69.109
	2007.48	0	1.0056	0.087	-59.36	0.297305	2.248	-65.577
	2007.48	3	0.0257	21.984	126.57	1.00000	3.136	4.666
	2007.48	1	0.0543	3.065	118.98	1.00000	1.613	12.278
	2007.52	0	1.3115	0.021	122.04	0.256973	2.584	-47.060
	2007.52	3	0.0248	25.479	128.73	1.00000	0.658	-5.088
	2007.58	0	1.0900	0.038	-150.81	0.455296	2.171	-36.499
	2007.58	2	0.0356	8.856	150.23	1.00000	0.000	-7.440
	2007.58	3	0.0155	22.317	136.21	1.00000	2.974	0.000
	2007.93	0	0.8893	0.071	145.37	0.524205	3.275	-33.133
	2007.93	3	0.0270	21.194	130.66	1.00000	4.828	-2.803
	2008.06	0	1.5123	0.056	-41.42	0.346102	2.682	-53.857
	2008.06	1	0.0713	3.265	123.19	1.00000	1.823	-11.853
$1124-186$	1997.38	0	0.8168	0.005	-103.10	0.342735	1.612	-16.999
	1997.38	2	0.0133	4.453	152.89	1.00000	0.000	168.917
	1997.56	0	0.7657	0.089	-18.67	0.00000	0.500	-30.566
	1997.56	1	0.0649	1.560	157.96	1.00000	1.434	18.080
	1997.69	0	0.6167	0.091	-15.02	1.00000	0.580	-36.299
	1997.69	2	0.0251	6.678	169.52	1.00000	2.541	13.758
	1998.29	0	0.8554	0.045	-14.83	0.509175	0.756	-15.893
	1998.29	1	0.0383	2.376	164.90	1.00000	2.758	-15.633
	1998.97	0	1.3257	0.117	5.46	1.00000	0.456	11.083
	1998.97	1	0.1426	1.311	-174.49	1.00000	0.900	-38.079
	2001.35	0	0.9674	0.013	-23.23	0.266434	1.676	-27.620
	2001.35	2	0.0101	5.619	48.57	1.00000	1.140	65.591
	2004.13	0	0.8947	0.100	-18.88	1.97137e-09	0.299	-18.258
	2004.13	1	0.0734	1.702	159.32	1.00000	0.826	143.701
	2004.54	0	0.9533	0.112	-5.98	1.00000	0.417	-6.161
	2004.54	2	0.0506	4.101	169.83	1.00000	2.392	33.141
	2007.52	0	0.6962	0.105	-12.65	0.00000	0.176	-32.342
	2007.52	2	0.0260	4.046	165.80	1.00000	1.375	13.758
$1144-379$	1997.08	0	1.2650	0.072	-37.23	0.00000	1.058	43.395
	1997.08	1	0.2258	1.680	150.20	1.00000	2.258	0.000
	1997.56	0	1.3340	0.025	-141.38	0.520288 1.591	-11.126	
	1997.56	99	0.0590	3.012	125.51	1.00000	1.657	33.141
	1998.97	0	1.1713	0.092	-15.06	0.337723	1.346	-29.755
	1998.97	1	0.1829	1.994	159.84	1.00000	3.523	0.000
	2001.35	0	1.1978	0.183	-20.63	1.00130e-09	1.638	-57.944
	2001.35	2	0.0526	5.209	121.60	1.00000	3.293	153.909

continue on next page...

...continued from previous page

Source Name	*Epoch*	*Component*	S (Jy)	a (mas)	ϕ (deg)	*Axial Ratio*	r (mas)	θ (deg)
	2002.04	0	0.5913	0.389	-24.08	1.00000	0.201	12.278
	2002.04	1	0.2370	1.954	156.81	1.00000	2.797	5.088
	2004.54	0	0.6965	0.046	162.90	0.438641	2.726	-33.798
	2004.54	3	0.0140	17.739	142.44	1.00000	0.000	-5.088
	2007.07	0	1.9768	0.163	-0.85	0.246532	6.493	9.325
	2007.07	3	0.0584	14.258	162.82	1.00000	3.117	19.603
	2007.48	0	1.9801	0.042	-139.47	1.00000	0.719	-9.271
	2007.48	1	0.1856	1.545	40.06	1.00000	2.720	-15.633
	2007.58	0	1.8917	0.010	22.60	0.250491	1.986	-33.625
	2007.58	2	0.2154	5.722	-107.85	1.00000	0.745	9.271
$1145-071$	1995.75	0	0.7795	0.046	46.99	0.384375	2.566	-63.948
	1995.75	2	0.0420	10.162	-55.14	1.00000	6.469	-145.861
	1997.08	0	0.7192	0.033	-92.37	0.297292	2.805	-69.152
	1997.08	2	0.0147	9.581	-57.21	1.00000	0.000	15.633
	1997.25	0	0.7174	0.012	-136.85	0.242305	2.744	-70.314
	1997.25	2	0.0208	10.587	-67.57	1.00000	4.076	8.569
	1997.38	0	0.7844	0.027	166.95	0.378105	2.821	-62.014
	1997.38	2	0.0508	10.949	-49.77	1.00000	10.604	-29.233
	1997.56	0	0.7164	0.015	135.48	0.308711	2.726	-66.005
	1997.56	2	0.0392	10.282	-53.24	1.00000	6.297	-153.909
	1997.69	0	0.7042	0.044	145.04	0.404078	2.664	-73.306
	1997.69	2	0.0432	10.378	-55.36	1.00000	8.640	0.000
	1997.96	0	0.6891	0.045	-57.75	0.281223	2.772	-73.211
	1997.96	2	0.0437	10.214	-60.67	1.00000	9.499	6.980
	1998.11	0	0.6326	0.043	-129.11	0.264112	2.854	-66.937
	1998.11	2	0.0435	11.482	-59.47	1.00000	9.448	0.000
	1998.29	0	0.7122	0.086	-95.26	0.310104	2.828	-68.957
	1998.29	2	0.0332	11.248	-48.42	1.00000	6.234	-5.088
	1998.48	0	0.6551	0.039	-50.06	0.477509	2.821	-65.312
	1998.48	2	0.0357	10.460	-55.74	1.00000	10.574	3.503
	1998.61	0	0.6352	0.068	-165.80	0.00000	2.796	-72.961
	1998.61	2	0.0416	12.116	-55.42	1.00000	9.251	14.955
	1999.47	0	0.5636	0.036	43.66	0.208985	2.865	-64.134
	1999.47	2	0.0333	10.345	-58.52	1.00000	8.107	-18.080
	2001.35	0	0.5453	0.035	147.45	0.192460	2.545	-66.314
	2001.35	2	0.0336	9.189	-58.86	1.00000	8.529	-3.297
	2002.04	0	0.3913	0.325	126.71	1.00000	0.567	23.523
	2002.04	1	0.2170	1.924	-62.50	1.00000	1.488	-11.083
	2002.04	2	0.0315	10.909	-54.40	1.00000	9.315	3.736
	2007.07	0	0.8127	0.057	132.30	0.00000	1.571	-43.672
	2007.07	1	0.1049	2.514	-53.17	1.00000	0.587	-156.477
	2007.07	2	0.0332	12.164	-49.85	1.00000	6.907	-4.666
$1253-055$	1997.03	0	7.7625	0.196	55.33	0.479477	2.679	63.658

continue on next page...

...continued from previous page

Source Name	*Epoch*	*Component*	S (Jy)	a (mas)	ϕ (deg)	*Axial Ratio*	r (mas)	θ (deg)
	1997.03	1	0.6083	14.805	-147.11	1.00000	5.127	10.097
	1997.56	0	7.7602	0.282	50.79	0.409632	3.017	62.726
	1997.56	1	0.5658	14.575	-146.83	1.00000	5.185	23.523
	1998.97	0	7.2977	0.820	50.03	0.508446	4.307	48.969
	1998.97	1	0.2946	14.761	-143.53	1.00000	0.000	36.299
$1255-316$	1997.38	0	1.0147	0.090	38.79	0.00000	3.065	13.139
	1997.38	2	0.1809	9.798	23.08	1.00000	0.008	0.000
	1997.38	3	0.0706	16.726	32.55	1.00000	0.755	-18.080
	1997.56	0	1.0810	0.232	-169.10	0.00000	3.389	27.070
	1997.56	1	0.1715	7.495	21.79	1.00000	0.906	180.000
	1997.56	3	0.1017	14.042	35.01	1.00000	5.232	-55.757
	1997.69	0	0.9710	0.105	-2.26	5.84387e-09	2.564	38.393
	1997.69	1	0.3413	7.269	30.95	1.00000	7.727	173.790
	1997.96	0	0.9963	0.094	-176.63	3.76214e-09	4.066	13.606
	1997.96	1	0.2938	7.222	23.97	1.00000	3.824	-18.080
	1997.96	3	0.0808	15.163	38.90	1.00000	2.644	-3.736
	2001.35	0	1.0255	1.832	164.33	1.00000	2.027	-6.335
	2001.35	1	0.2196	9.373	3.41	1.00000	3.693	7.965
	2004.54	0	1.6910	0.013	117.66	0.659293	2.810	-9.115
	2004.54	4	0.0643	26.032	28.73	1.00000	2.845	0.000
	2007.07	0	1.4143	0.092	-81.70	1.00000	1.239	5.885
	2007.07	3	0.0512	16.449	39.41	1.00000	1.216	-16.374
	2007.07	1	0.1733	12.379	20.13	1.00000	2.000	-12.736
	2007.24	0	0.9869	0.301	-171.89	1.00000	1.269	-15.633
	2007.24	1	0.2764	6.073	21.88	1.00000	3.960	-26.091
	2007.24	3	0.0607	16.211	33.02	1.00000	1.823	0.000
	2007.48	0	1.4515	0.086	-14.25	0.689781	2.444	34.680
	2007.48	1	0.0464	5.357	-128.04	1.00000	0.000	-31.471
	2007.48	4	0.0599	23.760	34.38	1.00000	1.014	-13.758
	2007.52	0	1.1310	0.159	-179.30	1.00000	1.019	-150.767
	2007.52	2	0.1348	10.578	20.61	1.00000	1.483	-10.097
	2007.52	3	0.0562	16.874	32.32	1.00000	0.513	-22.770
	2007.58	0	1.4717	0.033	-178.82	0.0921422	4.619	21.076
	2007.58	3	0.1058	16.495	40.99	1.00000	1.809	172.035
	2007.93	0	1.0158	0.506	-153.02	1.00000	1.104	0.000
	2007.93	1	0.2235	6.393	20.65	1.00000	1.353	-12.278
	2007.93	2	0.0456	11.870	43.25	1.00000	1.115	-22.199
	2007.93	4	0.0253	30.012	30.30	1.00000	0.000	-13.758
	2008.06	0	1.3769	0.084	-159.59	0.00000	4.765	28.974
	2008.06	2	0.1076	9.668	25.10	1.00000	5.874	-12.278
$1313-333$	1994.52	0	1.0584	0.065	30.10	0.382770	1.245	4.794
	1994.52	2	0.2568	4.606	-69.44	1.00000	3.248	7.965
	1997.08	0	1.0168	0.037	169.54	3.06382e-09	1.049	88.666

continue on next page...

...continued from previous page

Source Name	*Epoch*	*Component*	S (Jy)	a (mas)	ϕ (deg)	*Axial Ratio*	r (mas)	θ (deg)
	1997.08	2	0.1852	5.222	-83.85	1.00000	4.676	26.091
	1997.38	0	0.9405	0.019	-140.82	0.724851	1.506	-9.695
	1997.38	2	0.1196	6.229	-94.74	1.00000	3.210	-6.980
	1997.56	0	1.0715	0.049	178.29	5.52710e-09	1.232	84.648
	1997.56	2	0.1732	5.497	-87.71	1.00000	4.184	6.980
	1997.69	0	1.2116	0.186	164.93	0.619332	1.600	-67.633
	1997.69	2	0.1823	5.020	-81.53	1.00000	4.936	11.083
	1997.96	0	0.8265	0.088	170.60	0.00000	1.324	-84.164
	1997.96	2	0.1849	5.067	-71.84	1.00000	5.290	-173.790
	1998.11	0	0.9330	0.053	171.04	1.00000	1.246	83.676
	1998.11	2	0.1668	4.086	-86.26	1.00000	6.233	15.633
	1998.29	0	0.8586	0.095	155.15	0.904413	1.545	-28.296
	1998.29	2	0.1369	5.163	-82.57	1.00000	4.141	7.965
	1998.48	0	0.8551	0.109	52.57	0.874499	1.634	-38.719
	1998.48	2	0.1420	5.481	-69.97	1.00000	4.571	15.633
	1998.67	0	0.7712	0.011	-97.96	3.07351e-09	1.507	-89.655
	1998.67	2	0.1413	5.595	-89.21	1.00000	4.876	52.556
	1998.97	0	0.5643	0.059	-137.80	0.860190	1.795	-73.696
	1998.97	2	0.1479	5.855	-71.56	1.00000	5.271	11.083
	1999.47	0	0.4921	0.152	31.88	0.00000	2.524	89.928
	1999.47	2	0.0454	5.694	-97.22	1.00000	4.806	12.278
	2000.81	0	0.9263	0.055	32.68	1.00000	1.000	33.141
	2000.81	1	0.1162	2.973	-79.13	1.00000	0.000	6.211
	2000.81	2	0.0768	7.478	-74.01	1.00000	4.516	-135.597
	2001.35	0	0.7715	0.567	141.52	1.00000	0.000	-44.403
	2001.35	1	0.2760	3.559	-49.82	1.00000	2.862	-10.097
	2002.04	0	0.8065	0.505	161.66	4.28750e-09	0.804	-80.074
	2002.04	1	0.3321	2.908	-84.73	1.00000	5.985	0.000
	2004.13	0	0.5332	0.099	145.93	0.00000	0.917	-79.082
	2004.13	1	0.2171	4.139	-67.88	1.00000	4.848	10.097
$1334-127$	1994.52	0	3.4516	0.031	-34.45	3.50019e-09	1.642	-7.693
	1994.52	1	0.1697	2.829	145.33	1.00000	1.200	6.211
	1994.52	3	0.0193	25.742	146.31	1.00000	2.393	33.141
	1995.56	0	2.2960	0.132	-20.35	0.268352	1.914	-8.127
	1995.56	1	0.2721	2.197	152.14	1.00000	2.178	-153.909
	1995.56	3	0.0365	24.699	150.46	1.00000	12.523	18.080
	1997.08	0	1.9764	0.515	-19.61	0.306049	1.724	-11.407
	1997.08	1	0.7077	1.698	156.89	1.00000	1.018	-159.833
	1997.08	2	0.0397	6.379	133.50	1.00000	3.520	90.000
	1997.08	3	0.0189	28.859	150.20	1.00000	3.429	-153.909
	1997.25	0	2.5021	0.248	-18.35	0.253659	2.326	-16.587
	1997.25	1	0.4610	2.338	159.08	1.00000	1.406	22.770
	1997.38	0	2.1285	0.517	-21.76	0.308601	1.977	-16.392

continue on next page...

...continued from previous page								
Source Name	*Epoch*	*Component*	S (Jy)	a (mas)	ϕ (deg)	*Axial Ratio*	r (mas)	θ (deg)
	1997.38	1	0.6890	1.847	157.10	1.00000	1.054	-20.641
	1997.38	2	0.0316	7.631	141.36	1.00000	2.107	-20.167
	1997.38	3	0.0451	30.327	151.56	1.00000	10.267	0.000
	1997.56	0	1.4523	0.901	-21.26	0.344340	1.131	-20.732
	1997.56	1	1.0059	1.460	157.67	1.00000	0.958	-153.909
	1997.56	2	0.0601	6.566	146.48	1.00000	6.510	58.507
	1997.56	3	0.0237	28.300	147.64	1.00000	4.764	99.658
	1997.69	0	2.4647	0.178	-18.66	0.270836	3.088	-15.426
	1997.69	1	0.3049	2.691	157.14	1.00000	3.118	-165.045
	1997.96	0	1.7199	0.848	-22.03	0.00000	0.923	30.487
	1997.96	1	1.1193	1.574	157.39	1.00000	1.028	-166.242
	1997.96	2	0.0288	7.485	137.50	1.00000	1.747	8.569
	1997.96	3	0.0155	29.521	149.41	1.00000	1.059	6.980
	1998.11	0	1.6140	0.741	-20.70	0.390330	1.753	-12.499
	1998.11	1	0.7866	1.847	157.62	1.00000	0.993	-5.594
	1998.11	2	0.0299	7.846	140.11	1.00000	1.873	0.000
	1998.11	3	0.0225	28.954	150.49	1.00000	2.816	-50.757
	1998.29	0	2.2915	0.020	158.49	0.227146	3.281	-21.026
	1998.29	1	0.0566	2.917	134.18	1.00000	0.000	9.271
	1998.48	0	1.9039	0.006	97.28	0.211857	2.386	-31.574
	1998.48	2	0.0305	6.503	138.72	1.00000	0.000	-26.091
	1998.61	0	1.2902	0.741	-20.68	0.294835	1.729	-22.687
	1998.61	1	0.5898	1.890	158.86	1.00000	1.091	-23.523
	1998.61	2	0.0319	8.904	145.17	1.00000	1.801	6.211
	1998.61	2	0.0219	29.069	149.66	1.00000	3.258	71.204
	1998.97	0	1.5908	0.014	-9.89	0.245332	3.084	-25.789
	1998.97	3	0.0321	21.490	146.87	1.00000	7.371	-173.789
	1999.47	0	1.3988	0.286	-22.43	0.587787	1.715	-16.634
	1999.47	1	0.2082	3.379	156.78	1.00000	0.000	-139.988
	1999.47	2	0.0227	8.403	137.88	1.00000	0.038	62.955
	2001.35	0	2.6338	0.019	-26.05	0.284032	1.291	-35.617
	2001.35	1	0.0541	4.237	131.35	1.00000	3.708	-18.080
	2001.35	2	0.0181	12.629	150.31	1.00000	0.000	-13.758
	2002.04	0	2.2336	0.046	-16.69	0.329289	1.127	-39.425
	2002.04	1	0.1509	2.694	157.68	1.00000	2.741	5.594
	2004.13	0	2.2517	0.023	171.21	0.260248	2.556	-22.586
	2004.13	1	0.0789	3.929	143.98	1.00000	0.000	11.083
	2004.13	2	0.0301	10.568	149.22	1.00000	2.632	31.933
	2006.53	0	1.2699	0.013	175.34	0.371320	1.859	-26.083
	2006.53	2	0.0443	10.815	145.74	1.00000	1.089	-29.233
	2007.24	0	1.8536	0.005	154.71	0.425986	1.196	-29.174
	2007.24	2	0.0616	10.709	152.71	1.00000	2.801	5.594
	2007.48	0	3.0440	0.005	-42.29	1.00000	0.648	0.000

continue on next page...

...continued from previous page								
Source Name	*Epoch*	*Component*	S (Jy)	a (mas)	ϕ (deg)	*Axial Ratio*	r (mas)	θ (deg)
	2007.48	2	0.1055	8.525	155.06	1.00000	5.432	-4.002
	2007.52	0	2.3935	0.036	-45.53	0.398594	0.960	-17.349
	2007.52	1	0.0972	3.091	149.08	1.00000	0.000	7.965
	2007.52	2	0.0302	9.992	146.66	1.00000	2.629	18.080
	2007.58	0	1.7381	0.030	-7.52	0.00000	1.925	-1.618
	2007.58	2	0.0541	7.749	143.97	1.00000	4.502	0.000
	2007.93	0	2.4317	0.024	3.85	2.70294e-09	1.420	-30.195
	2007.93	2	0.0518	8.909	151.36	1.00000	0.914	18.080
	2008.06	0	2.5698	0.012	-27.60	0.432220	1.558	-15.883
	2008.06	2	0.0491	11.025	147.36	1.00000	4.341	-22.770
$1351-018$	1997.03	0	0.8767	0.010	56.94	4.80811e-09	1.048	-53.363
	1997.03	1	0.0325	11.597	-5.40	1.00000	6.029	-7.965
	1997.08	0	0.8390	0.013	75.87	0.738475	0.982	-47.826
	1997.08	1	0.0325	11.279	-4.11	1.00000	6.841	21.393
	1997.25	0	0.8434	0.004	25.04	1.00000	0.819	-15.633
	1997.25	1	0.0341	10.828	-11.79	1.00000	5.689	-44.403
	1997.38	0	0.8218	0.003	-82.88	0.750559	0.872	-24.427
	1997.38	1	0.0361	11.246	-8.86	1.00000	6.539	-34.433
	1997.69	0	0.8743	0.020	-177.47	1.00000	1.253	-31.471
	1997.69	1	0.0300	11.721	-7.66	1.00000	4.825	33.141
	1997.96	0	0.8404	0.007	61.51	0.568805	1.016	-62.885
	1997.96	1	0.0434	9.458	-14.37	1.00000	4.646	146.859
	2004.54	0	0.8104	0.014	20.09	0.571972	1.160	-76.123
	2004.54	1	0.0316	10.871	-1.37	1.00000	7.340	-9.271
	2006.70	0	0.7492	0.013	124.10	0.737025	1.313	25.279
	2006.70	1	0.0225	12.806	-9.53	1.00000	3.270	174.406
	2007.07	0	1.0235	0.005	161.40	0.660491	1.092	78.622
	2007.07	1	0.0224	10.019	-5.07	1.00000	1.571	-22.770
	2007.48	0	0.9958	0.003	174.89	0.00000	1.210	52.748
	2007.48	1	0.0258	11.179	-1.91	1.00000	0.000	-18.080
	2007.93	0	0.8047	0.036	142.36	1.00000	0.947	0.000
	2007.93	1	0.0301	13.463	-14.15	1.00000	5.596	-9.271
	2008.06	0	0.9762	0.023	-4.88	0.904107	1.095	17.528
	2008.06	1	0.0294	8.560	-2.02	1.00000	3.326	153.909
$1424-418$	1997.39	0	2.0502	0.107	-1.02	1.00000	1.469	-8.569
	1997.38	2	0.1580	16.484	163.06	1.00000	1.197	-15.633
	1997.56	0	2.4137	0.169	158.33	1.00000	1.636	-11.083
	1997.56	2	0.1444	15.148	134.28	1.00000	0.000	-6.573
	1997.97	0	2.2066	0.125	165.84	1.00000	1.604	53.474
	1997.97	2	0.7205	19.821	42.32	1.00000	21.526	-3.736
	1998.29	0	2.3167	0.026	66.43	0.733823	2.262	11.895
	1998.29	3	0.2898	23.381	46.68	1.00000	3.576	5.594
	1998.48	0	2.2578	0.021	-36.14	0.409334	2.552	-9.025
								continue on next page...

...continued from previous page

Source Name	*Epoch*	*Component*	S (Jy)	a (mas)	ϕ (deg)	*Axial Ratio*	r (mas)	θ (deg)
	1998.48	3	0.2622	27.361	40.51	1.00000	3.923	21.393
	1998.61	0	1.8077	0.136	170.84	1.00000	1.597	0.000
	1998.61	2	0.1928	15.259	72.49	1.00000	2.248	16.374
	1998.97	0	1.9102	0.287	-165.08	0.292626	4.913	13.693
	1998.97	3	0.3292	27.069	46.05	1.00000	8.361	0.000
	1998.97	1	0.1996	9.660	55.99	1.00000	6.571	0.000
	1999.47	0	1.8609	0.076	163.48	0.727975	1.476	-21.382
	1999.47	2	0.1052	17.622	29.03	1.00000	0.000	18.080
	1999.47	3	0.3183	23.109	51.17	1.00000	12.217	7.965
	2000.81	0	0.6882	0.080	2.06	0.00000	1.805	66.010
	2000.81	2	0.1319	19.201	159.56	1.00000	2.527	-4.666
	2001.35	0	0.9307	0.936	-27.02	1.00000	2.404	-12.736
	2001.35	2	0.2260	22.459	41.83	1.00000	4.515	-18.080
	2004.54	0	1.3446	0.298	-7.69	1.00000	1.847	-86.517
	2004.54	3	0.1701	27.262	49.18	1.00000	4.153	13.758
	2004.54	1	0.1125	9.884	60.58	1.00000	3.040	-10.406
	2006.70	0	1.2345	0.024	149.46	0.787427	1.205	45.619
	2006.70	1	0.0807	10.528	86.29	1.00000	1.103	-164.367
	2006.70	3	0.0681	25.769	48.57	1.00000	3.486	90.000
	2007.48	0	1.9471	0.017	154.44	1.00000	0.780	6.980
	2007.48	3	0.1311	25.885	45.75	1.00000	3.022	-12.977
	2007.48	1	0.0999	8.984	45.66	1.00000	0.000	-80.342
	2007.48	2	0.0638	16.043	98.30	1.00000	1.052	18.080
	2007.52	0	1.2793	0.011	-132.25	1.00000	0.180	23.997
	2007.52	3	0.1013	26.303	50.46	1.00000	4.855	5.088
	2007.52	1	0.0676	9.563	97.39	1.00000	1.457	36.299
	2007.52	99	0.0440	27.257	25.13	1.00000	3.589	-157.801
	2007.58	0	1.2880	0.040	-149.79	4.26091e-09	1.917	30.732
	2007.58	3	0.1018	25.462	72.21	1.00000	2.320	14.637
	2007.93	0	1.4513	0.097	-167.90	0.465793	2.363	-6.653
	2007.93	3	0.1852	24.374	51.51	1.00000	5.417	-146.859
	2007.93	2	0.0898	15.965	21.64	1.00000	4.255	11.083
	2008.06	0	1.6588	0.276	171.59	0.284329	3.328	-11.025
	2008.06	3	0.2852	25.941	43.77	1.00000	4.916	9.271
	2008.06	2	0.0786	15.607	-31.71	1.00000	0.000	-21.393
	2008.06	99	0.0646	38.673	148.80	1.00000	2.146	15.633
$1451-375$	1997.08	0	1.0276	0.086	9.76	0.00000	0.949	40.191
	1997.08	1	0.1120	5.560	-141.63	1.00000	2.445	0.000
	1997.25	0	1.3813	0.615	-168.08	1.00000	1.782	-78.938
	1997.25	2	0.1507	8.351	-120.53	1.00000	3.153	0.000
	1997.38	0	1.5540	0.009	106.87	1.00000	0.764	-66.366
	1997.38	2	0.1182	8.146	-144.45	1.00000	2.040	-20.167
	1997.56	0	1.4108	0.014	-0.94	0.00000	1.007	59.820

continue on next page...

...continued from previous page

Source Name	*Epoch*	*Component*	S (Jy)	a (mas)	ϕ (deg)	*Axial Ratio*	r (mas)	θ (deg)
	1997.56	2	0.1290	7.595	-141.00	1.00000	3.900	-13.758
	1997.96	0	1.3181	0.021	100.26	0.0507247	1.475	33.921
	1997.96	1	0.1027	5.906	-136.02	1.00000	3.608	-5.088
	1997.96	3	0.0628	15.807	-147.49	1.00000	3.982	10.406
	1998.11	0	1.2570	0.014	-136.29	0.401000 2.267	-1.406	
	1998.11	1	0.1169	6.230	-143.91	1.00000	3.358	-21.393
	1998.11	5	0.0191	35.171	-144.99	1.00000	0.000	4.666
	1998.29	0	1.4386	0.016	49.58	0.493268	1.400	28.650
	1998.29	2	0.1259	8.374	-145.52	1.00000	3.705	180.000
	1998.29	4	0.0299	22.900	-138.90	1.00000	4.551	-6.210
	1998.48	0	1.1068	0.175	30.58	1.00000	0.300	42.074
	1998.48	1	0.1376	4.362	-145.33	1.00000	3.551	-5.594
	1998.48	3	0.0629	15.589	-149.88	1.00000	5.226	-4.666
	1998.61	0	1.0348	0.024	-156.36	1.00000	1.358	11.092
	1998.61	5	0.0307	33.677	-149.92	1.00000	1.617	-146.859
	1999.47	0	1.0169	0.057	41.35	1.00000	0.713	40.595
	1999.47	2	0.1216	8.432	-142.77	1.00000	3.282	-20.167
	2000.81	0	0.6655	0.126	2.30	4.53884e-09	1.775	31.278
	2000.81	2	0.0903	8.536	-142.15	1.00000	1.743	10.097
	2002.04	0	1.1291	0.053	-52.53	1.00000	1.377	-5.594
	2002.04	3	0.0677	17.919	-144.68	1.00000	1.800	-167.722
	2006.53	0	0.5058	0.036	52.45	0.189414	2.283	18.952
	2006.53	3	0.0504	16.209	-146.27	1.00000	2.769	-156.477
$1514-241$	1997.08	0	1.4772	0.138	-13.52	0.0593834	2.576	-23.391
	1997.08	1	0.1613	8.200	157.88	1.00000	1.700	-11.083
	1997.08	2	0.1176	13.658	159.27	1.00000	3.984	30.440
	1997.08	5	0.0491	23.321	143.39	1.00000	4.447	13.758
	1997.25	0	1.3645	0.217	-16.69	0.103144	2.147	-24.908
	1997.25	1	0.1350	5.127	156.91	1.00000	1.707	-6.211
	1997.25	5	0.0604	21.251	149.28	1.00000	3.848	20.641
	1997.25	2	0.1711	10.462	159.19	1.00000	1.755	59.738
	1997.38	0	1.5167	0.258	-16.88	2.92573e-09	2.910	-23.701
	1997.38	1	0.1652	7.111	156.39	1.00000	1.414	0.000
	1997.38	2	0.1773	13.155	158.36	1.00000	4.990	0.000
	1997.38	5	0.0957	23.253	145.31	1.00000	7.991	7.965
	1997.54	0	1.8611	0.106	-17.80	0.0972471	2.778	-19.665
	1997.54	1	0.1370	8.657	157.14	1.00000	1.124	-36.299
	1997.54	2	0.1601	15.916	157.84	1.00000	4.579	-15.633
	1997.54	5	0.0483	24.906	143.89	1.00000	3.673	0.000
	1997.69	0	1.6126	0.280	-18.47	1.00000	0.658	-14.955
	1997.69	1	0.2440	9.356	159.76	1.00000	2.009	-5.594
	1997.69	3	0.1079	19.188	153.32	1.00000	6.054	0.000
	1997.96	0	2.0883	0.080	-33.41	0.272108	1.788	-19.904

continue on next page...

...continued from previous page

Source Name	Epoch	Component	S (Jy)	a (mas)	ϕ (deg)	Axial Ratio	r (mas)	θ (deg)
	1997.96	2	0.1471	11.893	159.94	1.00000	1.737	-6.210
	1997.96	3	0.1000	16.776	152.21	1.00000	3.038	0.000
	1997.96	1	0.1039	6.149	153.88	1.00000	1.060	0.000
	1997.96	5	0.0536	25.142	142.76	1.00000	3.733	36.299
	1998.11	0	2.0075	0.056	-15.23	0.234700	2.027	-23.463
	1998.11	2	0.2151	10.156	157.99	1.00000	2.595	30.440
	1998.11	3	0.0858	19.589	153.89	1.00000	2.120	19.279
	1998.11	6	0.0407	37.691	134.00	1.00000	4.264	5.088
	1998.11	5	0.0516	27.242	147.68	1.00000	3.310	36.299
	1998.29	0	2.0236	0.069	-26.86	0.208758	2.389	-21.742
	1998.29	1	0.1058	7.352	157.16	1.00000	1.526	-15.633
	1998.29	2	0.1394	12.739	159.81	1.00000	2.639	-30.440
	1998.29	3	0.0821	18.500	153.80	1.00000	2.713	-6.980
	1998.29	5	0.0418	25.595	146.11	1.00000	3.434	-29.233
	1998.48	0	1.9980	0.115	-26.47	0.220895	2.565	-22.654
	1998.48	2	0.0932	13.681	159.66	1.00000	2.070	-12.278
	1998.48	1	0.1318	6.281	151.47	1.00000	1.974	11.083
	1998.48	4	0.0919	18.330	151.78	1.00000	3.760	36.299
	1998.48	5	0.0380	27.049	143.91	1.00000	4.380	-11.083
	1998.61	0	1.9782	0.138	-20.62	0.182349	2.392	-23.699
	1998.61	2	0.1930	10.137	158.19	1.00000	2.352	-29.233
	1998.61	5	0.0370	25.759	138.99	1.00000	2.839	20.167
	1998.61	4	0.1242	19.133	153.33	1.00000	4.505	23.523
	1998.61	6	0.0244	36.118	131.89	1.00000	2.109	-12.278
	1998.97	0	1.8302	0.174	-17.46	0.00000	2.583	-27.605
	1998.97	1	0.1619	6.950	154.60	1.00000	2.514	-19.603
	1998.97	2	0.1167	15.207	159.39	1.00000	3.104	-5.594
	1998.97	5	0.0891	21.190	152.73	1.00000	3.777	44.403
	1998.97	6	0.0502	32.151	144.28	1.00000	6.834	-9.271
	1999.47	0	1.8287	0.073	-28.88	0.182496	2.900	-24.086
	1999.47	2	0.0797	13.861	158.54	1.00000	2.638	-26.091
	1999.47	1	0.1384	4.658	155.14	1.00000	2.411	11.083
	1999.47	3	0.1514	20.079	153.01	1.00000	6.532	7.965
	2000.81	0	1.1424	0.440	-24.60	0.298091	2.357	-14.163
	2000.81	1	0.3221	3.711	149.08	1.00000	1.609	18.080
	2000.81	2	0.1660	8.192	155.25	1.00000	1.304	13.758
	2000.81	5	0.0824	23.170	151.36	1.00000	3.690	-21.393
	2000.81	4	0.0780	18.274	155.81	1.00000	4.030	-12.278
	2002.04	0	1.6350	0.316	-30.43	0.312022	3.089	-26.404
	2002.04	1	0.3723	8.907	153.93	1.00000	2.178	6.980
	2002.04	5	0.1005	23.128	154.44	1.00000	2.763	0.000
	2007.07	0	2.2373	0.560	-20.84	5.38813e-09	2.890	-32.149
	2007.07	1	0.3922	10.315	152.65	1.00000	4.293	-23.523

continue on next page...

...continued from previous page								
Source Name	*Epoch*	*Component*	S (Jy)	a (mas)	ϕ (deg)	*Axial Ratio*	r (mas)	θ (deg)
	2007.07	5	0.2660	27.927	151.23	1.00000	4.636	10.097
$1622-253$	1994.52	0	1.6791	0.031	7.58	0.353461	1.826	47.811
	1994.52	5	0.0431	10.334	-28.30	1.00000	2.250	-9.271
	1995.56	0	0.9717	0.191	152.27	1.28606e-09	2.082	14.717
	1995.56	99	0.8855	0.358	-29.53	1.00000	2.037	-5.088
	1995.56	4	0.0431	6.433	-104.37	1.00000	5.513	-175.998
	1997.08	0	1.3031	0.012	-167.60	0.462860	1.374	80.530
	1997.08	4	0.0277	6.558	-47.27	1.00000	2.752	-4.666
	1997.25	0	1.4795	0.007	-125.01	0.00000	1.449	83.752
	1997.25	4	0.0301	7.662	-38.62	1.00000	2.249	11.083
	1997.38	0	1.0310	0.011	-140.37	1.00000	1.420	36.334
	1997.38	4	0.0398	6.176	-3.91	1.00000	1.244	0.000
	1997.56	0	1.2070	0.036	21.00	0.739369	1.938	14.416
	1997.56	4	0.0239	5.255	-49.53	1.00000	1.957	18.080
	1997.69	0	1.1980	0.214	168.45	1.00000	1.430	175.692
	1997.69	4	0.1243	5.561	-16.10	1.00000	5.152	-11.083
	1997.96	0	1.2806	0.051	121.04	0.524077	1.958	12.604
	1997.96	1	0.1095	2.483	-44.53	1.00000	1.562	6.980
	1997.96	5	0.0290	13.407	-17.44	1.00000	2.123	-20.167
	1998.11	0	1.5740	0.027	110.16	0.758384	1.712	8.388
	1998.11	1	0.0778	3.081	-50.77	1.00000	1.463	0.000
	1998.29	0	0.9748	0.195	-159.31	1.00000	1.133	38.368
	1998.29	1	0.2181	1.311	23.51	1.00000	1.708	-23.997
	1998.29	2	0.0413	4.825	-48.05	1.00000	0.000	-18.080
	1998.48	0	1.0896	0.123	169.78	0.703256	1.924	2.932
	1998.48	1	0.1454	2.302	-19.24	1.00000	4.062	5.088
	1998.61	0	1.0571	0.143	159.12	1.00000	0.988	-47.753
	1998.61	1	0.2255	2.010	-26.07	1.00000	2.907	180.000
	1998.97	0	1.1887	0.006	74.96	1.00000	1.292	-7.965
	1998.97	1	0.0567	2.829	-67.50	1.00000	1.341	90.000
	1999.47	0	1.5043	0.115	152.38	1.00000	0.754	62.955
	1999.47	1	0.2512	2.228	-25.01	1.00000	3.049	38.079
	2000.81	0	0.6326	0.087	64.25	0.745723	1.926	-2.318
	2000.81	1	0.0498	2.406	-61.35	1.00000	1.329	58.507
	2000.81	6	0.0218	16.200	-24.21	1.00000	4.021	-15.633
	2001.35	0	0.6003	0.255	157.39	1.00000	1.316	26.091
	2001.35	1	0.1037	2.819	-36.30	1.00000	4.174	49.606
	2002.04	0	0.9267	0.287	165.83	1.00000	1.520	40.012
	2002.04	3	0.0961	4.300	-19.96	1.00000	2.754	4.666
	2004.54	0	2.1842	0.092	152.64	1.00000	0.811	-50.632
	2004.54	1	0.2333	1.775	-27.26	1.00000	1.655	-44.403
	2006.53	0	1.7140	0.033	159.45	0.649120	1.949	-36.749
	2006.53	5	0.0278	11.745	-98.27	1.00000	0.421	-16.374
								continue on next page...

...continued from previous page								
Source Name	*Epoch*	*Component*	S (Jy)	a (mas)	ϕ (deg)	*Axial Ratio*	r (mas)	θ (deg)
	2007.07	0	1.9835	0.125	155.73	0.423561	2.426	-26.676
	2007.07	4	0.0510	6.843	-136.85	1.00000	1.313	-13.758
	2007.52	0	1.3696	0.093	159.08	0.906920	0.948	-82.807
	2007.52	3	0.0810	3.591	-17.33	1.00000	3.164	-26.091
	2007.52	5	0.0206	10.162	-64.29	1.00000	4.986	-14.452
	2008.06	0	0.9947	0.151	11.93	5.35193e-09	1.385	54.464
	2008.06	4	0.0190	7.160	-37.00	1.00000	2.374	5.329
	2008.06	7	0.0104	26.465	-32.73	1.00000	3.444	-4.666
$1741-038$	1995.56	0	1.7975	0.023	8.06	1.00000	0.600	24.324
	1995.56	1	0.0462	5.067	173.30	1.00000	1.301	40.012
	1995.78	0	1.7687	0.038	-9.24	1.00000	0.705	11.083
	1995.78	2	0.0481	8.110	170.80	1.00000	3.192	-26.091
	1997.08	0	1.9640	0.026	-7.70	1.00000	0.567	-50.595
	1997.08	1	0.0696	3.977	167.46	1.00000	2.273	3.736
	1997.25	0	2.3082	0.011	-2.84	1.00000	0.668	-19.068
	1997.25	1	0.0715	4.498	173.73	1.00000	2.279	146.859
	1997.38	0	2.6514	0.024	-11.95	0.629828	0.896	-30.273
	1997.38	1	0.0664	4.956	172.23	1.00000	2.383	36.299
	1997.56	0	2.3932	0.011	-12.60	1.00000	0.563	21.393
	1997.56	1	0.0547	5.108	170.39	1.00000	2.600	-11.853
	1997.69	0	2.6221	0.020	-14.71	0.477746	1.653	-3.916
	1997.69	2	0.0350	8.099	174.25	1.00000	2.893	-15.633
	1997.96	0	2.8265	0.007	-3.23	1.00000	0.684	5.922
	1997.96	2	0.0406	9.777	168.47	1.00000	3.490	-12.977
	1998.11	0	2.5350	0.045	-37.09	1.00000	0.675	-6.980
	1998.11	99	0.1440	1.137	145.79	1.00000	0.977	16.374
	1998.11	1	0.0325	6.156	-179.87	1.00000	2.105	20.167
	1998.29	0	3.0456	0.018	0.52	0.802779	1.056	-28.207
	1998.29	1	0.0805	3.990	172.21	1.00000	2.531	5.594
	1998.48	0	2.9488	0.008	6.05	0.613267	1.170	-27.171
	1998.48	1	0.0547	4.579	173.60	1.00000	2.817	0.000
	1998.61	0	2.5372	0.013	-1.15	0.671911	1.118	-38.666
	1998.61	1	0.0373	5.431	174.89	1.00000	2.817	41.394
	1998.97	0	2.9276	0.001	-109.71	0.677900	1.101	-27.759
	1998.97	1	0.0405	6.802	171.46	1.00000	4.394	0.000
	1999.47	0	3.8894	0.022	-6.38	0.496944	1.361	-35.609
	1999.47	1	0.0754	3.983	170.88	1.00000	3.111	0.000
	2001.35	0	2.8230	0.009	-17.85	1.00000	0.675	-3.114
	2001.35	2	0.1812	7.357	-136.24	1.00000	0.937	0.000
	2004.13	0	4.0327	0.011	-14.58	0.700577	0.972	-30.205
	2004.13	2	0.0790	9.635	161.24	1.00000	2.177	-11.083
	2004.54	0	3.6633	0.020	-9.31	1.00000	0.578	11.853
	2004.54	1	0.0887	4.143	158.62	1.00000	2.693	11.083
								continue on next page...

...continued from previous page

Source Name	*Epoch*	*Component*	S (Jy)	a (mas)	ϕ (deg)	*Axial Ratio*	r (mas)	θ (deg)
	2008.06	0	4.7254	0.044	-25.72	1.00000	0.861	-13.758
	2008.06	2	0.0484	8.353	178.34	1.00000	7.662	-14.955
$1908-201$	1997.08	0	1.5277	0.270	-108.19	0.504637	2.937	37.607
	1997.08	1	0.3693	2.551	53.23	1.00000	2.352	117.045
	1997.08	2	0.0985	5.453	68.96	1.00000	3.915	0.000
	1997.08	3	0.0172	14.132	73.17	1.00000	4.296	-4.002
	1997.25	0	1.4941	0.307	-124.22	0.505177	2.791	40.563
	1997.25	1	0.4739	2.427	51.62	1.00000	2.776	-12.278
	1997.25	2	0.0873	6.616	65.00	1.00000	6.483	0.000
	1997.38	0	1.7806	0.230	-60.74	0.514240	3.234	35.325
	1997.38	1	0.2606	2.870	57.69	1.00000	1.500	44.403
	1997.38	2	0.0995	5.368	73.61	1.00000	3.013	-26.091
	1997.56	0	1.8784	0.132	-46.58	0.469483	3.376	38.168
	1997.56	1	0.2053	3.347	60.62	1.00000	1.287	-15.633
	1997.56	2	0.0829	6.202	71.90	1.00000	3.284	-10.406
	1997.69	99	0.4965	1.905	-141.36	1.00000	1.962	80.597
	1997.69	0	1.0102	0.255	-95.49	1.00000	1.194	-159.833
	1997.69	1	0.7015	1.708	44.49	1.00000	2.474	-9.271
	1997.69	2	0.2051	4.057	58.65	1.00000	4.209	-9.271
	1997.69	3	0.0246	11.526	73.75	1.00000	5.392	11.853
	1998.11	0	2.0088	0.154	-133.45	0.448992	2.912	40.164
	1998.11	1	0.4266	3.116	53.82	1.00000	3.064	26.091
	1998.11	2	0.0403	7.184	62.04	1.00000	1.364	0.000
	1998.29	0	2.5813	0.109	-46.33	0.414024	2.539	42.715
	1998.29	1	0.3832	3.114	63.14	1.00000	1.580	-12.278
	1998.48	0	2.1491	0.169	-145.41	0.432560	3.315	32.460
	1998.48	1	0.4161	2.586	56.49	1.00000	4.861	0.000
	1998.61	0	2.1941	0.047	-76.37	0.395151	3.040	39.333
	1998.61	1	0.2024	3.398	56.63	1.00000	0.458	-5.594
	1998.61	2	0.0789	5.765	64.75	1.00000	2.316	146.859
	1998.61	3	0.0152	13.305	60.03	1.00000	3.996	-6.210
	1998.97	0	2.3068	0.114	-76.80	0.463125	2.775	41.386
	1998.97	1	0.2655	3.285	55.12	1.00000	1.438	172.035
	1998.97	2	0.0735	6.445	70.07	1.00000	2.386	0.000
	1999.47	0	2.7958	0.107	-101.18	0.475185	2.653	47.430
	1999.47	1	0.3515	3.365	62.07	1.00000	2.604	-13.758
	2000.81	0	2.3524	0.092	165.05	0.522476	2.335	45.372
	2000.81	2	0.5368	3.148	52.17	1.00000	3.123	-6.211
	2001.35	0	1.9476	0.103	-56.59	0.518944	2.690	42.202
	2001.35	1	0.4221	3.402	61.38	1.00000	3.385	-24.324
	2004.54	0	1.5618	0.110	-91.80	0.445869	3.979	17.873
	2004.54	3	0.2479	3.829	67.22	1.00000	4.476	4.666
	2006.53	0	1.5532	0.217	-157.15	0.00000	2.355	56.129

continue on next page...

...continued from previous page								
Source Name	*Epoch*	*Component*	S (Jy)	a (mas)	ϕ (deg)	*Axial Ratio*	r (mas)	θ (deg)
	2006.53	2	0.1804	6.996	141.69	1.00000	4.690	-174.912
	2006.53	3	0.1558	9.823	-9.25	1.00000	0.000	-19.603
	2006.70	0	1.5211	0.045	-20.10	0.611952	1.777	25.857
	2006.70	1	0.1177	3.276	82.47	1.00000	0.673	-49.606
	2007.07	0	2.1209	0.137	-78.96	0.453668	2.009	0.617
	2007.07	1	0.4007	2.894	63.96	1.00000	3.389	-39.220
	2007.07	4	0.0372	23.234	48.52	1.00000	2.383	180.000
	2007.24	0	1.8864	0.058	-112.02	0.581413	1.833	14.683
	2007.24	1	0.3184	3.555	48.98	1.00000	2.775	-14.955
	2007.24	4	0.0284	22.721	53.35	1.00000	3.029	-14.955
	2007.48	0	2.2174	0.057	-112.67	0.551068	2.647	8.058
	2007.48	1	0.3755	3.888	53.38	1.00000	3.894	-15.633
	2007.48	4	0.0330	24.069	56.23	1.00000	5.125	138.958
	2007.52	0	2.0849	0.086	-64.68	1.00000	1.529	32.295
	2007.52	1	0.3105	3.826	61.57	1.00000	5.247	-12.549
	2007.93	0	1.7786	0.272	-24.45	1.00000	1.447	13.207
	2007.93	1	0.2100	3.052	66.69	1.00000	0.000	-13.758
	2007.93	2	0.1472	5.667	74.34	1.00000	4.566	-13.758
$1921-293$	1994.52	0	10.9887	0.082	-117.15	0.445916	1.997	19.814
	1994.52	1	3.3527	4.516	38.38	1.00000	3.496	-10.097
	1994.52	2	1.2583	5.675	-152.78	1.00000	0.000	-50.757
	1995.56	0	9.0969	0.121	-133.86	0.461115	2.233	20.692
	1995.56	1	4.3594	4.794	32.36	1.00000	3.993	22.770
	1995.56	2	0.6888	5.077	-151.16	1.00000	1.342	-8.569
	1995.75	0	12.1628	0.394	-17.62	1.00000	2.030	77.358
	1995.75	1	2.4260	3.754	50.94	1.00000	2.047	-6.211
	1997.08	0	8.0183	0.088	-160.58	0.264867	1.802	47.679
	1997.08	1	3.9182	4.363	37.05	1.00000	4.172	-11.083
	1997.08	2	0.9579	5.426	-154.32	1.00000	0.000	-9.271
	1997.25	0	7.4655	0.230	-157.42	0.559824	2.077	24.914
	1997.25	1	4.1088	4.070	33.20	1.00000	3.881	-7.965
	1997.25	2	0.7032	5.371	-149.45	1.00000	0.000	-15.633
	1997.38	0	8.2683	0.083	-111.79	0.621713	1.902	26.933
	1997.38	1	5.2679	4.518	34.01	1.00000	3.723	180.000
	1997.56	0	9.9587	0.473	-156.31	0.261632	2.525	27.024
	1997.56	1	4.6851	4.650	34.56	1.00000	3.086	23.523
	1997.69	0	9.2398	0.932	-30.03	1.00000	1.753	76.242
	1997.69	1	4.3289	3.592	52.10	1.00000	3.430	173.789
	1997.96	0	9.3143	0.187	-24.62	0.504194	2.809	11.725
	1997.96	1	3.0147	4.201	43.37	1.00000	3.035	-16.770
	1997.96	2	1.2811	6.276	-158.09	1.00000	0.000	-4.002
	1998.11	0	8.4964	0.164	-26.71	0.554079	1.845	28.934
	1998.11	1	3.6377	4.557	39.93	1.00000	3.505	0.000
								continue on next page...

...continued from previous page								
Source Name	*Epoch*	*Component*	S (Jy)	a (mas)	ϕ (deg)	*Axial Ratio*	r (mas)	θ (deg)
	1998.11	2	0.9103	6.288	-162.49	1.00000	0.000	-167.023
	1998.29	0	8.3365	0.162	-61.53	1.00000	1.332	7.965
	1998.29	1	5.2419	3.700	34.98	1.00000	4.095	-26.091
	1998.48	0	8.4959	0.091	-55.65	0.457175	3.370	9.766
	1998.48	1	2.9919	4.659	43.91	1.00000	3.138	-19.603
	1998.48	2	0.3713	6.300	-155.74	1.00000	0.000	0.000
	1998.61	0	7.2225	0.134	-21.68	0.233581	2.149	57.615
	1998.61	1	2.3569	4.321	49.03	1.00000	2.799	0.000
	1998.61	2	0.6451	6.207	-160.74	1.00000	0.000	-26.091
	1998.97	0	5.6829	0.256	-34.04	1.00000	1.625	77.301
	1998.97	1	4.0772	4.352	33.69	1.00000	4.236	-30.440
	1998.97	2	0.7975	6.519	-163.68	1.00000	1.676	-173.789
	2000.81	99	3.6049	2.344	-157.57	1.00000	0.904	28.575
	2000.81	99	4.4016	3.060	32.87	1.00000	3.777	-3.503
	2001.35	0	4.8298	0.171	-145.17	0.00000	2.151	54.514
	2001.35	1	3.4906	5.256	30.91	1.00000	4.690	165.045
	2001.35	2	1.3289	6.120	-149.97	1.00000	1.807	-8.569
	2004.13	0	4.1365	0.187	-24.07	1.00000	2.581	-170.729
	2004.13	1	1.7238	4.780	48.64	1.00000	3.764	0.000
	2004.13	2	0.5810	6.746	-159.67	1.00000	0.000	-29.740
	2006.70	0	6.6843	0.033	-92.51	0.507246	2.416	34.960
	2006.70	3	0.4065	10.369	47.74	1.00000	1.180	-173.789
	2007.07	0	6.4493	0.149	-44.98	0.497032	1.713	-34.499
	2007.07	2	2.4774	7.267	30.19	1.00000	4.132	0.000
	2007.24	0	2.1351	0.184	-145.86	5.68780e-09	2.785	-41.476
	2007.24	1	2.1058	4.401	27.96	1.00000	3.885	-7.440
	2007.48	0	4.9123	0.199	-2.83	0.465474	3.353	0.716
	2007.48	2	2.9196	7.099	29.29	1.00000	3.992	-167.722
	2007.93	0	5.4308	0.044	-26.75	1.00000	1.734	0.000
	2007.93	3	0.7542	9.192	47.21	1.00000	2.380	-13.758
$1954-388$	1997.08	0	2.7550	0.009	-17.49	4.03699e-09	0.695	71.153
	1997.08	5	0.0209	22.755	-167.42	1.00000	0.000	62.954
	1997.25	0	2.5885	0.019	-173.15	1.00000	0.586	-50.895
	1997.25	1	0.0349	5.766	-127.51	1.00000	1.644	0.000
	1997.38	0	2.5213	0.082	175.35	1.00000	0.655	-67.216
	1997.38	1	0.0886	5.496	-18.18	1.00000	6.824	12.278
	1997.56	0	2.3292	0.003	11.71	4.11952e-09	0.797	62.350
	1997.56	2	0.0236	8.773	-143.64	1.00000	3.020	18.080
	1997.69	0	2.2819	0.048	169.16	0.663303	1.447	-9.623
	1997.69	3	0.0369	12.495	-6.72	1.00000	0.953	-36.299
	1997.96	0	2.2290	0.011	-44.09	3.80800e-09	0.952	50.707
	1997.96	3	0.0434	10.037	-27.93	1.00000	3.398	5.594
	1998.29	0	2.7208	0.013	-10.99	0.318051	1.456	18.243
								continue on next page...

...continued from previous page								
Source Name	*Epoch*	*Component*	S (Jy)	a (mas)	ϕ (deg)	*Axial Ratio*	r (mas)	θ (deg)
	1998.29	2	0.0426	7.912	-140.81	1.00000	5.813	-11.853
	1999.47	0	1.6119	0.032	175.47	1.00000	0.718	-11.583
	1999.47	3	0.0146	13.188	-35.31	1.00000	1.307	0.000
	2000.81	0	0.8589	0.099	-49.55	1.00000	0.985	64.038
	2000.81	5	0.0166	20.177	-85.36	1.00000	3.068	-52.556
	2000.81	1	0.0174	6.837	-51.15	1.00000	2.095	6.211
	2002.04	0	0.9293	0.046	-11.62	0.506610	2.543	-1.469
	2002.04	3	0.0141	15.094	-106.81	1.00000	2.945	175.334
	2004.54	0	2.1847	0.021	25.41	0.235647	4.192	5.344
	2004.54	2	0.0281	11.468	-53.66	1.00000	2.580	-8.569
	2006.70	0	2.0459	0.043	103.90	1.00000	0.602	87.096
	2006.70	4	0.1873	2.642	-141.98	1.00000	1.126	-38.079
	2007.48	0	2.6019	0.037	-164.64	1.00000	1.187	-13.758
	2007.48	2	0.0545	8.627	-43.24	1.00000	0.000	-31.471
	2007.52	0	1.9436	0.012	-40.97	1.00000	1.233	1.351
	2007.52	5	0.0222	22.065	-96.98	1.00000	1.200	-36.299
	2007.93	0	1.9669	0.025	111.46	1.00000	0.562	4.778
	2007.93	2	0.2132	8.492	-153.32	1.00000	1.501	-26.091
	2007.93	99	0.2030	8.743	24.92	1.00000	2.636	-29.233
	2008.06	0	2.6876	0.033	-10.90	0.330863	2.646	18.552
	2008.06	1	0.0575	4.981	-116.73	1.00000	1.816	-13.758
$1958-179$	1995.52	0	0.3067	0.344	52.33	1.00000	0.528	30.517
	1995.52	1	0.1364	1.144	-123.53	1.00000	1.110	180.000
	1995.75	0	0.4761	0.129	48.25	1.00000	1.063	13.627
	1995.75	1	0.0717	1.945	-143.28	1.00000	1.087	-33.141
	2004.54	0	1.7611	0.013	8.77	1.45180e-09	0.922	-61.219
	2004.54	99	0.0271	7.972	-158.35	1.00000	1.060	-18.080
	2007.24	0	1.5490	0.028	13.45	4.76921e-09	0.580	32.204
	2007.24	1	0.0794	2.927	-1.48	1.00000	1.450	18.080
	2007.24	2	0.1176	1.844	-170.21	1.00000	2.047	0.000
$2052-474$	1997.69	0	1.3686	0.032	-165.55	0.716238	1.882	-88.742
	1997.69	1	0.0623	24.522	-142.18	1.00000	1.915	-11.083
$2243-123$	1997.03	0	1.7328	0.113	178.75	0.127008	2.590	26.814
	1997.03	2	0.3243	9.104	35.45	1.00000	2.652	8.569
	1997.08	0	1.6717	0.047	124.99	0.163752	2.822	24.037
	1997.08	2	0.3066	9.281	34.95	1.00000	2.818	-6.211
	1997.25	0	1.2250	0.640	-159.26	1.00000	0.499	14.955
	1997.25	2	0.2845	9.499	34.72	1.00000	2.374	33.141
	1997.25	1	0.5696	1.827	24.01	1.00000	1.097	-5.088
	1997.25	3	0.0375	12.218	68.60	1.00000	4.142	18.080
	1997.38	0	1.9318	0.052	159.93	1.00000	1.690	-9.271
	1997.38	2	0.3514	9.354	33.49	1.00000	3.907	0.000
	1997.56	0	1.4791	0.417	-161.53	0.170954	1.660	10.986
								continue on next page...

...continued from previous page								
Source Name	*Epoch*	*Component*	S (Jy)	a (mas)	ϕ (deg)	*Axial Ratio*	r (mas)	θ (deg)
	1997.56	2	0.2907	9.506	34.56	1.00000	2.633	0.000
	1997.56	1	0.4361	2.075	28.96	1.00000	1.087	-18.080
	1997.56	3	0.0350	13.347	65.77	1.00000	2.480	-3.297
	1997.69	0	1.9448	0.165	153.07	1.00000	1.806	-4.666
	1997.69	2	0.3312	9.488	34.34	1.00000	3.635	5.594
	1997.96	0	1.7928	0.067	173.43	0.108411	2.965	25.264
	1997.96	2	0.3009	9.287	34.57	1.00000	2.948	0.000
	1998.11	0	1.1638	0.746	-159.25	1.00000	0.673	12.278
	1998.11	2	0.2396	9.527	34.40	1.00000	2.455	14.955
	1998.11	1	0.4833	2.010	21.69	1.00000	1.237	-20.167
	1998.11	3	0.0391	12.487	66.56	1.00000	4.724	21.393
	1998.29	0	1.7774	0.102	14.57	0.302343	2.993	20.279
	1998.29	2	0.2672	9.712	34.50	1.00000	2.939	0.000
	1998.48	0	0.9962	0.751	-164.56	1.00000	0.488	0.000
	1998.48	2	0.2249	9.570	34.27	1.00000	2.533	-29.233
	1998.48	1	0.5995	1.779	26.01	1.00000	1.478	-20.167
	1998.48	3	0.0210	12.175	74.99	1.00000	3.010	0.000
	1998.61	0	1.0428	0.766	-163.08	1.00000	0.000	13.758
	1998.61	2	0.2361	9.503	34.92	1.00000	2.598	-11.083
	1998.61	1	0.5676	1.762	28.28	1.00000	1.044	-6.980
	1998.61	3	0.0168	13.712	61.55	1.00000	1.401	-18.080
	1998.97	0	1.4240	0.090	96.63	0.193455	3.395	23.719
	1998.97	2	0.2182	9.291	35.14	1.00000	2.196	0.000
	1999.47	0	1.3279	0.105	-153.97	0.340943	3.056	25.577
	1999.47	2	0.1978	8.999	36.09	1.00000	2.667	0.000
$2255-282$	1994.52	0	0.9257	0.300	53.49	1.00000	0.534	14.955
	1994.52	1	0.4971	2.704	-137.46	1.00000	1.486	-13.758
	1994.52	2	0.0482	14.671	-119.11	1.00000	2.086	0.000
	1995.56	0	0.8227	0.316	52.97	1.00000	0.885	12.977
	1995.56	1	0.3607	2.831	-138.29	1.00000	1.559	-26.091
	1995.56	2	0.0785	10.728	-123.73	1.00000	8.353	-21.393
	1995.75	0	1.2408	0.152	-112.07	0.565793	3.963	33.622
	1997.08	0	0.9135	0.875	39.25	1.00000	0.000	28.112
	1997.08	1	0.4085	2.729	-136.84	1.00000	1.268	159.833
	1997.08	2	0.0446	11.840	-112.67	1.00000	6.295	2.337
	1997.25	0	1.2541	0.282	35.78	0.00000	3.205	41.569
	1997.25	1	0.1484	3.466	-129.16	1.00000	2.339	-48.222
	1997.25	2	0.0352	11.872	-102.40	1.00000	4.876	3.297
	1997.38	0	1.0925	0.575	40.53	1.00000	0.735	-16.069
	1997.38	1	0.3977	3.299	-141.50	1.00000	1.584	-3.114
	1997.38	2	0.0294	13.035	-104.49	1.00000	3.908	4.308
	1997.56	0	1.0283	0.713	38.25	1.00000	0.288	12.977
	1997.56	1	0.4209	3.008	-139.05	1.00000	1.903	13.758

continue on next page...

...continued from previous page								
Source Name	*Epoch*	*Component*	S (Jy)	a (mas)	ϕ (deg)	*Axial Ratio*	r (mas)	θ (deg)
	1997.56	2	0.0414	13.033	-115.10	1.00000	5.189	0.000
	1997.69	0	1.0922	0.415	31.24	1.00000	1.234	0.000
	1997.69	1	0.3955	3.196	-139.50	1.00000	2.302	175.998
	1997.96	0	1.0816	0.578	38.67	1.00000	0.095	4.666
	1997.96	1	0.3880	3.229	-136.61	1.00000	1.579	-18.080
	1997.96	2	0.0364	12.738	-117.26	1.00000	4.346	4.002
	2006.70	0	0.7010	0.032	-2.13	1.00000	0.772	6.980
	2006.70	1	0.0714	9.125	-141.81	1.00000	0.000	176.264
	2007.07	0	1.0182	0.426	157.29	1.00000	3.164	-7.280
	2007.07	1	0.0863	5.709	-131.34	1.00000	0.000	-13.758
	2007.07	2	0.0277	23.130	-134.85	1.00000	0.000	-9.271
	2007.48	0	0.8172	0.085	48.29	1.00000	2.045	2.951
	2007.48	1	0.1590	5.017	-133.45	1.00000	1.853	-28.851
	2007.48	2	0.0153	29.635	-134.00	1.00000	4.049	-10.097
	2007.58	0	0.8900	0.061	-25.60	1.00000	2.392	0.000
	2008.06	0	0.8675	0.157	63.89	1.00000	1.527	9.271
	2008.06	1	0.0872	9.338	-143.36	1.00000	0.000	180.000